AD-A045 801 CHARLES STARK DRAPER LAB INC CAMBRIDGE MASS F/G 8/3
THE C. S. DRAPER LABORATORY ROLE IN THE MOORING DYNAMICS EXPERI--ETC(U)
APR 77 W A VACHON, J R SCHOLTEN N00014-75-C-1065
UNCLASSIFIED R-1093 NL

1 OF 2
ADA045801

AD A045801

12

R-1093

FINAL REPORT ON THE C. S. DRAPER LABORATORY ROLE IN THE MOORING DYNAMICS EXPERIMENT

by

William A. Vachon
James R. Scholten

April 1977

DDC
RECEIVED
OCT 20 1977
C

The Charles Stark Draper Laboratory, Inc.
Cambridge, Massachusetts 02139

AD No.
DDC FILE COPY

Approved for public release; distribution unlimited.

SECURITY CLASSIFICATION OF THIS PAGE *(When Data Entered)*

REPORT DOCUMENTATION PAGE

READ INSTRUCTIONS BEFORE COMPLETING FORM

1. REPORT NUMBER: R-1093	2. GOVT ACCESSION NO.
3. RECIPIENT'S CATALOG NUMBER	
4. TITLE *(and Subtitle)*: ~~Final Report on~~ the C. S. Draper Laboratory Role in the Mooring Dynamics Experiment.	5. TYPE OF REPORT & PERIOD COVERED: ~~Interim~~ Report, March 1975-June 1977
	6. PERFORMING ORG. REPORT NUMBER
7. AUTHOR(s): William A. Vachon; James R. Scholten	8. CONTRACT OR GRANT NUMBER(s): N00014-75-C-1065
9. PERFORMING ORGANIZATION NAME AND ADDRESS: Charles Stark Draper Laboratory, Inc. 555 Technology Square Cambridge, MA 02139	10. PROGRAM ELEMENT, PROJECT, TASK AREA & WORK UNIT NUMBERS: 113 P.
11. CONTROLLING OFFICE NAME AND ADDRESS: NORDA, Code 450 NSTL Station Bay St. Louis, Miss. 39529	12. REPORT DATE: April 1977
	13. NUMBER OF PAGES: 104
14. MONITORING AGENCY NAME & ADDRESS *(if different from Controlling Office)*: SAME	15. SECURITY CLASS. *(of this report)*: Unclassified
	15a. DECLASSIFICATION/DOWNGRADING SCHEDULE

16. DISTRIBUTION STATEMENT *(of this Report)*

Distribution unlimited

DISTRIBUTION STATEMENT A
Approved for public release;
Distribution Unlimited

17. DISTRIBUTION STATEMENT *(of the abstract entered in Block 20, if different from Report)*

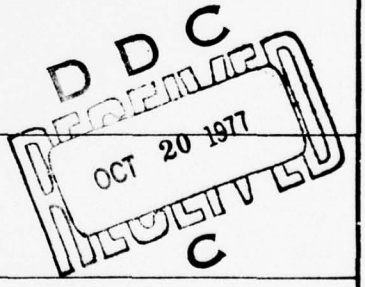

18. SUPPLEMENTARY NOTES

19. KEY WORDS *(Continue on reverse side if necessary and identify by block number)*

Moorings — Oceanographic Moorings
Mooring Dynamics
Buoys
Oceanographic Buoys

20. ABSTRACT *(Continue on reverse side if necessary and identify by block number)*

This report describes the details of the ONR/NDBO Mooring Dynamics Experiment (MDE) that was conducted at the Pacific Missile Range Facility (PMRF) during October and November of 1976. Specific emphasis is placed on describing the instruments built, calibration techniques employed, and results achieved by the C. S. Draper-supplied equipment. In addition, though, considerable emphasis is placed on describing the details of the test moorings, experiment timelines, summary results, and other pertinent data that would be useful in applying the

DD FORM 1 JAN 73 1473 EDITION OF 1 NOV 65 IS OBSOLETE

408 386

SECURITY CLASSIFICATION OF THIS PAGE *(When Data Entered)*

R-1093:

measured data to the verification of mathematical models of mooring response.

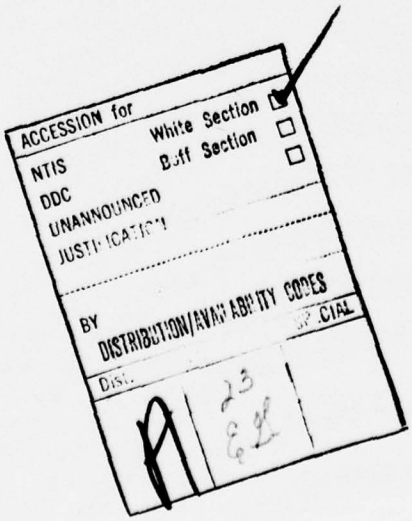

R-1093

FINAL REPORT ON THE C. S. DRAPER LABORATORY ROLE IN THE MOORING DYNAMICS EXPERIMENT

by

WILLIAM A. VACHON
JAMES R. SCHOLTEN

THE CHARLES STARK DRAPER LABORATORY, INC.
555 Technology Square
Cambridge, Massachusetts 02139

April 1977

TECHNICAL REPORT

Approved: Philip N. Bowditch Date: 10-11-77

Philip N. Bowditch
Head, Scientific Research Dept.

Approved for public release; distribution unlimited

ACKNOWLEDGEMENT

This research was jointly sponsored by the Office of Naval Research (ONR) and the NOAA Data Buoy Office (NDBO) through contract number N00014-75-C-1065 from ONR to the C. S. Draper Laboratory, Inc.

The authors wish to thank all of the organizations and individuals who worked with us on the mooring dynamics experiment. Special thanks are due to Mr. John Gregory and Lt. Tom Christensen of NORDA (formerly ONR) as well as Cmdr. Charles Niederman and Lt. Don BeBok of NDBO for their support and assitance throughout the program. In addition, special thanks are due to Mr. Robert Walden, and the personnel at the Woods Hole Oceanographic Institute for their assistance and co-operation throughout the program, to Mr. Stewart V. Burley and the staff of the Pacific Missile Range Facility (PMRF) for their assistance in the field test phase, and to the officers and crew of the USNS DeSteiguer for their support during marine operations. Within the Draper Laboratory the following individuals made invaluable contributions toward the program success: Mr. John Dahlen for the initial design of the mooring instrumentation scheme and for his guidance throughout the program; Mr. Narender Chhabra for mathematical simulations of mooring motion and assistance with data analysis; Mr. John McKenna for the design modification, and test of the electronics systems as well as field support during the experimental phase; to Mr. Joseph Marino for his assistance with the electronic design and test; to Mr. Richard Araujo and Mr. Matti Soikkeli for their assistance in the instrument modifications, test and field test support; to Mr. William DeRusso, Mr. Carmen Martorella and Mr. Edward Scioli for their unselfish contributions during the instrument assembly, calibration and checkout phase; and to Mr. Huey Lane, Mr. Don Black and all the individuals in the system assembly division for their painstaking work in the fabrication of the system electronics. Special thanks are also due to Catherine Hall for her typing of the manuscript.

R-1093

Final Report of C. S. Draper Lab Role in the Mooring Dynamics Experiment

Table of Contents

Section	Description	Page
	Abstract	
1.0	Introduction	1
2.0	Summary of Field Test Program	3
	2.1 Mooring Descriptions	3
	2.1.1 Current Meter Mooring	3
	2.1.2 Discus Surface Moorings (Experiments #1 and #3)	9
	2.1.3 Spar/Sphere Mooring (Experiment #2)	10
	2.1.4 High Performance Intermediate Mooring (Experiment #4)	14
	2.1.5 CEL Subsurface Mooring (Experiment #5)	15
	2.2 Summary of Results	15
3.0	Instrument Descriptions	24
	3.1 Force Vector Recorder (FVR)	24
	3.2 High Frequency Temperature-Pressure Recorders (HFTP)	29
	3.3 Low Frequency Temperature-Pressure Recorders (LFTP)	32
4.0	Pre and Post Experiment Instrument Tests and Calibrations	33
	4.1 FVR Pressure and Load Tests	33
	4.2 FVR Sensor Calibration Procedure	36
	4.2.1 Accelerometer Calibrations	36
	4.2.2 Tension Load Cell Calibration	37
	4.2.3 Magnetometer Calibration	37
	4.3 HFTP and LFTP Sensor Calibration Procedure	37
	4.4 System Synchronization Procedure	39
	4.5 System Integration Test	39

Table of Contents (Cont.)

Section	Description	Page
5.0	FVR Euler Angle Determination	42
6.0	FVR Magnetometer Calibrations and Error Analysis	53
7.0	Archived Data Tape Constants	65
	References	68
Appendix A -	Summary of Averaged T/P Field Data	69
Appendix B -	T/P Timing, Calibrations and Word Structure	92
Appendix C -	FVR Timing, Calibrations and Word Structure	99

LIST OF TABLES

Table	Description	Page
1	Modelling Parameters for Key Elements of MDE Moorings	13
2	Experiment No. 1 Summary	17
3	Experiment No. 2 Summary	18
4	Experiment No. 3 Summary	19
5	Experiment No. 5 Summary	20
6	System Timing of Burst Instruments Employed in Mooring Dynamics Experiment	25
7	Force Vector Recorder Characteristics	28
8	Nominal Ranges and Scaling of Temperature-Pressure Recorders	31
9	Summary of Kauai Magnetometer Calibrations	60
10	Magnetometer Scale Factors and Estimated Alignment Errors During MDE Field Experiment	62
11	MDE-Magnetometer Calibration Data Summary	64
A-1 through A-22	Summary of Averaged T/P Field Test Data	69-91
B-1	HFTP "Time Count" Description	94
B-2	LFTP "Time Count" Description	95
B-3	HFTP Casette Tape Format	96
B-4	LFTP Casette Tape Format	97
B-5	Data Format for Archived T/P Records	98
C-1	FVR Bit Formatting	100
C-2	FVR Casette Tape Format - After 1st Frame	101
C-3	FVR Casette Tape Format - First Frame	102
C-4	Load Cell & Accelerometer Calibration Summary	103
C-5	FVR Archived Data Format	104
C-6	FVR Euler Angle Archived Data Format	104

LIST OF FIGURES

Figure	Description	Page
1	Schematic of Current Meter Mooring	4
2	Schematic of NDBO Discus Moorings	5
3	Schematic of Spar/Sphere Mooring	6
4	Schematic of High Performance Intermediate or DOCMS Mooring	7
5	Schematic of Subsurface CEL Mooring	8
6	Deep-Can Pinger Outline Sketch	11
7	Sub-Can and Drop-Sonde Pinger Outline Sketch	12
8	Photo of Force Vector Recorder within its Flotation Shell	27
9	Photo of High Frequency Temperature-Pressure Recorder	30
10	FVR Simultaneous Pressure and Tension Test at CEL - Pressure History	34
11	Photo of FVR Simultaneous Pressure and Load Test at CEL	35
12	Instrument Configuration During System Integration Test	41
13	Normalized 3-D Magnetometer Response to Angular Changes within the Earth's Magnetic Field	43
14	Force Vector Recorder Axis Definitions	45
15	FVR Euler Angle Definitions	46
16	"Azimuth Scan" Magnetometer Field Calibration Setup	57
17	"Elevation Scan" Magnetometer Field Calibration Setup	58

1.0 INTRODUCTION

In the early phase of the Mid Ocean Dynamics Experiment (MODE) in 1970 and '71 it was statistically shown that the dynamics of surface moorings lead to a greater contamination of current meter records than subsurface moorings (Gould and Sambuco, 1975). At the same time numerous controlled laboratory tests of current measurement sensors were illustrating the problems of sensor errors in the presence of dynamics (Kalvaitis, 1974). It became painfully obvious, though, that in order to accurately simulate the dynamics of ocean sensors in the laboratory it was necessary to know the nature of the dynamics on particular mooring types. Lacking hard, measured data on real mooring systems, numerous investigators resorted to pure mathematical simulation of these moorings (Dillon, 1973). These mathematical simulations further illustrated the types of problems that could be encountered, but none of the results were verified. As the first step an effort to inject some real data into this morass of mathematica, ONR contracted the C. S. Draper Laboratory to conduct an instrumented test of a deep ocean current measurement mooring (Chhabra, 1974 and Chhabra et al 1974) of the type normally used by the Woods Hole Oceanographic Institute (Heinmiller and Walden, 1973). This work gave indications of the errors that could be expected from any current sensors from low frequency mooring motions. In addition, the measured current meter records were used as the forcing function in a revised estimate of the mooring line drag coefficient that was needed in order to result in the type of mooring motion that was acoustically measured.

Coincident with and following this program, specialized instrumentation was developed that permitted the at-sea measurement of engineering parameters, some of which are specifically related to surface moorings. This included the development of Temperature-Pressure Recorders (Wunsch and Dahlen,1974) for monitoring mooring depth excursions, a Portable Ocean Platform Motion Instrumentation Package (POPMIP) for monitoring buoy dynamics, and a Force Vector Recorder (FVR) for measuring the dynamics and forces on a mooring line. With these instruments available, a well-co-ordinated, well-planned series of mooring experiments was conducted in Hawaii in October and November of 1976. The participants in these experiments were from numerous laboratories and

agencies within the U. S., all of whom had a common interest of making useful measurements in the deep ocean. The goal of these experiments was the acquisition of all of the requisite data for the verification of both sub-surface and surface mooring math models. This report outlines the instruments and the role of the C. S. Draper Lab in what become known as the Mooring Dynamics Experiment (MDE) (Walden et al, 1977).

2.0 SUMMARY OF FIELD TEST PROGRAM

The section will describe the field test program; giving a description of the moorings installed, their locations and a summary of the results.

2.1 Mooring Descriptions

Six moorings in all were employed in the MDE. One mooring was installed as merely a current measurement mooring which monitored the current forcing on the other five experimental or test moorings. It was the first mooring installed-recording data throughout the period of the field test program. The five test moorings contained an abundance of dynamic sensing systems on each. Due to a limited quantity of such systems, the test moorings had to be installed serially such that the sensor systems were refurbished between mooring installations.

The six moorings employed in the MDE are illustrated in Figures 1 - 5 (Figure 2 deployed twice at different scopes). The information contained in these figures is available through the courtesy of the Woods Hole Oceanographic Institute (WHOI) which did the mooring detailed design, installation and retrieval. The six moorings will be described below. The objectives for installing each type of mooring are well-described in Walden el al (1977). The locations of each sensor system and their ranges were selected by employing either the NBDO Hull/Mooring Dynamic Simulation model (frequency domain model) or the C. S. Draper Lab time domain mooring simulation model (for the spar/sphere mooring only), (Chhabra, 1976). The mathematical models predicted the mooring responses at specific locations resulting from assumed wave or current inputs. The results were employed to place FVRs at the most energetic or interesting regions of moorings and to place T/Ps at key positions whose depth history was important in describing mooring shape and dynamics. Furthermore, the T/Ps acted as a measure of redundancy should the acoustic pingers fail and also to give specific high-accuracy calibration points for the XBTs used throughout the experiments.

2.1.1 Current Meter Mooring

The first mooring installed, and the last retrieved after the field test program was over, was the current meter mooring shown in Figure 1. It was placed in the northern part of the test range as close to the test moorings as

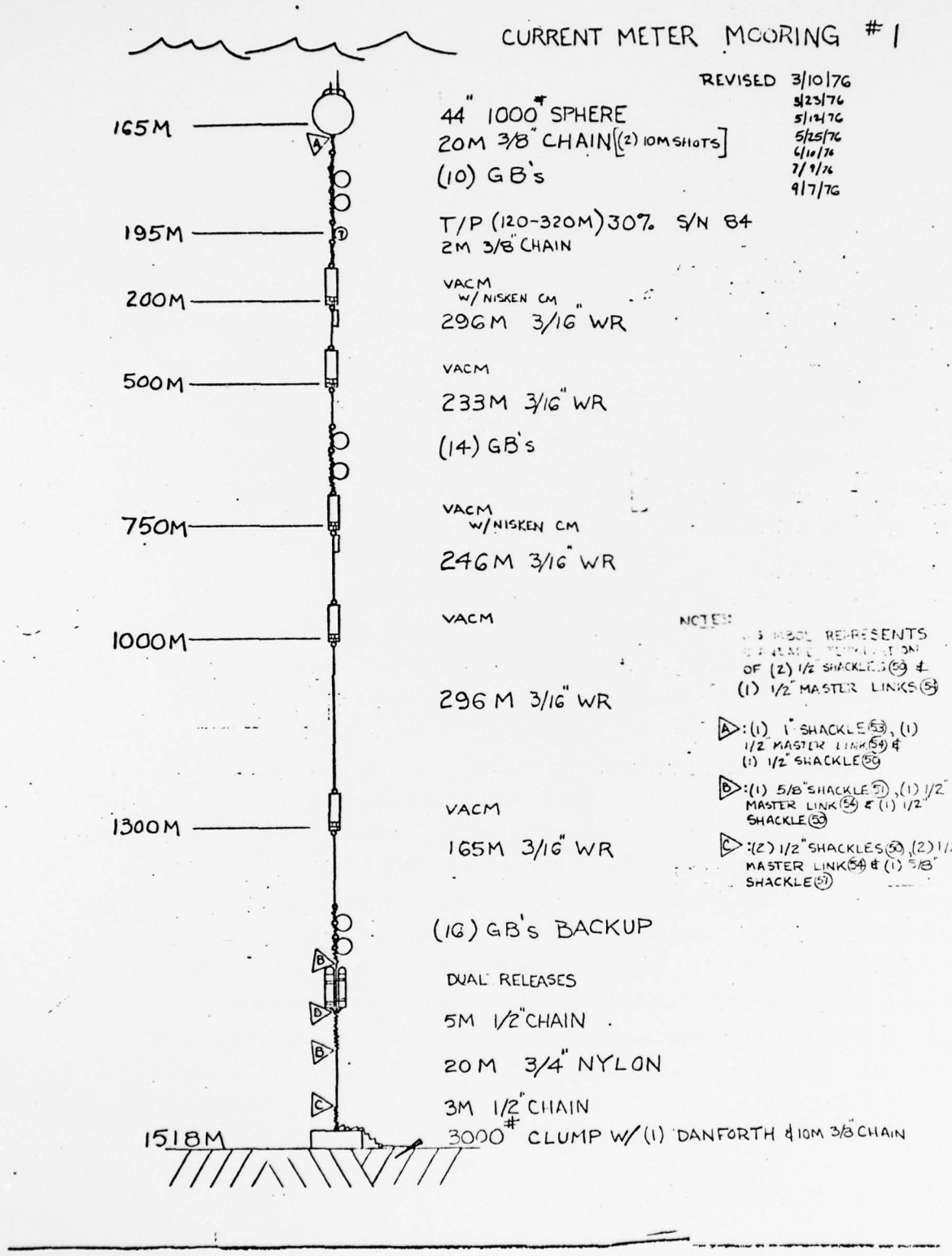

Figure 1 - Current Meter Mooring

(Supplied by WHOI)

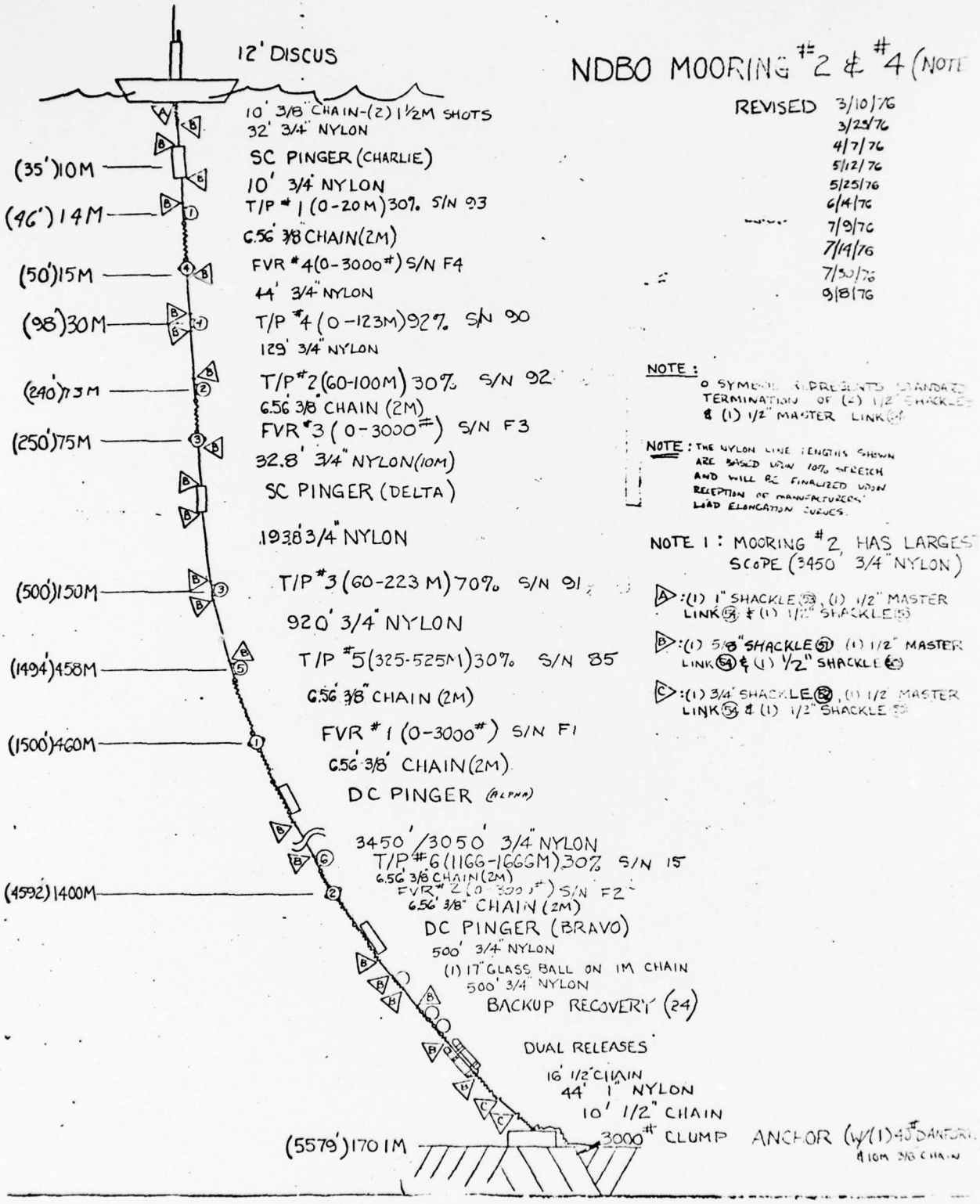

Figure 2 - NDBO Discus Moorings

(Experiment No. 1, slack and
Experiment No. 3, taut)
(Supplied by WHOI)

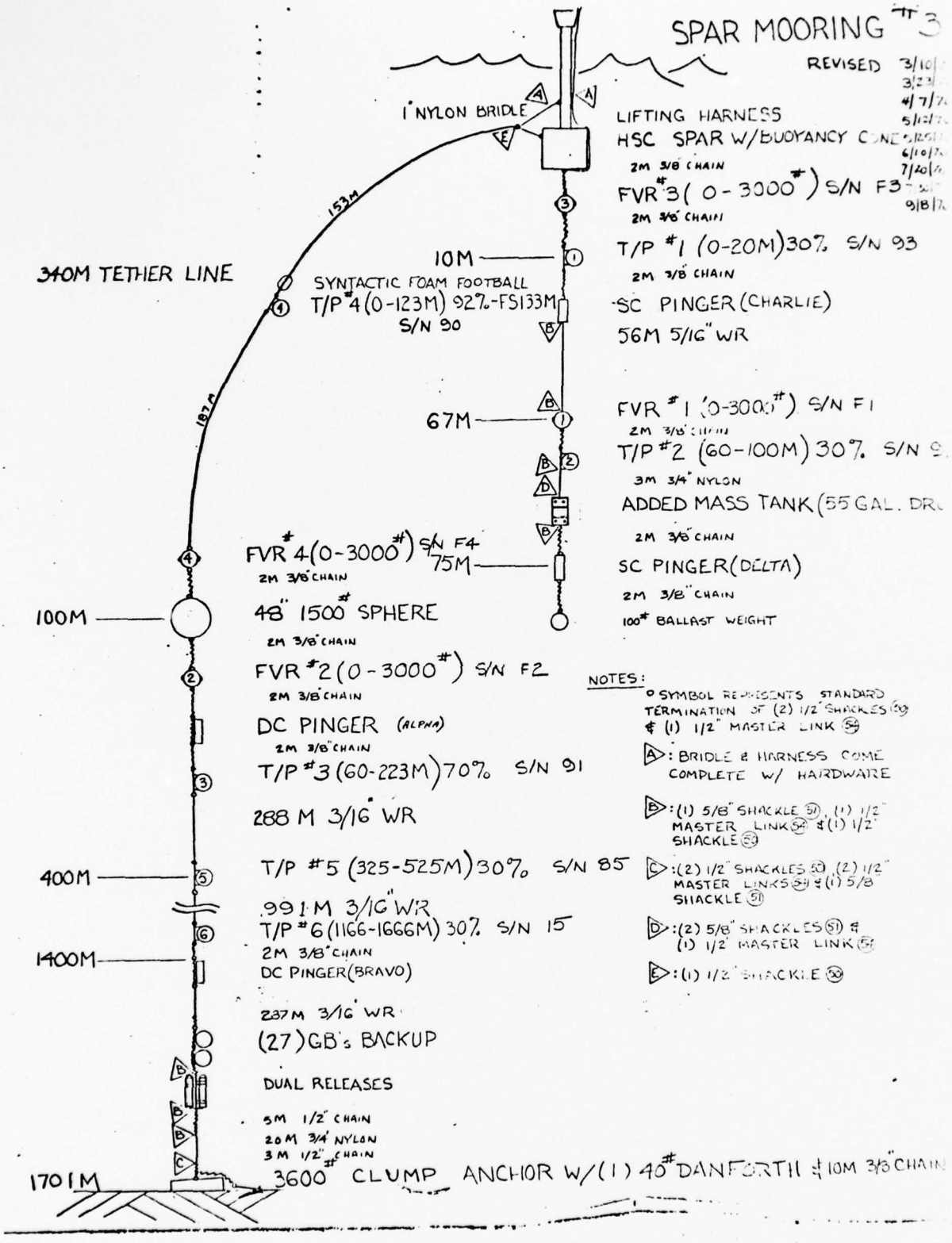

Figure 3 - Spar/Sphere Mooring

(Experiment No. 2)
(Supplied by WHOI)

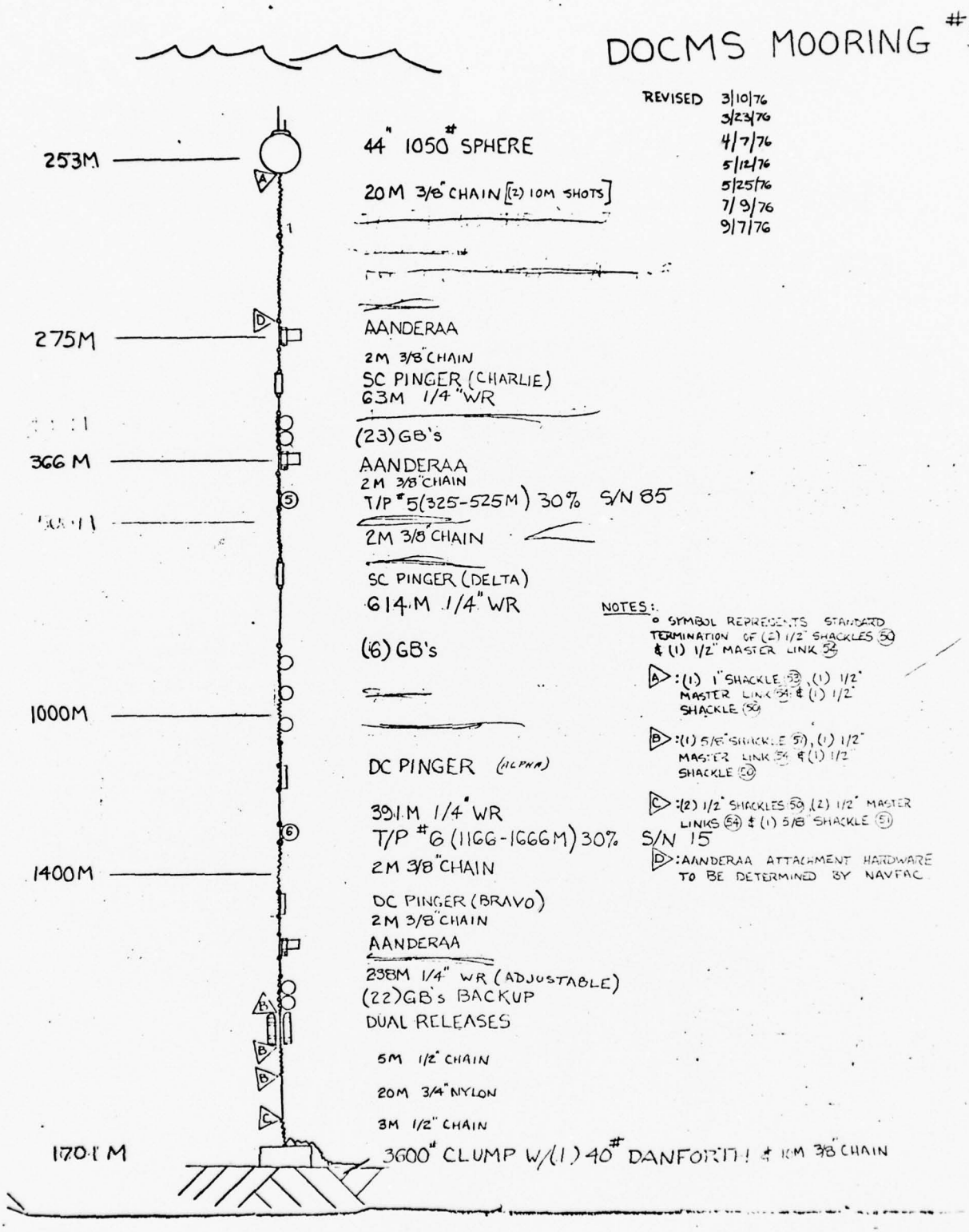

Figure 4 - High Performance Intermediate Mooring
(Experiment No. 4) or DOCMS Mooring
(Supplied by WHOI)

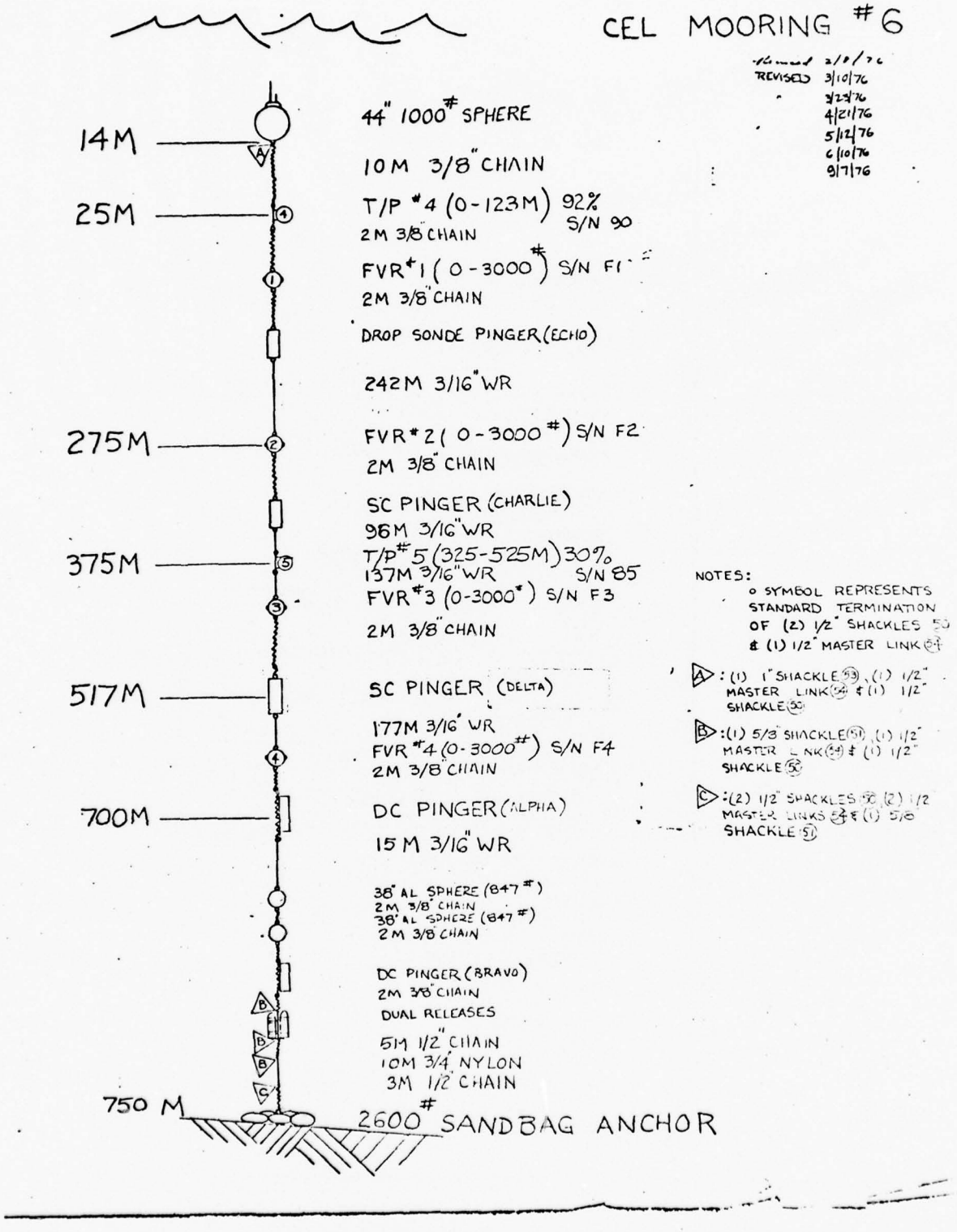

Figure 5 - Subsurface CEL Mooring (Experiment No. 5)
(Supplied by WHOI)

practical. It contained five VACM currentmeters, two Niskin current meters, and a Low Frequency Temperature/Pressure Recorder to measure mooring lean over. Computer simulations of this mooring were run in order to specify the flotation. The design goal was to keep lean over to less than 15^{o} in the maximum operational current profile of 1 knot from the surface to the bottom. The VACMs and their data were prepared by the Pacific Marine Environmental Lab (PMEL), Seattle, Washington.

2.1.2 Discus Surface Moorings (Experiments #1 and #3)

Figure 2 is a schematic representation of the discus mooring that was installed twice. The first time it was installed at a scope of 1.078 to 1 (Experiment #1) and the second time (Experiment #3) at a scope of 1.006 to 1. The first installation (Exp. #1) was at the following co-ordinates with the given total magnetic field strength value:

Latitude: 22^{o} 10' 31.0" N.
Longitude: 159^{o} 56' 55.6" W.
Magnetic Total Intensity: 37,350 γ

while the second installation (Exp. #3) was at the following position:

Latitude: 22^{o} 10' 22.6" N.
Longitude: 159^{o} 56' 39.4" W.
Magnetic Total Intensity: 37,350 γ

The discus mooring is typical of that used by the NOAA Data Buoy Office (NDBO) for environmental monitoring. The buoy itself was a discus shape, 3.65 meters in diameter, containing the POPMIP dynamic sensing package. Details of the dynamic modelling parameters and techniques for the discus itself are available from NDBO and from Kaplan et al (1972). It should be observed in Figure 2 that this mooring contains 2 different lengths of 3/4" diameter nylon between the 460-meter and 1400-meter depth. It was in this section of line that the mooring scope was varied. The details of mooring line materials, diameters, and lengths (in a relaxed condition) are shown in Figure 1. Some of the details of in-air weights, wetted weights, lateral areas and buoyancies

required for modelling the instruments are found in Table 1. Certain lateral areas in Table 1 are left blank because the information is difficult to assess. The sketches of the deep can and sub can pingers are shown in Figures 6 and 7 - allowing a computer modeller to arrive at their own assessment of area and added mass. The 17-inch (43 cm) diameter glass balls, employed for buoyancy at many locations on the mooring, contained protective hard hats and as a result the added mass may be difficult to estimate. The lateral area is, however, given in Table 1 which includes 1 meter of chain. Individual mooring modellers should make their own assessment of these parameters.

2.1.3 Spar/Sphere Mooring (Experiment #2)

Figure 3 is a sketch of the mooring configuration employed in Experiment #2. It was located as follows:

Latitude: 22° 10' 31.0"
Longitude: 159° 56' 41.0"
Magnetic Total Intensity: 37,350 γ

The POPMIP was installed in the lower half of the spar itself in order to monitor its dynamics. Because there were fears that POPMIP might not function up to its full expectations, the FVR (S/N F3) was moved up and attached directly to the bottom of the spar. This change, not reflected in Figure 3, was possible because the all-aluminum spar buoy would theoretically not interfere with the earth's magnetic field which the FVR relied on for azimuth orientation. A rigid yoke was expeditiously built in Kauai which supported and constrained the FVR from rotations while allowing it to sense forces along the longitudinal axis of the buoy. The placement of the FVR at this location gave a measure of tension at the buoy which would have not otherwise been available.

In order to increase the natural heave period of the spar an added mass tank (55 gallon oil drum with many holes drilled) was added to the bottom of the section beneath the spar. In order to ballast the buoy upright and keep that section of mooring line vertical, a 45 kg weight was placed at the bottom of the added mass tank.

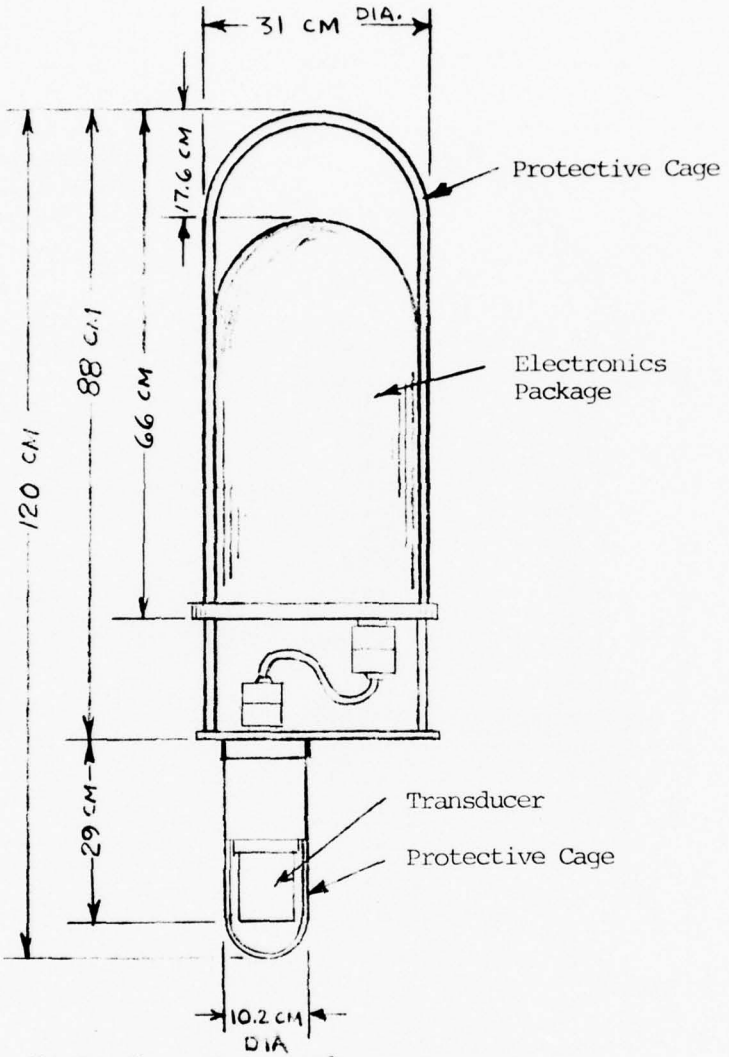

Notes: (1) Drawing not to scale.

(2) Pinger attached to and in parallel with 2 m., 3/8" chain.

(3) Weights, excl. of chain: 64.9 Kg (in air), 34.4 Kg (in water).

Figure 6 - Deep-Can Pinger Outline Sketch
(Information supplied by WHOI)

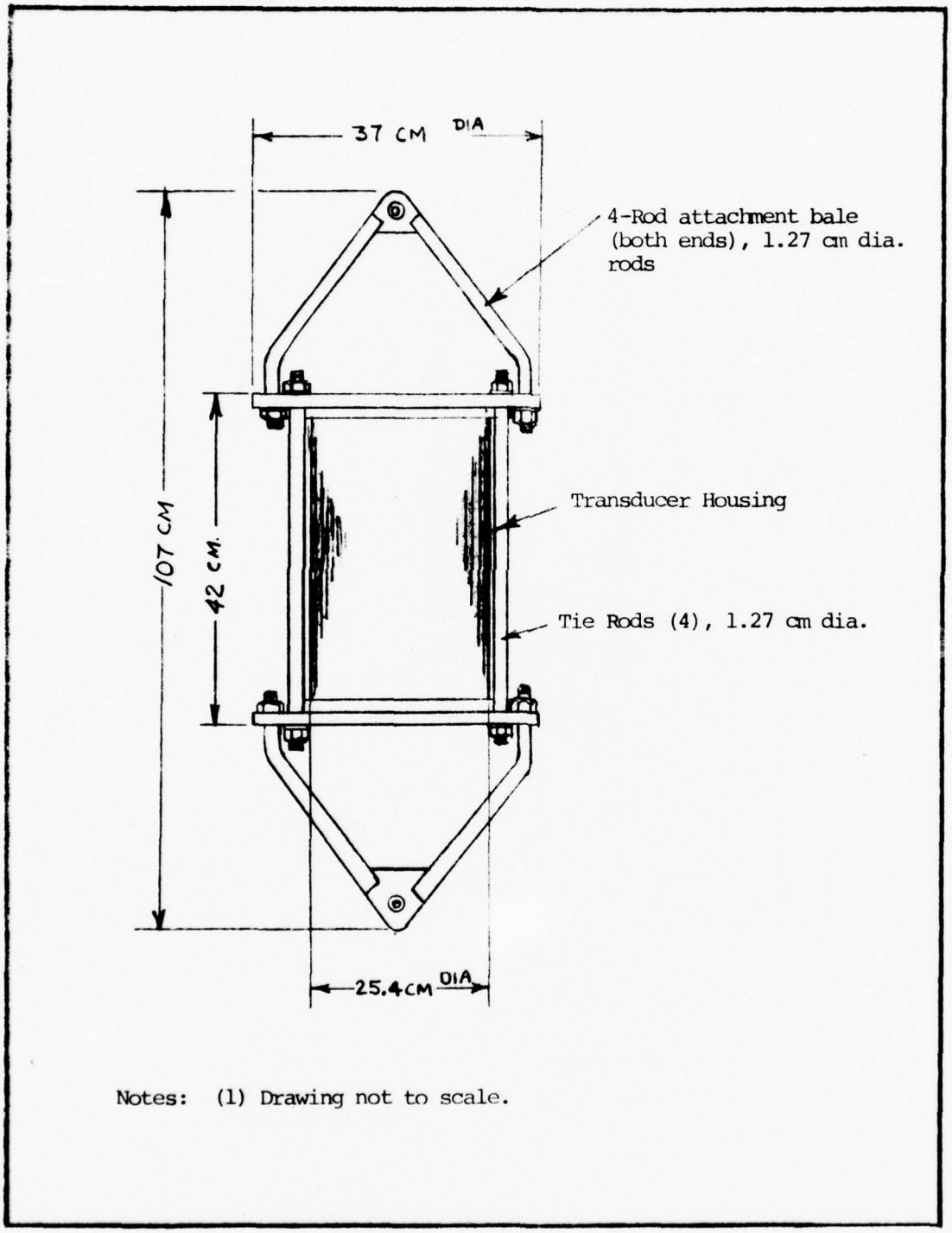

Notes: (1) Drawing not to scale.

Figure 7 - Sub-Can and Drop-Sonde Pinger Outline Sketch
(Information supplied by WHOI)

Mooring Element	Wt. in Air (Kg)	Wt. in Water (KG) (*)	Lateral Area (m^2)
FVR	59.46	-1.8	.183
LFTP	29.51	9.08	.080
HFTP	29.51	9.08	.080
Deep Can (DC) Pinger (**) (with 2 m. 3/8" chain)	69.4	39.04	N. A. (see sketches)
Sub Can (SC) in Cage (**) (no chain)	44.80	20.11	N. A. (see sketches)
17" - dia. (43 cm) (**)	24.51	-23.60	.2696 (**)
Glass Balls in Hard Hats (with 1 m. 3/8" chain)			
Added Mass Tank (55 gal. steel drum)	20.8 (**)	18.1	N. A.
Steel Hardware for Added Mass Tank (braces, rod, etc.)	25.3 (**)	22.1	N. A.
Flotation Cone on Top of Spar Buoy (**)	26.7	Not applic.	N. A.
Buoyant Tether Line (**) (3.86 cm dia.)	.77 Kg/m	-.36 Kg/m @ surface -.33 Kg/m @ 200 psi	Varies with mooring shape
Concrete Anchors (Qty = 2), § Dimensions = 1.45 m x 1.45 m x .43 m (hi)	2262 (**)	∿1337.	Varies with orientation
Concrete Anchors (Qty = 2), + dimensions unsure but approx. 1.45 m x 1.45 m x .53 m (hi)	2762	∿1632.	Varies with orientation
Assumed Mass of Water-filled tank + Hardware (including added mass assumption) (**)		≈ 508 Kg-mass	

(*) Assuming ρ_{water} = 1026 Kgm/m^3

(**) Data provided by R. Walden (WHOI)

§ Used on experiments 1 and 3 only.

\+ Used on experiments 2 and 4 only.

Table 1 - Modelling Parameters for Key Elements on MDE Moorings

In order to monitor the excursions of a stiff, buoyant tether between the spar and the subsurface sphere, a HFTP was placed in the middle of the line. In order to monitor the level of dynamic forcing acting on the subsurface sphere and the effect of the sphere itself, a FVR was placed both above and below the sphere as shown. T/Ps were again placed at other strategic locations on the line in order to monitor dynamics.

An interesting feature of the use of two HFTPs in Experiments 1, 2 and 3 is to compare the time history of the pressure record from each in an effort to use the data for wave height measurement. This feature seems possible because T/P S/N 93 (at ~ 7 m depth) will experience a pressure signal change from both wave height and buoy vertical displacement. T/P S/N 92 (at ~70 m depth) will experience an output change which is dominated by buoy motion only in all but rather heavy seas (not encountered here). These two pieces of data with two unknowns (wave height and buoy displacement) should allow a cut at a solution. The synchronized vertical accelerometer in the buoy-mounted FVR should allow an independent estimate of buoy displacement by a double integration of the z-axis sensor (assuming buoy tilt is rather small).

2.1.4 High Performance Intermediate Mooring (Experiment #4)

Figure 4 contains a sketch of the High Performance Intermediate Mooring which has been called a Deep Ocean Current Measurement System (DOCMS). Two LFTPs were placed on the mooring for three purposes:

(1) Help define the mooring shape in the vertical direction with possibly better accuracy than the range pingers.

(2) Act as an element of redundancy in defining mooring shape if range pingers should fail.

(3) Accurately measure low frequency mooring lean over for correcting current meter records for mooring motion.

(4) Provide high accuracy Temperature-Depth data in order to refine XBT data for acoustic ray traces of pinger position.

The mooring and the results of this experiment will be discussed in a forthcoming Woods Hole blue cover report.

2.1.5 CEL Subsurface Mooring (Experiment #5)

Figure 5 contains a sketch of the Civil Engineering Laboratory (CEL) test mooring. It was located at the following position and with the given earth's magnetic intensity:

Latitude: 22° 04' 01.0" N.
Longitude: 159° 53' 38.0" W.
Magnetic Total Intensity: 36,250 γ

In order to simplify mathematical modelling, this mooring contained only aluminum spheres for buoyancy, both at the top and bottom. Furthermore, it contained only chain and wire rope for mooring line elements.

During data bursts of the HFTP and the four FVRs, mathematically modellable dynamic events were imposed on the mooring. These events contained the anchor launch and release as well as five other events, during intermediate bursts which involved artifically pulling the top of the mooring over and suddenly releasing it. Such events caused a step function in lateral force. The results of this experiment should be well documented by CEL reports.

2.2 Summary of Results

Appendix A contains a summary of average data from both the HFTPs and LFTPs for all of the experiments. These data are averaged either over a burst (for HFTPs) or every hour (LFTPs). This section contains a narrative summary of the qualitative results from each experiment plus a description of the timing of each experiment and the manner in which the time word is written on the archived tapes.

Timing

Low Frequency Temperature/Pressure Recorders (LFTPs) - The LFTPs were all started together at 1130 hours local Boston time or 1530 Zulu on September 27, 1976. They all recorded data continuously every four minutes from that time to the end of the experiment period recording, data whether in

the ocean or not. The archived tapes only contain data from the ocean, however. The time designated as t = 0 on the data tapes is when the instruments were started. The time word, written in the first column of the data tapes is the number of minutes after t = 0. For example, 20:00:00 hours (Zulu) on 12 October 1976 just before the anchor launch for Experiment No. 1 is a time count of 21,870 minutes after t = 0. The anchor was launched at 20:27:27 Zulu on 12 October (see Table 2) or at approximately 21,897 minutes on the LFTP data tape. All times for subsequent experiments should be figured relative to the same t = 0 for the LFTPs.

HFTPs and FVRs - The timing word which is archived for both the High Frequency Temperature/Pressure Recorders (HFTP) and the Force Vector Recorders (FVR) is relative to a t = 0 at the beginning of the first recorded burst in a given experiment. The precise times at which each burst began are given in Tables 2 through 5 for Experiments 1, 2, 3, and 5. It should be observed in these tables that for Experiments 1 and 3 (i.e., Tables 2 and 4) the first burst for both the FVRs and HFTPs occur at the same time. In experiments 2 and 5 (i.e., Tables 3 and 5), however, the first burst from the HFTPs occurs 43 minutes and 41 seconds, or one HFTP burst repetition period, before the first FVR burst. This difference arose due to the differing times that the recorder enabling (or ON/OFF) magnet was removed from the instruments relative to when they would normally have a data recording burst. Because the HFTPs would burst approximately every 43 1/2 minutes versus approximately every 87 minutes for the FVRs, a magnet removal from all instruments just prior to the HFTP-only burst would lead to the timing condition shown in Tables 3 and 5.

Current Meter Mooring

The Low Frequency Temperature/Pressure Recorder that was installed at the top of the mooring (S/N 84) was bumped and became inoperable at launch. It did not record any further data during the experiment. It was found that an inadvertent impact with the stern of the ship during launch had unlatched the tape recorder cassette such that it did not record. The data that would

MDE MOORING SUMMARY

WV 12-21-76

MOORING NUMBER: 2 | EXPERIMENT NO. 1, DISCUS

DATE: 10-12-76 | SYNCHRONIZATION DATE/TIME: 10-12-76 8:48:14 Z

ANCHOR LAUNCH TIME: 20:27:27 Z | ANCHOR RELEASE TIME: 10-13-76 18:43 Z

BURST TIMES

FVR BURST No.	FVR TIME (LOCAL & Z)	HFTP BURST No.	HFTP TIME (ZULU)
1	06:04:55	1	16:04:55
	16:04:55 Z	2	16:48:36
2	07:32:18	3	17:32:18
	17:32:18 Z	4	18:15:59
3	09:00:00	5	19:00:00
	19:00:00	6	19:43:41
4	10:27:23	7	20:27:23
	20:27:23 Z	8	21:11:04
5	11:54:46	9	21:54:46
	21:54:46 Z	10	22:38:27
6	13:22:09	11	23:22:09
	23:22:09 Z	12	00:05:50
7	14:49:32	13	00:49:32
	00:49:32 Z	14	01:33:13
8	16:16:54	15	02:16:54
	02:16:54 Z	16	03:00:35
9	17:44:17	17	03:44:17
	03:44:17 Z	18	04:27:58
10	19:11:40	19	05:11:40
	05:11:40 Z	20	05:55:21
11	20:39:03	21	06:39:03
	06:39:03	22	07:22:44
12	22:06:26	23	08:06:26
	08:06:26	24	08:50:07
		25	09:33:48
		26	10:17:29
		27	11:01:10

INSTRUMENT SUMMARY

SYSTEM S/N	F1	F2	F3	F4
MAGNET OFF TIME (ie. ENABLE)	15:55 Z 10-12-76	15:54 Z 10-12-76	15:53 Z 10-12-76	15:54 Z 10-12-76
TIME IN WATER	18:02 Z 10-12-76	18:45 10-12-76	17:11 10-12-76	16:58 10-12-76
TIME OUT OF WATER	20:25 Z 10-13-76	19:26 10-13-76	20:29 10-13-76	20:41 10-13-76
TIME MAGNET ON	20:11 Z 10-13-76	19:37 Z 10-13-76	20:35 Z 10-13-76	20:51 Z 10-13-76
COMMENTS		X-ACCEL. FAILED AFTER 4th BURST	REPLACED Y-ACCEL. WITH SCHAEVITZ AFTER TEST. DATA OK BUT SIGNAL QUESTIONED	
SYSTEM S/N	90	91	92	93
MAGNET OFF TIME (ie. ENABLE)	15:51 Z 10-12-76	15:54 Z 10-12-76	15:53 Z 10-12-76	15:52 Z 10-12-76
TIME IN WATER	17:03 Z 10-12-76	17:23 Z 10-12-76	17:09 Z 10-12-76	16:57 Z 10-12-76
TIME OUT OF WATER	20:37 Z 10-13-76	20:18 Z 10-13-76	20:29 Z 10-13-76	20:42 Z 10-13-76
TIME MAGNET ON	20:49 Z 10-13-76	20:22 Z 10-13-76	20:34 Z 10-13-76	20:48 Z 10-13-76
COMMENTS		SLIGHTLY INTER-MITENT TEMP. RECORD, THERMISTOR SOLDERED		RESCALE p-SENSOR AFTER EXP'T TO RG.~ 9 to 29 m.

NOTE: FVR: BURST DURATION = 15M 41.2S, BURST REP. PERIOD = 87M 22.8S

HFTP: BURST DURATION = 28M 50.5S, BURST REP. PERIOD = 43M 41.4S

TABLE 2 – EXPERIMENT #1 SUMMARY

MDE MOORING SUMMARY

MOORING NUMBER: 3	EXPERIMENT NO. 2, SPAR
DATE: 10-18,19-76	SYNCHRONIZATION DATE/TIME: 10-18-76 07:48:20 Z
ANCHOR LAUNCH TIME: 20:27:45 Z	ANCHOR RELEASE TIME: 10-19-76 10:00:00 Z

BURST TIMES

FVR		HFTP	
BURST NO.	TIME (LOCAL & Z)	BURST NO.	TIME (ZULU)
1	05:05:14	1	14:21:33
	15:05:14 Z	2	15:05:14
2	06:32:37	3	15:48:56
	16:32:37 Z	4	16:32:37
3	08:00:00	5	17:16:19
	18:00:00 Z	6	18:00:00
4	09:27:23	7	18:43:41
	19:27:23 Z	8	19:27:23
5	10:54:46	9	20:11:04
	20:54:46 Z	10	20:54:46
6	12:22:09	11	21:38:27
	22:22:09 Z	12	22:22:09
7	13:49:32	13	23:05:50
	23:49:32 Z	14	23:49:32
8	15:16:55	15	00:33:13
	01:16:55 Z	16	01:16:55
9	16:44:17	17	02:00:36
	02:44:17 Z	18	02:44:17
10	18:11:40	19	03:27:59
	04:11:40 Z	20	04:11:40
11	19:39:03	21	04:55:22
	05:39:03 Z	22	05:39:03
12	21:06:26	23	06:22:45
	07:06:26 Z	24	07:06:26
		25	07:50:07
		26	08:33:49
		27	09:17:30

INSTRUMENT SUMMARY

SYSTEM S/N	F1	F2	F3	F4
MAGNET OFF TIME (ie. ENABLE)	14:10 Z 10-18-76	14:11 Z 10-18-76	14:09 Z 10-18-76	14.11 Z 10-18-76
TIME IN WATER	14:41 Z 10-18-76	17:47 Z 10-18-76	15:59 Z 10-18-76	17:23 Z 10-18-76
TIME OUT OF WATER	13:59 Z 10-19-76	14:48 Z 10-19-76	13:18 Z 10-19-76	14:38 Z 10-19-76
TIME MAGNET ON	14:02 Z 10-19-76	14:53 Z 10-19-76	13:35 Z 10-19-76	14:44 Z 10-19-76
COMMENTS				

SYSTEM S/N	90	91	92	93
MAGNET OFF TIME (ie. ENABLE)	14:15 Z 10-18-76	14:15 Z 10-18-76	14.14 Z 10-18-76	14:15 Z 10-18-76
TIME IN WATER	16:48 Z 10-18-76	17:58 Z 10-18-76	14:40 Z 10-18-76	15:24 Z 10-18-76
TIME OUT OF WATER	14:27 Z 10-19-76	14.58 Z 10-19-76	14:03 Z 10-19-76	13:44 Z 10-19-76
TIME MAGNET ON	14:32 Z 10-19-76	15:08 Z 10-19-76	14:05 Z 10-19-76	13:46 Z 10-19-76
COMMENTS		DATA BREAK-UP AFTER BURST 21. RCDR REPLACED		

NOTE: FVR: BD = 15M 41.2 S , BRP = 87M 22.88 S
HFTP: BD = 28M 50.56 S , BRP = 43M 41.44 S

TABLE 3 - SPAR/SPHERE MOORING SUMMARY (EXP. #2)

MDE MOORING SUMMARY

MOORING NUMBER: 4 | EXPERIMENT NO. 3, DISCUS

DATE: 10-22-76 | SYNCHRONIZATION DATE/TIME: 10-22-76 02:33:00 Z

ANCHOR LAUNCH TIME: 15:44:28 Z | ANCHOR RELEASE TIME: 10-23-76 05:05 Z

BURST TIMES

FVR		HFTP	
BURST No.	TIME (LOCAL & Z)	BURST No.	TIME (ZULU)
1	02:44:40	1	12:44:40
	12:44:40 Z	2	13:28:21
2	04:12:03	3	14:12:03
	14:12:03 Z	4	14:55:44
3	05:39:26	5	15:39:26
	15:39:26 Z	6	16:23:07
4	07:06:49	7	17:06:49
	17:06:49 Z	8	17:50:30
5	08:34:12	9	18:34:12
	18:34:12 Z	10	19:17:53
6	10:01:35	11	20:01:35
	20:01:35 Z	12	20:45:16
7	11:28:57	13	21:28:57
	21:28:57 Z	14	22:12:38
8	12:56:20	15	22:56:20
	22:56:20 Z	16	23:40:01
9	14:23:43	17	00:23:43
	00:23:43 Z	18	01:07:24
10	15:51:05	19	01:51:05
	01:51:05 Z	20	02:34:46
11	17:18:28	21	03:18:28
	03:18:28 Z	22	04:02:09
12	18:45:51	23	04:45:51
	04:45:51 Z	24	05:29:32
		25	06:13:14
		26	06:56:55
		27	07:40:37

INSTRUMENT SUMMARY

SYSTEM S/N	F1	F2	F3	F4
MAGNET OFF TIME (ie. ENABLE)	12:41 Z 10-22-76	12:43 Z 10-22-76	12:42 Z 10-22-76	12:42 Z 10-22-76
TIME IN WATER	15:44 Z 10-22-76	17:47 Z 10-22-76	15:59 Z 10-22-76	17:23 Z 10-22-76
TIME OUT OF WATER	07:03 Z 10-23-76	14:48 Z 10-23-76	13:18 Z 10-23-76	14:38 Z 10-23-76
TIME MAGNET ON	07:07 Z 10-23-76	06:42 Z 10-23-76	07:27 Z 10-23-76	07:36 Z 10-23-76
COMMENTS				

SYSTEM S/N	90	91	92	93
MAGNET OFF TIME (ie. ENABLE)	12:41 Z 10-22-76	12:42 Z 10-22-76	12:41 Z 10-22-76	12:38 Z 10-22-76
TIME IN WATER	13:04 Z 10-22-76	13:24 Z 10-22-76	13:10 Z 10-22-76	12:54 Z 10-22-76
TIME OUT OF WATER	07:31 Z 10-23-76	07:15 Z 10-23-76	07:25 Z 10-23-76	07:37 Z 10-23-76
TIME MAGNET ON	07:31 Z 10-23-76	07:17 Z 10-23-76	07:27 Z 10-23-76	07:38 Z 10-23-76
COMMENTS				

NOTE: FVR BD = 15M 41.2S, BRP = 87M 22.88S

HFTP BD = 28M 50.56S, BRP = 43M 41.44S

TABLE 4 - EXPERIMENT #3 SUMMARY

MDE MOORING SUMMARY

MOORING NUMBER: 6	EXPERIMENT NO. 5, CEL
DATE: 11-1-76	SYNCHRONIZATION DATE/TIME: 11-1-76 07:03:15 Z
ANCHOR LAUNCH TIME: 11-1-76 17:17 Z	ANCHOR RELEASE TIME: 11-2-76 03:27:35 Z

BURST TIMES

FVR		HFTP	
BURST NO.	TIME (LOCAL & Z)	BURST NO.	TIME (ZULU)
1	05:47:37	1	15:03:56
	15:47:37 Z	2	15:47:37
2	07:15:00	3	16:31:18
	17:15:00 Z	4	17:15:00
3	08:42:23	5	17:58:41
	18:42:23 Z	6	18:42:23
4	10:09:46	7	19:26:04
	20:09:46 Z	8	20:09:46
5	11:37:09	9	20:53:27
	21:37:09 Z	10	21:37:09
6	13:04:31	11	22:21:50
	23:04:31 Z	12	23:04:31
7	14:31:54	13	23:48:12
	00:31.54 Z	14	00:31:54
8	15:59:18	15	01:15:35
	01:59:18 Z	16	01:59:18
9	17:26:40	17	02:42:59
	03:26:40 Z	18	03:26:40
10		19	04:20:21
		20	
11		21	
		22	
12		23	
		24	

INSTRUMENT SUMMARY

SYSTEM S/N	F1	F2	F3	F4
MAGNET OFF TIME (ie. ENABLE)	14:51 Z 11-1-76	14:50 Z 11-1-76	14:49 Z 11-1-76	14:48 Z 11-1-76
TIME IN WATER	15:12 Z 11-1-76	15:40 Z 11-1-76	15:58 Z 11-1-76	16:12 Z 11-1-76
TIME OUT OF WATER	04:28 Z 11-2-76	04:49 Z 11-2-76	05:07 Z 11-2-76	05:18 Z 11-2-76
TIME MAGNET ON	04:33 Z 11-2-76	04:55 Z 11-2-76	05:12 Z 11-2-76	05:31 Z 11-2-76
COMMENTS				
SYSTEM S/N	90	91	92	93
MAGNET OFF TIME (ie. ENABLE)	14:52 Z 11-1-76			
TIME IN WATER	15:19 Z 11-1-76			
TIME OUT OF WATER	04:20 Z 11-2-76			
TIME MAGNET ON	04:27 Z 11-2-76			
COMMENTS				

NOTE: FVR BD = 15M 41.2S, BRP = 87M 22.88S
HFTP BD = 28M 50.56S, BRP = 43M 41.44S

TABLE 5 - EXPERIMENT #5 SUMMARY

have been recorded was to be used in estimating the lean over of the current meter mooring in the presence of currents. Mathematical, computer estimates can still be made based on both the value of current measured by the VACMs and the Dropsonde data.

Experiment Number 1 - Slack Discus Surface Mooring

Table 2 is a tabular listing of the timing associated with Experiment #1. It can be seen that the anchor-launch dynamic transient was measured by all of the FVRs, HFTPs, LFTPs, and Pingers. The anchor was dropped approximately 4 seconds after the beginning of the fourth burst. The anchor took approximately 19 minutes to hit bottom in 1700 meters of water. As a result, the FVRs were unable to record the full launch transient because a burst was less than 16 minutes in duration. The HFTPs and LFTPs did, however, record the full transient.

The data from the near-bottom FVR load cells in general show an initial 15 to 30 second increase in tension followed by a decrease in tension following anchor deployment. Then there is a gradual buildup in tension as the anchor settles to the bottom. In subsequent bursts the tension value had diminished to a much lower level. The maximum tension measured during the launch transient was recorded on the deepest FVR, installed at a 1400-meter depth. Just prior to the anchor bottoming the tension had built up to approximately 750 pounds. At the beginning of the next burst, approximately 72 minuted later, the tension had dropped to approximately 250 pounds as the mooring assumed its steady orientation in the water column.

The FVRs, HFTPs, and LFTPs recorded approximately 98% of the possible data during the deployment. The sensor signals appear to be clean and distinctive, indicating that much useful information for both spectral and time response correlation can be derived. Problems that were encountered during this deployment are briefly described on the right side of Table 2. FVR S/N F2 had a failure of the x-axis accelerometer after the anchor launch transient burst. S/N F2 was the deepest and, as a result, the coldest of all FVRs. It may have been a thermally-induced problem. The unit was replaced by a spare sensor and the problem solved. HFTP S/N91 encountered a problem with an intermittent thermistor connection. Most of the temperature data are, however,

good. The connection was resoldered and the problem also solved. HFTP S/N 93 was scaled to operate in the depth range of 0 to 19 meters. For some undetermined reason the unit ended up at a depth of approximately 19 meters such that the dynamic pressure record clipped with each wave cycle to depths greater than 19 meters. This problem is reflected in the summary found in Table A-4 (Appendix A). The unit was rescaled to a range of 7.4 to 28.4 meters and no further problem encountered in later deployments. Table 2 also indicates that FVR S/N F3 had a y-axis accelerometer replaced after the experiment. The data recorded during the experiment appear to be excellent, but sensor oscillations were found later during a lab checkout. Again a sensor replacement solved the problem.

The seas encountered during the 17-hour duration of Experiment #1 were the most severe of all the five experiments. Swells as high as approximately two meters were measured by a wave rider buoy. Thus the dynamics encountered should enable a good test of the mathematical models.

Experiment Number 2 - Spar/Sphere Mooring

A 99 + % data return was achieved from the FVRs, HFTPs and LFTP during the second mooring deployment. A slight problem developed with HFTP S/N 91 near the end of the experiment such that its data became unreadable. Otherwise all instruments functioned flawlessly giving data of high quality. The timing of all bursts and key events are given in Table 3.

Although the anchor-launch and release transients were mot measured because they occurred between bursts and after the experiment respectively, voluminous quantities of data are available from the spar mooring which will immensely help mooring designers assess the following types of effects:

(1) The attenuation of wave motion by the spar portion of the mooring.

(2) The response of the spar/added mass tank and vertical section to wave input.

(3) The role of the buoyant tether line as a motion isolator for the subsurface flotation sphere.

(4) The degree to which the subsurface flotation sphere attenuates buoyant tether line motion.

The seas encountered during this deployment were nearly calm with long-period (approx. 12-second) swells of up to 2 meters. The lack of large wave inputs during the deployment is somewhat unfortunate, but the mooring still experienced considerable action from the swells which will allow the models to be exercised.

Experiment Number 3 - Taut Discus Surface Mooring

The anchor for this mooring was deployed approximately five minutes into the third FVR burst - permitting over ten minutes of useful FVR dynamic measurement during the launch. The FVRs, HFTPs and LFTPs functioned 100% during this deployment. The data derived are much like that measured in Experiment number 1, although the dynamics are less owing to a greatly-reduced sea state. The timing details are given in Table 4.

Experiment Number 4 - High Performance Intermediate Mooring

The LFTPs deployed during the DOCMS mooring functioned 100% and are expected to yield useful data on the mooring shape and vertical excursions in the water column caused by "lean over."

Experiment Number 5 - Civil Engineering Lab (CEL) Mooring

The four FVRs, single HFTP and single LFTP deployed on this mooring functioned 100%. Seven individual dynamic events were recorded during seven different bursts. Included in this list is the anchor-launch and anchor release transients as well as five other events caused by the near-surface element of the mooring line being drawn to the side and suddenly released. (See Table A-21, Appendix A.) The data are of high quality - clearly illustrating the significant events. A summary of the timing of bursts and significant events associated with Experiment number 5 are given in Table 5.

3.0 INSTRUMENT DESCRIPTIONS

This section describes the three types of instruments provided by the C. S. Draper Laboratory for the MDE. Other key instruments that were employed in the MDE, but will not be described here, are the 4 acoustic pingers employed for measuring the mooring line position, shape, and dynamics and the POPMIP dynamic sensing package mounted in the buoy. The pinger positions were sampled every .5 seconds by the range operations room at the Pacific Missile Range Facility (PMRF) for 17 hours. The 17-hour experiment duration was specified by the nominal pinger battery life at the defined ping rate.

The POPMIP package as well as the 4 Draper Lab Force Vector Recorders (FVRs) and 4 High Frequency Temperature/Pressure Recorders (HFTPs) are burst instruments. That is, the instruments periodically turn on the recording portions and record data at a high rate - shutting down in between bursts. Table 6 is a summary of the system timing employed in the MDE. The other instruments supplied by the C. S. Draper Lab were 3 Low Frequency Temperature/Pressure Recorders (LFTPs). They recorded a sample every 4 minutes which was an accumulated average of 64 points taken every 3.75 seconds. The primary function of the LFTPs was to augment the pinger data for mooring line shape definition, but also to act as a redundancy should a pinger fail.

3.1 Force Vector Recorder (FVR)

The primary tool for the acquisition of high frequency (0 - 1 Hz) dynamic data on the mooring line was the Force Vector Recorder (FVR). A FVR is a self-contained, battery-operated motion sensing package which records digital data on an internal tape cassette. The electronic data acquisition system is an outgrowth of a system designed for Temperature/Pressure Recorders used in the Mid Ocean Dynamics Experiment (MODE) funded by NSF. The FVR contains six sensor channels, including three mutually orthogonal servo accelerometers, two magnetometers aligned perpendicular to its longitudinal axis for azimuth reference, and either a strain gage pressure sensor for depth or a similar load cell for mooring line tension. In the MDE, a tension load cell with a full scale range of 3000 pounds was employed. Time is recorded

	Portable Ocean Platform Motion Instrumentation Package (POPMIP)	Force Vector Recorder (FVR)	High Frequency Temperature/Pressure Recorder (HFTP)
Sampling Rate (frames/sec)*	4	1.92	.48 (temperature) 1.92 (pressure)
Burst Duration (BD)	approxi. 16 min.	15.6867 min.	28.8427 min.
Burst Repetition Period (BRP)	87.38 min.	87.3813 min.	43.6907 min.
Total Record Time if Operated Continuously	4..... hours	3.18 hours	12.89 hours
Number of Burst Recordable During Mooring Dynamics Experiment	approxi. 15	12.18	26.82

* A data frame consists of a complete scan of all sensor channels.

TABLE 6 System Timing of Burst Instruments Employed in Mooring Dynamics Experiment

by updating a 6-bit frame count associated with each data word recorded. (See Appendix C.) Every .52 seconds (i.e., frame count period) the frame count changed on each of the 6 channels. It samples each of the six channels at up to once every 0.52 seconds, giving a frequency response of 0 to 1 Hz on all axes. This rate can, however, be reduced. It can be programmed to record data in a "burst" mode with variable record burst lengths and burst repetition frequencies - filling a data tape in approximately three hours if operated continuously at the highest rate. If operated at short burst lengths and low burst repetition frequencies, a FVR can periodically record useful dynamic information for months. Because the data from the experiments described should be useful in verifying time as well as frequency domain mooring math models, the data recorded by each instrument (including that from POPMIP and the High Frequency Temperature/Pressure Recorders, HFTPs) should be synchronized in time. In order to accomplish synchronization, two leads are brought out of the pressure case of both the FVRs and HFTPs allowing burst and sample synchronization of four FVRs, four HPTPs and the POPMIP package in the buoy.

Physically, a FVR is a sphere, approximately nineteen inches in diameter. This includes a syntactic foam flotation shell which renders the complete unit neutrally buoyant in water while weighing 130 pounds in air. Without the flotation shell the FVR is approximately 13-inches in diameter, weighing 85 pounds in air and approximately 45 pounds in water. The mooring line is attached in line with the centerline of the sphere. Figure 8 is a photograph of the FVR with half of its flotation shell removed for viewing. A summary of the FVR characteristics is found in Table 7.

It should be noted that Table 7 contains no mention of accuracy. The accuracy of each FVR sensor channel is made up of 2 sources - some systematic and estimatable, and others random. For example, the variation of sensor outputs with temperature or drift are generally systematic and have been found to be of such low order that they can be neglected. Other estimatable errors are those due to sensor misalignments as well as calibration errors. Section 6 will discuss some aspects of these errors in relation to the magnetometers. In general the accelerometer and load cell calibrations narrow the total non-random errors to approximately .2 percent of the full scale output. In some cases

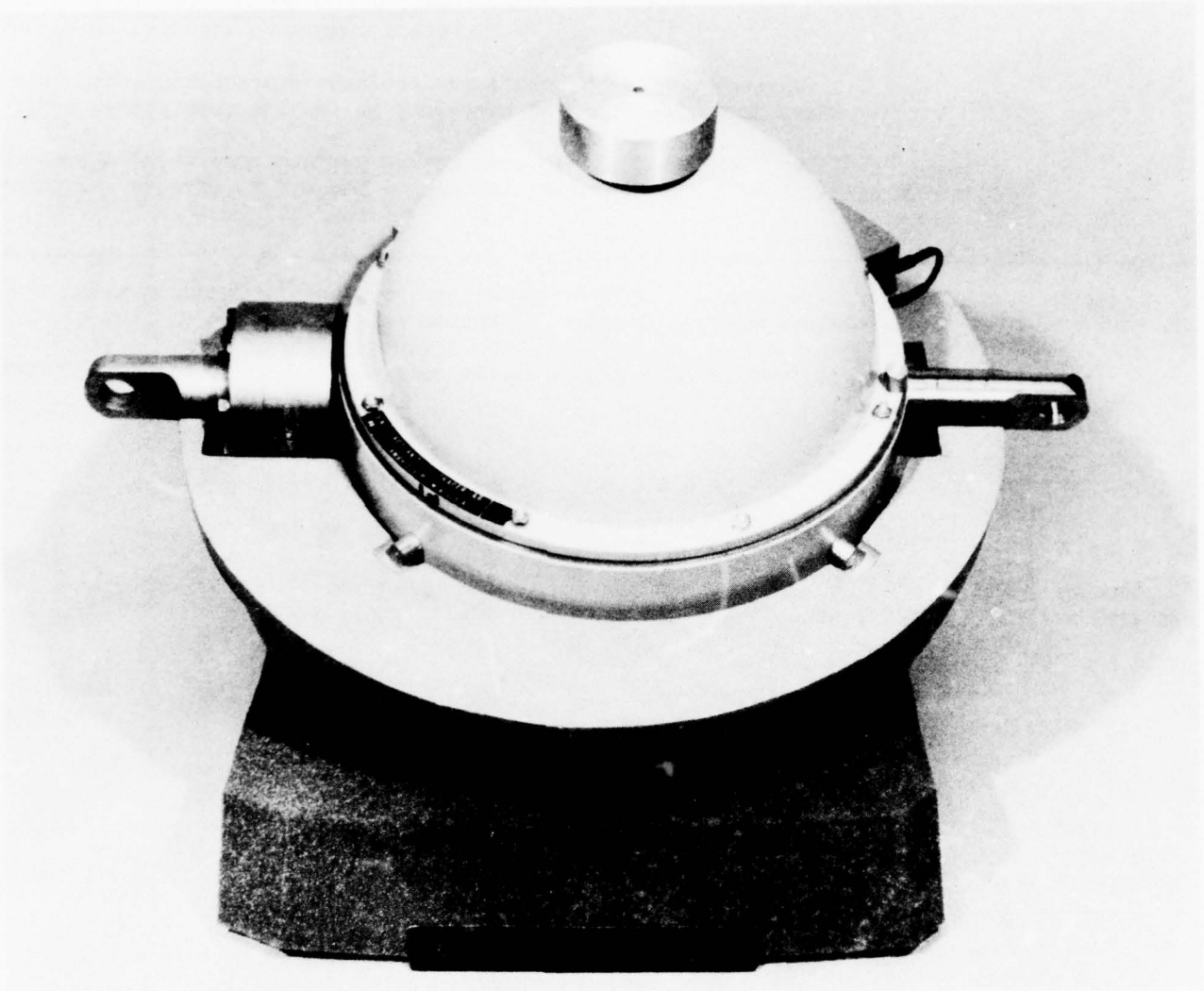

Figure 8. Force vector recorder within its flotation shell.

Measurement	Sensor	Maximum Ranges	Sensor* Frequency Response	Maximum + Resolution (10 bit word)
Acceleration - 3 mutually orthogonal axes	Force Balance Accelerometer	±2g	48 Hz	.001 x Full Scale (eg. .004g for ± 2g unit)
Azimuth Reference - 2 axes orthogonal to mooring line	Magnetometer	0-360°	N.A.	~.1° (Max.)
Tension	Strain Gage Bridge Load Cell	0-3,000 pounds	~0-10 KHz	.001 x Full Scale = 3 pounds
Or				
Pressure	Strain Gage Bridge	0-10,000 psi	0-10 Khz	.001 x Full Scale

General Capabilities: Pressure: 10,000 psi maximum external pressure on case, 5,000 psi on load cell, 3,400 psi on flotation shell.
Life: To approximately 6 months on internal battery package.
Data Recording: Burst or continuous mode at 2,6-word scans/Sec. (10 bit words).

---

* Overall FVR frequency response is limited to Nyquist frequency of $f_{Ny} = \frac{1}{2\Delta t} = .96$ Hz where Δt is interval between data samples of .52 seconds.

\+ Resolution of lease significant bit may be increased by reducing sensor range. Select Full Scale output for optimum accuracy and range in any applicating.

TABLE 7 - Force Vector Recorder Characteristics

no attempt will be made to correct for this error source because it may so vastly complicate the math (see Section 6) that data handling is much encumbered and very little is gained in model verification work. Notes of error values will, however, be made. The random errors are of the order of ± one-half of one least significant bit (LSB) (i.e., approximately 0.1 percent of full scale) arising primarily from the analog-to-digital converter selection of the LSB and any electronic noise.

In order to avoid the possibility of high frequency energy altering the recorded energy spectrum of the FVR, first order analog filters were installed on each sensor channel. The filters were scaled to have a break frequency of 0.5 Hz.

3.2 High Frequency Temperature/Pressure Recorder (HFTP)

Two types of temperature/pressure recorders (TPs) were employed during the mooring dynamics experiment - four high frequency TPs (HFTP) and three low frequency TPs (LFTP). All such instruments employed calibrated thermistors for temperature measurement and strain gages bonded to a diaphragm for pressure measurement. The instruments were both 11 1/2-inch diameter spheres containing a mooring line tension carrying rod mounted tangentially as shown in Figure 9.

The HFTPs are burst recording instruments just like the FVR - containing the same recorder and data acquisition system but different sensors. A HFTP records a temperature word every 2.08 seconds and a pressure word on the average every 0.52 seconds, allowing the computation of temperature variations to 1/4 Hertz and pressure to 1 Hertz. A 10-bit time word is written every 2.08 seconds. Both the sample timing and burst characteristics can be altered by an internal wiring change. As with the FVR, a HFTP records a 10-bit data word from each sensor, giving a least significant bit strength of approximately .001 times the sensor range. In many cases the temperature and pressure sensor ranges were scaled to be considerably less than their full scale capability. A summary of the ranges and scaling employing in both the high and low frequency TPs is summarized in Table 8.

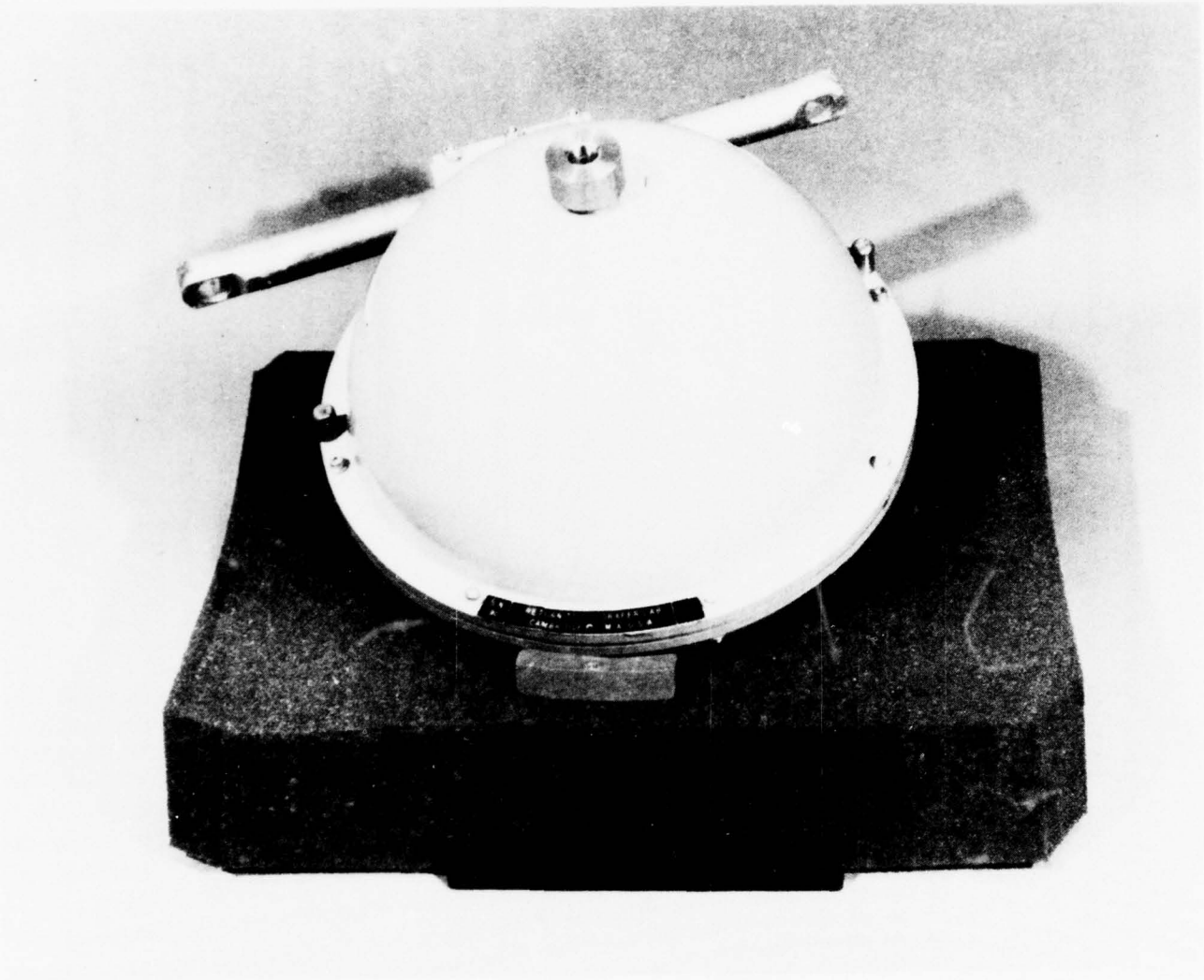

Figure 9. High frequency temperature - pressure recorder (HFTP) (same externally as LFTP).

	High Frequency Temperature - Pressure Recorder (HFTP)				Low Frequency Temperature - Pressure Recorder (LFTP)		
Instrument Serial Number (S/N)	90	91	92	93	15	84	85
Temperature Range (^{o}C)	2.86 - 30.31	2.86 - 30.31	2.86 - 30.31	10.68 - 29.67	0-20	10-26	0-20
Temperature Least Significant Bit, LSB_T (^{o}C)	.027	.027	.027	.019	.02	.016	.02
Pressure Sensor Full Scale Capability (meters of Water)	127	229	127	58.3	1703	683	683
Pressure Sensor Range (Meters)	0-127	60-229	60-100	0-20	1167-1667	120-320	325-525
Pressure Sensor Least Bit Significant Bit, LSB_p (cm)	12.7	16.9	4	2	50	20	20

TABLE 8 Nominal Ranges and Scaling of Temperature-Pressure Recorders Employed in Mooring Dynamics Experiment

3.3 Low Frequency Temperature/Pressure Recorders (LFTP)

The LFTPs are continuous internally-recording instruments so long as the external on/off magnet is removed. As already mentioned, during the Mooring Dynamics Experiment they sampled temperature, pressure, and time every 3.75 seconds but only wrote an accumulated word for each parameter every 64 samples (i.e., 4 minutes). The LFTPs can operate continuously in the ocean for longer than 1 year at the proper sampling rate.

4.0 PRE AND POST EXPERIMENT INSTRUMENT TESTS AND CALIBRATIONS

Prior to and following the field test the FVRs, HFTPs and LFTPs were put through a series of tests in order to ensure their proper function, timing, and calibration. This section describes the general nature of these tests. The final calibration values derived from these tests are summarized in the Appendices.

4.1 FVR Pressure and Load Test

Because of the nature of the FVR design requirements it was helpful to support the unit by tether line tension passing through the geometric center of the sphere. In such a way the hydrodynamic forces on the FVR would not cause moments and induce unwanted rotations. As a result, the main FVR housing had to support both tension (to above the rated breaking strength of the mooring line or 9,000 pounds) plus sealing against water leaks. In the MDE the maximum external working pressure could be as high as 2,300 psi if the instrument were on the bottom of a mooring line in approximately 1,600 meters of water or fell to the bottom in the event of a flotation failure.

In order to verify that the FVR could simultaneoulsy withstand maximum tension expected in the experiment (i.e., 3,000 pounds) and the maximum depth without mechanical failure or leaking, the system was tested in a pressure tank. The most expedient means of simultaneously achieving a tension of approximately 3,000 pounds (in water) was to suspend a sufficient quantity of weight beneath the instrument while in the pressure tank. The most readily available site for such a test was the Civil Engineering Lab (CEL) of the Naval Construction Battalion at Port Heuneme, California. With the kind cooperation of Mr. Dallas Meggitt and others at CEL, two FVRs were pressure tested to the time line shown in Figure 10 in May of 1976. The in-air weights and in-water weights are also shown in Figure 10. Figure 11 is a photo of the two FVRs supporting the pallet of weights beneath.

During the test no electronics were installed within the FVR housings for fear that a leak would ruin costly equipment. Both units were helium mass spectrometer leak tested before and after the test. Dryed silica gel bags were weighed before and after installation as evidence of gross water leakage.

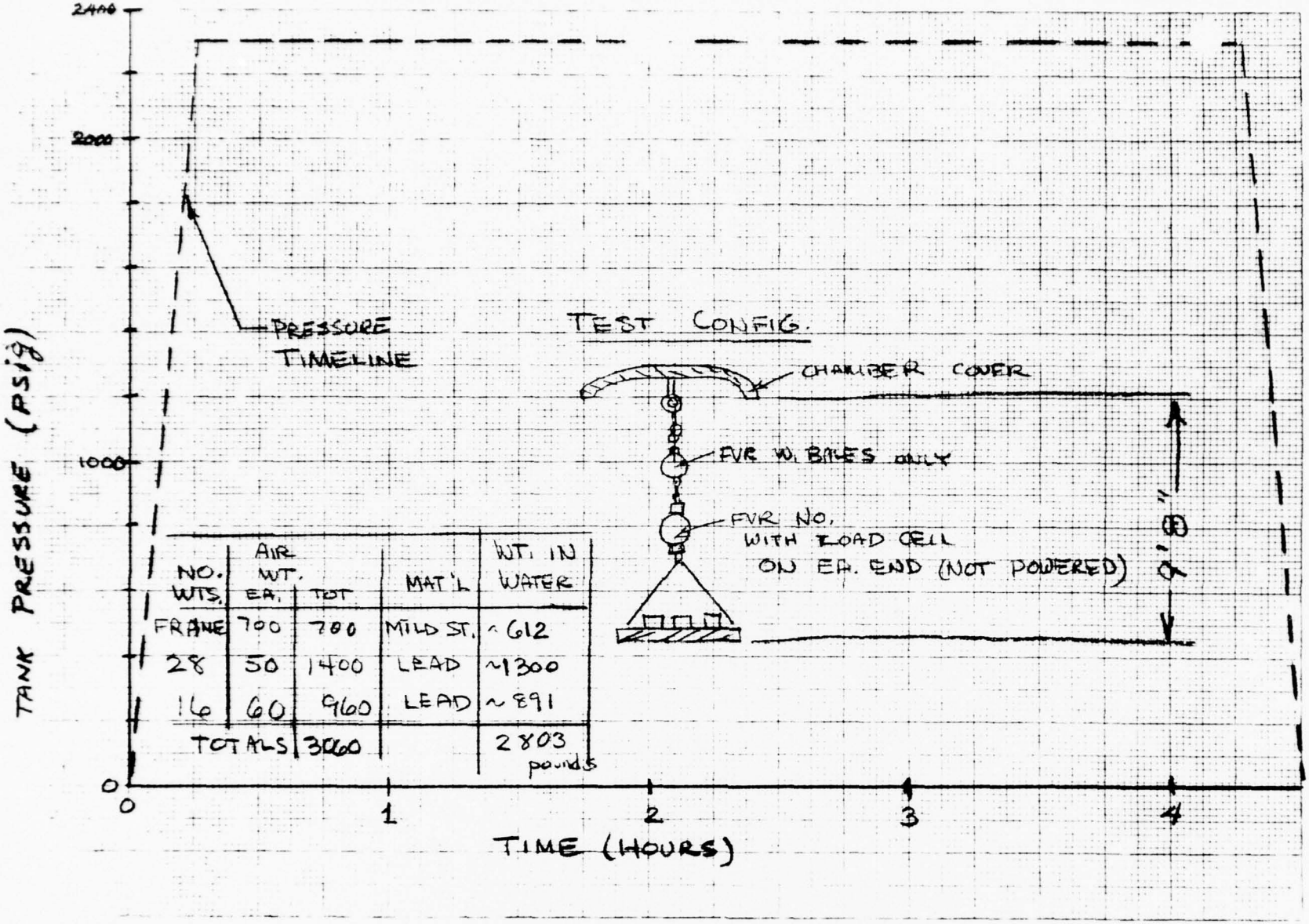

NO. WTS.	AIR WT. EA.	TOT	MAT'L	WT. IN WATER
FRAME	700	700	MILD ST.	~612
28	50	1400	LEAD	~1300
16	60	960	LEAD	~891
TOTALS		3060		2803 pounds

FIGURE 10 FVR SIMULTANEOUS PRESSURE & TENSION TEST AT CEL (PORT HUENEME, CAL) MAY 27, 1976

JJV 6/1/76

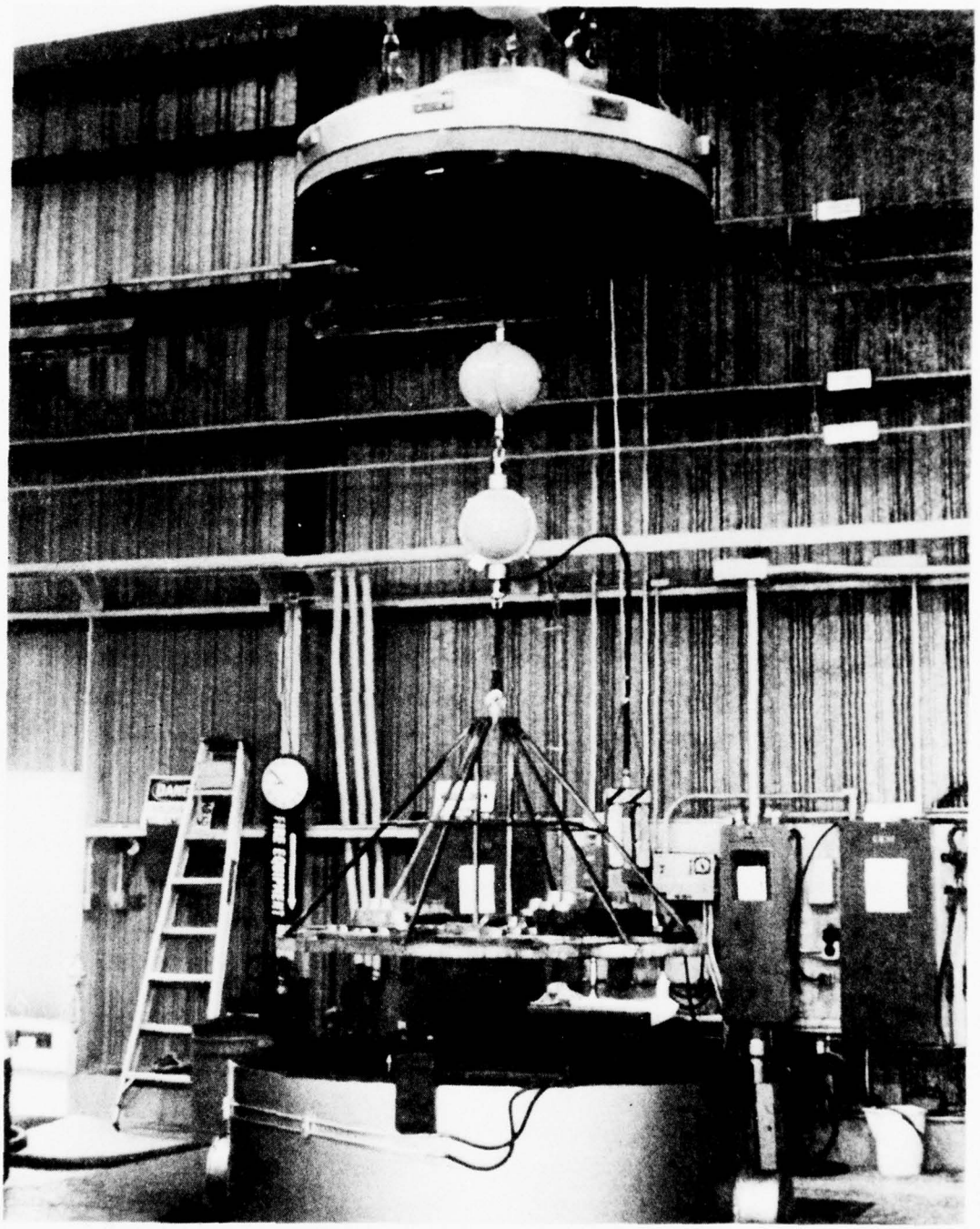

Figure 11. FVR simultaneous pressure and load test at CEL.

All bolts, bales, tension cells, and feed-thrus were torqued to the specification value that they would see in final assembly. Plastic bags were taped within the housings around key areas of potential leaks as an aid to isolating sources should a gross leak be found.

The results showed no leak in either unit. In many subsequent installations in the Hawaii field test program, no leaks were encountered also.

Just prior to shipment to the field test site, all FVRs were assembled in their final configuration and pressure tested to 2,300 psi for about 3 hours each. The tests were conducted at Benthos Inc. at Falmouth, Massachusetts. The goal was to look for any leaks in the semi-permanent seals associated with load cells, electrical feed-thrus, and unused pressure sensor parts. All systems passed the test.

4.2 FVR Sensor Calibration Procedure

The three types of sensors within the FVR required three entirely different types of calibrations. In most cases, where the sensors are linear devices, it is only really necessary to know their bias and scale factor values as a suitable calibration. In the case of the magnetometers, however, this is not sufficient because the value and direction (i.e., dip angle) of the local earth's field vary strongly with geographic location. Therefore, it is necessary to always calibrate the magnetometers locally or find that the magnetic survey charts are sufficiently explicit and accurate that one can know the dip angle and then ratio the scale factor value from another calibration site. Barring confidence in the latter approach the magnetometers were calibrated at PMRF. The procedure will be described in section 4.2.3.

4.2.1 Accelerometer Calibrations

The precise and detailed description of the accelerometer calibration procedure is found in Appendix A-2 of the Mooring Dynamics Experiment Test Plan available from the NOAA Data Buoy Office (NDBO). In summary, the sensor plate of each FVR was sequentially mounted to an accurately-aligned precision tilt table. The table was then incrementally rotated through 10^{o} steps such that each axis was exposed to $\pm$1g of acceleration input. The 10^{o} steps would not be necessary if one were only looking for bias and scale factor. Such a

procedure did find problems of stickiness with various accelerometer sensors (which were rejected) and early in the program revealed a subtle quantization problem with the electronic A to D converter.

4.2.2 Tension Load Cell Calibration

The four fully-assembled and working FVRs were sequentially installed in a precision Instron tensile testing machine in order to calibrate the load cells. The FVRs were powered up and read out in digital counts. The FVRs were installed in the tensile tester with the load cell downward such that the FVR did not measure its own weight at zero applied load. The applied load was accurate to approximately .1 to .2 percent of the full scale Instron range (5,000 pound range for loads over 2,500 pounds). The applied load was varied in approximately 500 pound increments up to 3,000 pounds and down again incrementally. No hysteresis was discovered in the load cell response.

4.2.3 Magnetometer Calibration

In order to calibrate the magnetometers most easily and reliably, a mechanical trunnion assembly was fabricated of aluminum (in order to minimize magnetic disturbances). The FVR was supported in this trunnion such that it could be freely rotated about the z-axis, which is normally in line with the mooring line. The trunnion contained leveling screws in 2 planes such that the z-axis could be pointed straight up and leveled or perfectly horizontal with the x-y body axis plane pointing north. The goal of these calibrations is to derive a value for the number of counts the instrument registers when both the x and y axes point north (horizontally), down, and along the magnetic vector (which for Hawaii was approximately 39 degrees below horizontal). As described later in Chapter 6 these types of tests enable the estimation of the key variables required in order to permit an estimation of Euler angles as well as any misalignment of magnetometer axes within the unit.

4.3 HFTP and LFTP Sensor Calibration Procedure

The detailed written procedure for the laboratory calibration of the HFTPs and LFTPs is a large, single document - occupying approximately 35 pages. A copy

is resident at the C. S. Draper Laboratory for each unit. This section will only explain the procedure employed in a very general manner. The detailed assembly and checkout procedures employed during the field test program are again found in the MDE Test Plan document (Appendix A-3) at NDBO.

Temperature Calibration

The thermistors employed within the TPs are supplied by Fenwal Inc. of Ashland, Massachusetts. With each thermistor is supplied a set of calibration data points of resistance versus temperasture. These data are fitted in a least squares manner to a curve obeying the following general form:

$$\frac{1}{T} = C_1 + C_2 \ell n\ R + C_3 \ell n\ R^3$$

where T is temperature in degrees centigrade and R is in ohms. The precise values of C_1, C_2, and C_3 result from the curve fit appropriate to each thermistor.

The output of the TPs in instrument counts is then measured as a function of a simulated thermistor resistance at eight points over the expected measurement range. The thermistor resistance is simulated by a precising resistance substitution box (General Radio Model GR1433-B good to $\pm$ .02% of range). A curve of instrument counts as a function of temperature is then possible by applying the above equation. This same procedure is carried out at room temperasture, 14°C, and 0°C by placing the TPs in a refrigerator but the resistance box outside. This type of test looks for the sensitivity of the temperature sensing circuitry to the ambient temperature itself. Small order variations are usually found.

Pressure Calibration

The pressure sensor employed in the TPs is a temperature compensated bonded strain gage device. It is generally scaled to work over a small portion of its usable range in order to boost sensitivity. Furthermore, these types of sensors are very linear. Therefore, the instrument output (in counts) is measured as a function of an accurately applied pressure at approximately

one-quarter and three-quarters of the useful range. The pressure is applied by a precision dead-weight tester of two types. For system S/N 93 (i.e., low pressure unit) an Ametek unit good to 0.025% of the applied pressure was used. For all other TPs an Ashcroft unit good to 0.1% of the applied pressure was used. The above test was carried out at room temperature and at $0^{\circ}C$ by bringing pressure hose leads to the tester outside of the refrigerator. A comparison of sensor output curves indicates any sensitivity of the pressure sensing circuitry (as a whole) to ambient temperature (i.e. $\frac{\partial p}{\partial T}$).

4.4 System Synchronization Procedure

Because of the desire for time domain data as well as that from the frequency domain (i.e., spectra) all high frequency burst instruments; including the FVRs, HFTPs, and POPMIP; were required to burst and measure data in synchronism. To accomplish this the C. S. Draper Lab designed and fabricated a start-up box. It artifically introduced a 5.12 second delay to both the POPMIP and HFTP instruments in order to match the starting time of the FVR with its own built-in delay of 5.12 seconds. The synchronization procedure employed in the MDE is given in Appendix C-1 of the MDE Test Plan.

4.5 System Integration Test

On July 21 to 22, 1976 all of the burst instruments subject to the synchronization procedure described in section 4.4 were brought together at the Draper Lab in order to answer the following questions:

(1) Did the start-up synchronization box do its job properly or did some unique electronic interface problems (e.g., unstable oscillation when connected) inhibit its proper function?

(2) Did each sensor system record the presence of dynamic events at the same and correct time as given by a computerized data evaluation of real data tapes in the same manner as would be done after Hawaii?

The former question checked for functional as well as mechanical cabling problems. The latter question was essentially an end-to-end check on the timing of each instrument and its associated software routines. This test was dubbed the System Integration Test.

In order to accomplish the test all of the instruments were mounted in boxes on or strapped directly to a large wooden platform. The whole platform was suspended by 2 chains from the lab ceiling 15-feet overhead in order to permit the whole platform to oscillate at approximately a 4-second period in the manner of a pendulum. Platform oscillations constituted as "event," common to all dynamic motion-sensing systems, that could be initiated at a precise time within each data burst. Figure 12 is a photo of the suspended platform will all instruments (4 HFTPs, 4 FVRs, and 1 POPMIP) aboard the platform awaiting the initiation of an "event," which in this case was the release of a pelican hook allowing the platform to swing free.

Because the HFTPs could not sense platform motion, a magnetic reed switch was wired in place of the thermistor such that, when a magnet was removed from the outside of the TP housing, the resistance of the thermistor lead appeared to go from zero to infinity. Such an "event" gave a clear indication on the computer output of the time that the magnet was removed.

The test was successful in that it pointed out 2 differences between the POPMIP and the Draper Lab instruments. One revolved around when POPMIP was to precisely get its timing signal in order to give a 5.12 second delay and the other involved the software interpretation of the POPMIP data. The differences were worked out and the systems henceforth had the capability of being synchronized. This fact was verified in a phone hook-up synchronization test in mid-September 1976 in which the units were manually started synchronously in Boston and Mississippi (POPMIP) by voice link. Ninety minutes later, during the second data burst, a second telephone conversation allowed both parties to synchronously (within a fraction of a second) initiate an event. The subsequent computerized specification of that time was essentially the same for both POPMIP and the C. S. Draper Lab FVRs and HFTPs.

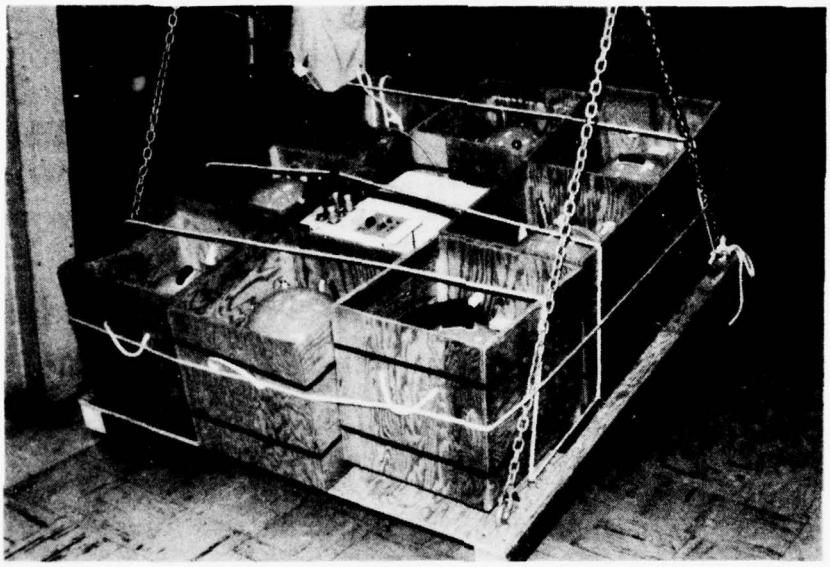

Figure 12. Instrument configuration during system integration test (note PIPMIP package surrounded by 4 FVR's and 4 HFTP's).

5.0 FVR EULER ANGLE DETERMINATION

This section will outline a single set of Euler angles that could be used in conjunction with the FVR data. Further, a method of using the FVR data in order to get Euler angles will be employed. Certain assumptions will be made in order to expeditiously derive the angles. In reality, however, it may be found that the outlined method of measuring Euler angles is in error by an amount which increases as the dynamics experienced by the FVR increases. Such can be true because, as will be seen, in order to derive the first two Euler angles it must be assumed that the dynamic acceleration, or the average over a period of time, is zero. This is necessitated because the FVR contains accelerometers which really are specific force receivers obeying the equation:

$$\vec{f} = \vec{a} - \vec{g} \qquad (5\text{-}1)$$

(sign convention seen later)

This equation says that the output of the sensor, $\vec{f}$, is composed of a dynamic component, $\vec{a}$, and a component of gravity, $\vec{g}$. With the math that will be discussed there is no real way of separating out the two elements in the sensor signal other than to assume that $\vec{a}$ is zero or averages to zero over the time period of interest. If the FVR had gyros as angle sensors such an assumption would not be necessary.

There are possibly two ways around this limitation on calculating Euler angles. The first is directly applicable to the presently-intended use of the FVR data. That is, in verifying the math models of moorings on which the FVR has measured data, it is suggested that the modeller model not only the mooring (with the FVR attached) but also the FVR output to the calculated mooring motion. In so doing the output of the simulation could be two-fold - it would give all x, y, z, θ, ϕ, ψ (positions and Euler angles) co-ordinates (assuming a 3-D model) and additionally derived quantities of specific force (f_x, f_y, & f_z) and magnetometer counts (M_x & M_y) in instrument units. These derived quantities could then be compared with the measured values and the model changed where needed to bring about agreement.

The other way around the limitation described is to use the x and y -axis (nominally horizontal axes) magnetometers as angle sensors for rotations about

the x and y -axis at each data point every .52 seconds. In order to do this the FVR orientation within the magnetic field of the earth must be known. In other words, to do this the Euler angles must be known to begin with. This suggested method implies an iterative scheme which is undefined at present. The result would be a comparison between the estimated angle change indicated by the magnetometer and that indicated by the accelerometers. Any difference could be largely attributed to dynamic acceleration. A limitation to using the magnetometers in this way is that they cannot sense rotation along the magnetic field vector of the earth. A conceptualized plot of the normalized magnetometer sensitivity to rotations is illustrated in Figure 13. This figure shows the earth's field vector $\vec{B}_e$, where sensitivity is indicated by the length of radial lines emanating from the origin. In 3-D space the figure shown is a torus with zero inner diameter.

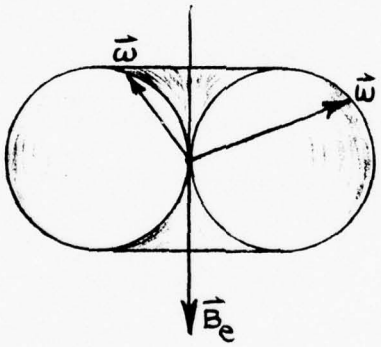

Figure 13 - Normalized 3-D Magnetometer Response to Angular Changes within the Earth's Magnetic Field, $\vec{B}_e$

The rotation vector $\vec{w}$ could be any generalized rotation. Figure 13 shows that for rotations about $\vec{B}_e$, if an axis is pointing parallel to $\vec{B}_e$ and the body is rotating about that axis, the signal change from that axis is zero. The axis normal to it will be changing but will exhibit a symmetrical positional ambiguity to either side of a plane determined by the $\vec{B}_e$ and $\vec{g}$ vectors for pure

rotations about the $\vec{B}_e$ vector. Such a situation is very unique and chances of its occurrence are slim. The data could, however, be difficult to interpret in such a case.

In determining Euler angles under a very specific set of assumptions, the set of axes shown in Figure 14 are assumed. It should be observed that the X, Y, Z co-ordinate system is assumed fixed with respect to inertial space while the x, y, z system is fixed to and moves with the instrument. Figure 15 defines the three Euler angles to be employed in defining the FVR attitude. The following definitions are also employed in deriving the angles:

$\vec{a}$ = acceleration of FVR w.r.t. inertial space (acceleration LT^{-2})

$\vec{f}$ = specific force on FVR (acceleration LT^{-2})

$\vec{g}$ = gravitational field of earth (acceleration LT^{-2})

$\vec{\gamma}$ = earth's magnetic field (Mag. flux density $MT^{-1}Q^{-1}$)

$\gamma_h = \gamma_X$ = horizontal component of the earth's magnetic field

$\gamma_v = \gamma_Z$ = vertical component of the earth's magnetic field

The basic equation relating accelerations is given by equation (5-1). In order to convert any vector $\vec{\ell}$ (i.e., $\vec{\ell} = \ell_X\vec{i}_X + \ell_Y\vec{i}_Y + \ell_Z\vec{i}_Z = \ell_x\vec{i}_x + \ell_y\vec{i}_y + \ell_z\vec{i}_z$) from inertial to body-fixed axes, it is necessary to derive a transformation matrix. By reference to Figure 15, the first rotation (ψ), about the Z-axis, is described by the following transformation for which positive rotations are for x rotated towards y.

$$\begin{Bmatrix} x_1 \\ y_1 \\ z_1 \end{Bmatrix} = A \begin{Bmatrix} X \\ Y \\ Z \end{Bmatrix} = \begin{bmatrix} \cos\psi & \sin\psi & 0 \\ -\sin\psi & \cos\psi & 0 \\ 0 & 0 & 1 \end{bmatrix} \begin{Bmatrix} X \\ Y \\ Z \end{Bmatrix} \qquad (5\text{-}2)$$

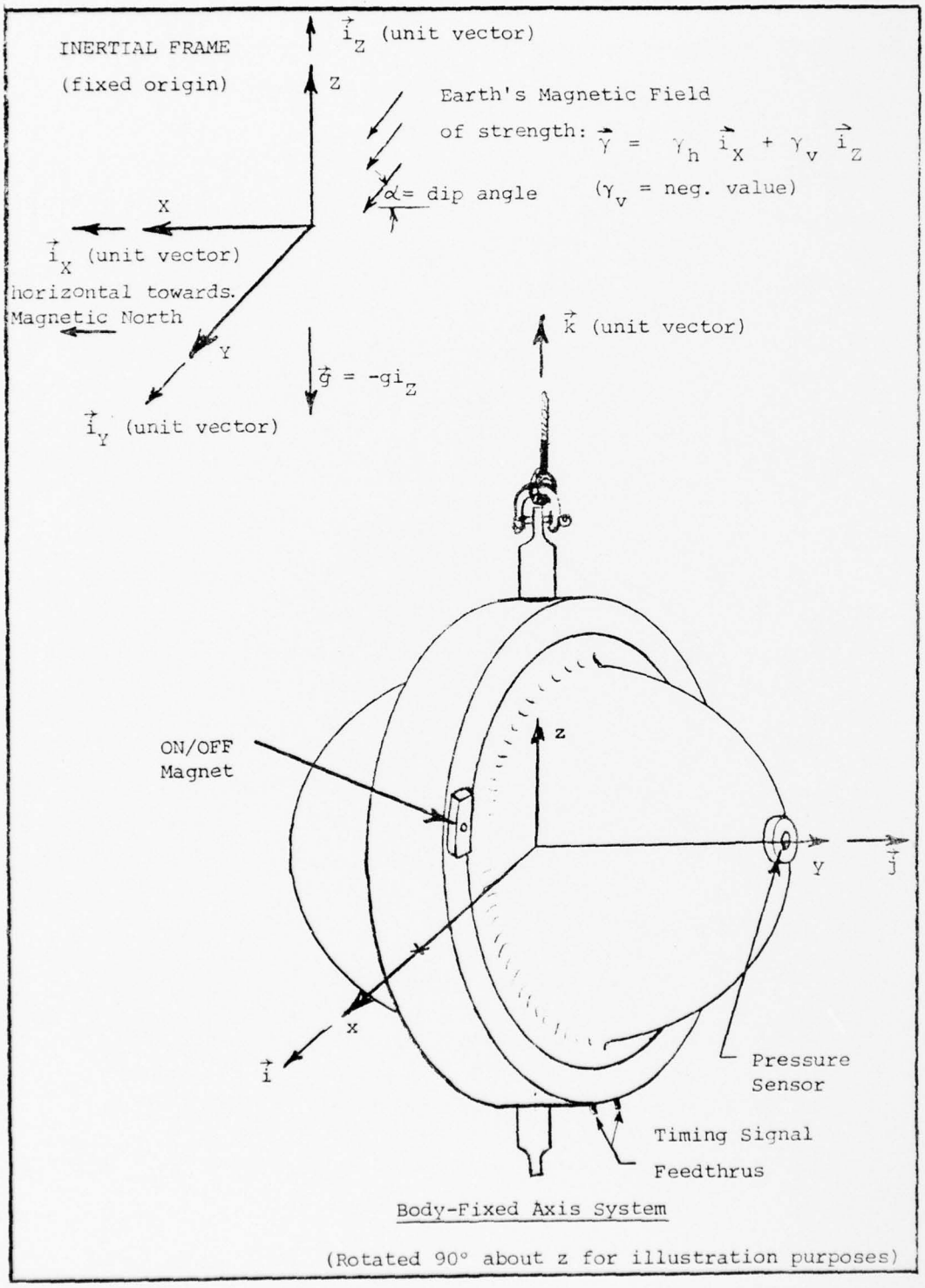

Figure 14. Force Vector Recorder axis definitions.

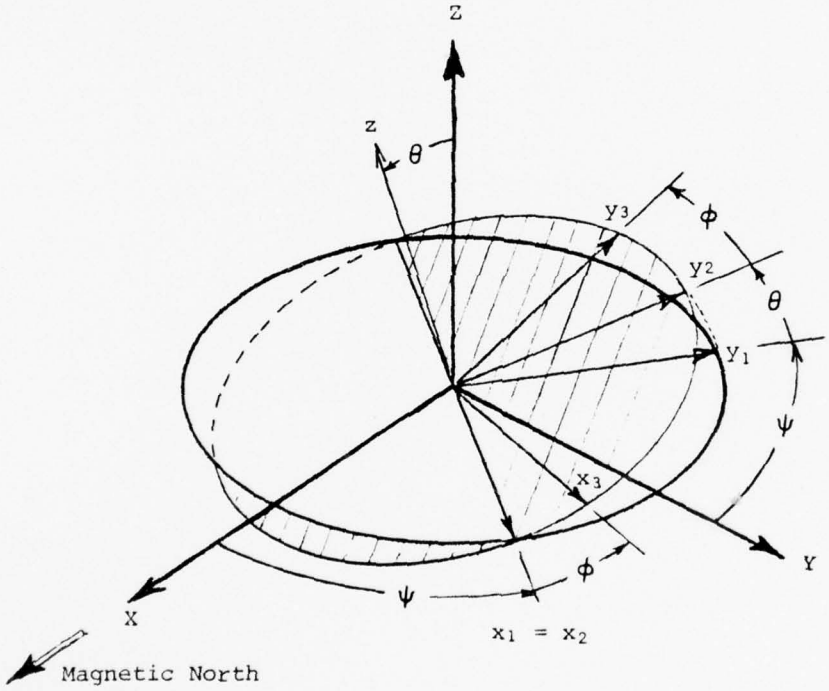

Summary Definition of Rotations

(1) ψ = Rotation about z-axis (aligned with Z-axis). (pos. for x rotated into y)

(2) θ = Rotation about displaced x-axis. (positive for y into z)

(3) ϕ = Rotation about tilted z-axis. (positive for x into y)

Figure 15. FVR Euler Angle Definitions

or:

$$\{\vec{\ell}_1\} = A\,\{\vec{\ell}_0\} \tag{5-3}$$

The second rotation (θ) is about the displaced x-axis (i.e., x_1 axis) and is described by the following transformation in which positive angles are for y into z.

$$\begin{Bmatrix} x_2 \\ y_2 \\ z_2 \end{Bmatrix} = B \begin{Bmatrix} x_1 \\ y_1 \\ z_1 \end{Bmatrix} = \begin{bmatrix} 1 & 0 & 0 \\ 0 & \cos\theta & \sin\theta \\ 0 & -\sin\theta & \cos\theta \end{bmatrix} \begin{Bmatrix} x_1 \\ y_1 \\ z_1 \end{Bmatrix} \tag{5-4}$$

or:

$$\{\vec{\ell}_2\} = B\ \{\vec{\ell}_1\} \tag{5-5}$$

The third and last rotation (ϕ) is about the displaced z-axis (i.e., z_2) and given by the following transformation for which x is rotated into y.

$$\begin{Bmatrix} x_3 \\ y_3 \\ z_3 \end{Bmatrix} = \begin{bmatrix} \cos\phi & \sin\phi & 0 \\ -\sin\phi & \cos\phi & 0 \\ 0 & 0 & 1 \end{bmatrix} \begin{Bmatrix} x_2 \\ y_2 \\ z_2 \end{Bmatrix} \tag{5-6}$$

or:

$$\{\vec{\ell}_3\} = C\{\vec{\ell}_2\} \tag{5-7}$$

The complete transformation matrix is given by the relation:

$$\{\vec{\ell}_3\} = \begin{Bmatrix} x_3 \\ y_3 \\ z_3 \end{Bmatrix} = [CBA] \begin{Bmatrix} x \\ y \\ z \end{Bmatrix} \tag{5-8}$$

$$CBA = \begin{bmatrix} \cos\phi\cos\psi - \sin\phi\sin\psi\cos\theta & \sin\psi\cos\phi + \cos\psi\sin\phi\cos\theta & \sin\phi\sin\theta \\ -\cos\psi\sin\phi - \sin\psi\cos\phi\cos\theta & -\sin\phi\sin\psi + \cos\phi\cos\psi\cos\theta & \cos\phi\sin\theta \\ \sin\psi\sin\theta & -\cos\psi\sin\theta & \cos\theta \end{bmatrix} \quad (5\text{-}9)$$

A useful property of the transformation matrix (5-9) is that its inverse $(CBA)^{-1}$ is equal to its transpose $(CBA)^{T}$.

For the static case (i.e., $\vec{a} = 0$) the values of θ and ϕ are determined from equation (5-1) at each data point. If the time average for $\vec{a}$ is assumed to be zero over many wave periods the same equations hold but the average values of θ, ϕ, and ψ can only be evaluated at lower frequencies. For both cases the accelerometer outputs are given as follows (where $\vec{g} = -g\vec{k}$):

$$\hat{f}_x = -\hat{g}_x = g(\sin\theta\hat{}\sin\phi) \quad (5\text{-}10)$$

$$\hat{f}_y = -\hat{g}_y = g(\sin\theta\hat{}\cos\phi) \quad (5\text{-}11)$$

The $\hat{}$ symbol denotes the average value over a time interval. The static assumption appropriate to equations (5-10) and (5-11) assumes that $\hat{a}_x = \hat{a}_y = 0$. This assumption may also be a fair approximation in some buoy dynamic situations. It is further assumed that $(\sin\theta\hat{}\cos\phi)$ and $(\sin\theta\hat{}\sin\phi)$ are equal to $\hat{\sin}\theta\ \hat{\cos}\phi$ and $\hat{\sin}\theta\ \hat{\sin}\phi$ respectively. This is true for the static case and probably a fair approximation in some buoy dynamic situations. Therefore, the following equations result:

$$f_x = g\ \hat{\sin}\theta\ \hat{\sin}\phi \quad (5\text{-}12)$$

$$f_y = g\ \hat{\sin}\theta\ \hat{\cos}\phi \quad (5\text{-}13)$$

Equations (5-12) and (5-13) may be solved for $\hat{\sin}\theta$, $\hat{\theta}$, and $\hat{\phi}$ under the assumptions that $\hat{\sin}\theta = \sin\hat{\theta}$, $\hat{\sin}\phi = \sin\hat{\phi}$, and $\hat{\cos}\phi = \cos\hat{\phi}$. The value of $\hat{\phi}$ is uniquely found from the relation:

$$\tan\phi = {}^{f_x}/_{f_y} \quad (5\text{-}14)$$

when a computer routine looks at the individual signs of both f_x and f_y. This value is then plugged back into either (5-12) or (5-13) in order to get a unique value for $\hat{\theta}$. The equation chosen depends on the value of $\hat{\phi}$. If one assumes that $\hat{\phi}$ may have a slight error in it, the best equation to use for $\hat{\theta}$ would be chosen as follows:

(a) If $|\sin\phi| > |\cos\phi|$, find θ from equation (5-12) and use equation (5-13) to resolve the ambiguity.

(b) If $|\sin\phi| < |\cos\phi|$, find θ from equation (5-13) and use equation (5-12) to resolve the ambiguity.

With the above procedure, the value of $\cos\phi$ or $\sin\phi$ has the least variation with errors in ϕ.

In order to employ the magnetometers as a sensor for the remaining Euler angle, ψ, it is necessary to have information on the local magnetic field and also the bias values for the two magnetometers (x and y-axes). If the bias values of the magnetometer outputs are given by B_x and B_y, and the output sensitivities are given by G_x and G_y, the output of the magnetometers are given by the relations:

$$m_x = B_x - G_x\gamma_x \quad \text{(counts)}^*$$
$$m_y = B_y - G_y\gamma_y \quad \text{(counts)}^* \qquad (5\text{-}15)$$

Because the magnetometers are used as angle sensors it is desirable to calibrate the magnetometers without having to know the local magnetic field strength in gamma, only the ratio to some other geographic location at which they were calibrated. In the test procedure it is necessary to know the outputs of the magnetometers when their input axes are pointed toward magnetic north (i.e., m_{xh} and m_{yh}) and vertically down (i.e., m_{xv} and m_{yv}) in the same field area where the FVR is to be used:

$$m_{xh} = B_x - G_x\gamma_h \qquad m_{yh} = B_y - G_y\gamma_h$$
$$m_{xv} = B_x - G_x\gamma_v \qquad m_{yv} = B_y - G_y\gamma_v \qquad (5\text{-}16)$$

Hence m_{xh}; m_{yh}; m_{xv} and/or m_{yv} are measured constants for the local axes.

*Negative sensitivities because of polarity of installed sensors.

In order to eliminate the instrument sensitivity, G, from the calibration, equations (5-15) and (5-16) are employed to get:

$$\frac{\gamma_x}{\gamma_h} = \frac{m_x - B_x}{m_{xh} - B_x}$$

$$\frac{\gamma_y}{\gamma_h} = \frac{m_y - B_y}{m_{yh} - B_y} \tag{5-17}$$

and:

$$\frac{\gamma_v}{\gamma_h} = \frac{m_{xv} - B_x}{m_{xh} - B_x} \quad \underline{\text{or}} \quad \frac{\gamma_v}{\gamma_h} = \frac{m_{yv} - B_y}{m_{yh} - B_y} \tag{5-18}$$

In equations (5-18) $\gamma_v/\gamma_h = \tan\alpha$ where α is the value of the dip angle of the local magnetic field. By our definitions $\tan\alpha$ is negative because γ_v is a negative quantity.

For the static case the components of the magnetic field sensed by the FVR are given by the following equations in body co-ordinates:

$$\gamma_x = \gamma_h\ (\cos\phi\ \cos\psi - \sin\phi\ \sin\psi\ \cos\theta) + (\sin\phi\ \sin\theta)\ \gamma_v$$

$$\gamma_y = \gamma_h\ (-\cos\psi\ \sin\phi - \sin\psi\ \cos\phi\ \cos\theta) + (\cos\phi\ \sin\theta)\ \gamma_v \tag{5-19}$$

where $\hat{\cos}\theta = \cos\hat{\theta}$, etc. Equations (5-19) can be multiplied by $\sin\phi$ and $\cos\phi$ repsectively and added in order to solve for ψ in terms of θ, ϕ, γ_x, γ_y, γ_v, and γ_h as follows:

$$\sin\psi = \frac{\gamma_v}{\gamma_h}\tan\theta - \frac{\gamma_x}{\gamma_h}\frac{\sin\phi}{\cos\theta} - \frac{\gamma_y}{\gamma_h}\frac{\cos\phi}{\cos\theta} \tag{5-20}$$

In a similar way equations (5-19) can be multiplied by $\cos\phi$ and $\sin\phi$ respecitvely and added to give the following:

$$\cos\psi = \frac{\gamma_x}{\gamma_h}\cos\phi - \frac{\gamma_y}{\gamma_h}\sin\phi \tag{5-21}$$

The values of $\frac{\gamma_v}{\gamma_h}$, $\frac{\gamma_x}{\gamma_h}$, and $\frac{\gamma_y}{\gamma_h}$ as shown in equations (5-17) and (5-18)

are substituted into equations (5-20) and (5-21) in order to arrive at the following equations in terms of measureable quantities:

(where again γ_v / γ_h should have a negative sign and equals tan α = tan (dip angle))

$$\sin\psi = \frac{m_{xv}-B_x}{m_{xh}-B_x} \tan\theta - \frac{m_x-B_x}{m_{xh}-B_x} \frac{\sin\phi}{\cos\theta} - \frac{m_y-B_y}{m_{yh}-B_y} \frac{\cos\phi}{\cos\theta} \tag{5-22}$$

$$\cos\psi = \frac{m_x-B_x}{m_{xh}-B_x} \cos\phi - \frac{m_y-B_y}{m_{yh}-B_y} \sin\phi \tag{5-23}$$

Other useful relationships could also be derived by which ψ can be derived. The most accurate procedure is to use the most sensitive equation. If, for example, the x magnetometer input axis were pointing near North, a small error in m_x would result in a large error in ψ if we were to use Equation (5-23) because small errors in $\cos\psi$ result in large errors in ψ for values of the argument near zero. Based on this thinking it is recommended that the following be applied.

If $|\sin\psi| < |\cos\psi|$ use (5-22) to calculate ψ and use (5-23) to resolve the ambiguity.

If $|\sin\psi| > |\cos\psi|$ use (5-23) to calculate ψ and use (5-22) to resolve the ambiguity.

In summary, with the suggested calibration scheme, the magnetometers require a knowledge of the local value of the dip angle of the magnetic field (derived from the charts or measured during calibrations), the instrument biases (measured in the lab), plus the values of the horizontal and vertical components of the local magnetic field in instrument counts (not Webers per square meter or gammas). These values are combined with the θ and ϕ values derived from the FVR accelerometers in order to get ψ, the azimuth angle of the FVR with respect to magnetic north. The frequency range over which the values

of Euler angle, derived by the above method, are valid is determined by the nature of the particular response being measured and also the period over which the dynamic component of acceleration, $\vec{a}$, is assumed to average to zero. In most cases, the longer this period is assumed to be the more correct the assumption for moorings whose shape and orientation does not change greatly during the averaging period. The archived Euler angles computed from FVR data taken during the MDE were derived in the manner described except the average value of each sensor output (i.e., f_x, f_y, f_z, M_x, M_y) were averaged over 117-second intervals in order to derive 8 nearly uniform length averages over a burst, yet each average contains approximately 20 wave periods and 10 periods at the swell frequency of approximately 1/12 Hz. The 117-second interval contains 225 frames of FVR data at 0.52 seconds per frame.

6.0 FVR MAGNETOMETER CALIBRATIONS AND ERROR ANALYSIS

The magnetometer calibrations were carried out in two tests for each FVR unit. For these tests the FVR was mounted in an all-aluminum test fixture (aluminum, in order to minimize disturbances to the local earth's field). The first test is referred to as an azimuth scan in which the full unit is incrementally rotated 360^{o} about its z-axis which is vertically aligned. This test produces a sinusoidal output signal from both the x and y axis magnetometer sensors, of amplitude equal to the horizontal component of the earth's field in instrument counts. From this test it is also possible to get an estimate of the sensor biases.

The second magnetometer calibration test is conducted with the instrument z-axis aligned horizontally and the plane determined by the instrument x-y axes aligned in a North-South direction. This test is referred to as the elevation scan. Again this test produces a sinusoidally-varying magnetometer signal for each sensor axis of amplitude equal to the equivalent strength of the earth's field (in instrument counts). If the x and y axes are accurately aligned at the start of the test, the phase angles of the sinusoids are a measure of the dip angle of the local earth's magnetic field. Again, the biases of each sensor are determined from this test and theoretically should agree with the value measured in the azimuth scan test. This, however, is not the case in general. This section will attempt to theoretically illuminate how this difference arises and in so doing show that magnetometer sensor misalignment errors can give rise to this difference.

6.1 Modified Co-ordinate Conversion Matrix

It can be shown that the only magnetometer misalignment error that gives rise to a sensor bias change during the described calibration is if a sensor is inclined towards (or away from) the body z-axis. These postulated magnetometer misalignment errors will be defined as follows:

ε_{xz} = misalignment of x-axis in z-axis direction

ε_{yz} = misalignment of y-axis in z-axis direction.

Employing the same Euler angles defined in section 5, a new set of co-ordinate conversion matrices can be developed which include the above misalignment errors. Equations (6-1) through (6-3) are the three new rotation matrices originally described in section 5. Carrying out the matrix multiplication CBA, and assuming the ε_{xz} and ε_{yz} are small angles (such that $\sin \varepsilon_{xz} = \varepsilon_{xz}$ and $\varepsilon_{xz}\varepsilon_{yz} \approx 0$, etc.) the resulting matrix equation (6-4) results.

ψ-rotation (+ for x into y)

$$\begin{Bmatrix} x_1 \\ y_1 \\ z_1 \end{Bmatrix} = \mathbf{A} \begin{Bmatrix} X \\ Y \\ Z \end{Bmatrix} = \begin{bmatrix} \cos\psi & \sin\psi & \sin\varepsilon_{xz} \\ -\sin\psi & \cos\psi & \sin\varepsilon_{yz} \\ 0 & 0 & 1 \end{bmatrix} \begin{Bmatrix} X \\ Y \\ Z \end{Bmatrix} \qquad (6\text{-}1)$$

θ-rotation (+ for y into z)

$$\begin{Bmatrix} x_2 \\ y_2 \\ z_2 \end{Bmatrix} = \mathbf{B} \begin{Bmatrix} x_1 \\ y_1 \\ z_1 \end{Bmatrix} = \begin{bmatrix} 1 & 0 & \sin\varepsilon_{xz} \\ 0 & \cos(\theta+\varepsilon_{yz}) & \sin(\theta+\varepsilon_{yz}) \\ \sin\varepsilon_{xz} & -\sin\theta & \cos\theta \end{bmatrix} \begin{Bmatrix} x_1 \\ y_1 \\ z_1 \end{Bmatrix} \qquad (6\text{-}2)$$

ψ-rotation (+ for x into y)

$$\begin{Bmatrix} x_3 \\ y_3 \\ z_3 \end{Bmatrix} = \mathbf{C} \begin{Bmatrix} x_2 \\ y_2 \\ z_2 \end{Bmatrix} = \begin{bmatrix} \cos\phi & \sin\phi & \sin\varepsilon_{xz} \\ -\sin\phi & \cos\phi & \sin\varepsilon_{yz} \\ 0 & 0 & 1 \end{bmatrix} \begin{Bmatrix} x_2 \\ y_2 \\ z_2 \end{Bmatrix} \qquad (6\text{-}3)$$

$$
CBA = \begin{bmatrix}
\cos\phi\cos\psi - \sin\phi\cos(\theta+\varepsilon_{yz})\sin\psi + \varepsilon_{xz}\sin\theta\sin\psi & \cos\phi\sin\psi + \sin\phi\cos(\theta+\varepsilon_{yz})\cos\psi - \varepsilon_{xz}\sin\theta\cos\psi & \sin\phi\sin(\theta+\varepsilon_{yz}) + 2\varepsilon_{xz}\cos\phi + \varepsilon_{yz}\cos(\theta+\varepsilon_{yz})\sin\phi + \varepsilon_{xz}\cos\theta \\
-\sin\phi\cos\psi - \cos\phi\cos(\theta+\varepsilon_{yz})\sin\psi + \varepsilon_{yz}\sin\theta\sin\psi & -\sin\psi\sin\phi + \cos\phi\cos(\theta+\varepsilon_{yz})\cos\psi - \varepsilon_{yz}\sin\theta\cos\psi & \cos\phi\sin(\theta+\varepsilon_{yz}) - 2\varepsilon_{xz}\sin\phi + \varepsilon_{yz}\cos\theta + \varepsilon_{yz}\cos(\theta+\varepsilon_{yz})\cos\phi \\
\sin\theta\sin\psi & -\sin\theta\cos\psi + \varepsilon_{xz}\sin\psi & \cos\theta - \varepsilon_{yz}\sin\theta
\end{bmatrix} \tag{6-4}
$$

The earth's magnetic field sensed by the two magnetometers is given by the following equation:

$$
\begin{Bmatrix} \gamma_x \\ \gamma_y \\ - \end{Bmatrix} = CBA \begin{Bmatrix} \gamma_h \\ 0 \\ \gamma_v \end{Bmatrix} \tag{6-5}
$$

where no z-axis magnetometer is present in the FVR.

In this case the earth's magnetic field vector is given by the relation:

$$
\vec{\gamma} = \gamma_h \vec{i}_Z + \gamma_v \vec{i}_Z \tag{6-6}
$$

where the unit vectors $\vec{i}_X$ $\vec{i}_Y$ and $\vec{i}_Z$ are earth-fixed axes and defined as shown in Figure 14. Therefore, the magnetic field sensed by the x and y axis magnetometers is given as follows by expanding equation (6-5):

$$\gamma_x = [\cos\phi\cos\psi - \sin\phi\cos(\theta+\varepsilon_{yz})\sin\psi + \varepsilon_{yz}\sin\theta\sin\psi]\gamma_h$$

$$+ [2\varepsilon_{xz}\cos\phi + \varepsilon_{xz}\cos(\theta+\varepsilon_{yz})\sin\phi + \sin\phi\sin(\theta+\varepsilon_{yz}) + \varepsilon_{xz}\cos\theta]\gamma_v \quad (6\text{-}7)$$

and

$$\gamma_y = [-\sin\phi\cos\psi - \cos\phi\cos(\theta+\varepsilon_{yz})\sin\psi + \varepsilon_{yz}\sin\theta\sin\psi]\gamma_h$$

$$+ [-2\varepsilon_{xz}\sin\phi + \cos\phi\sin(\theta+\varepsilon_{yz}) + \varepsilon_{yz}\cos\theta + \varepsilon_{yz}\cos(\theta+\varepsilon_{yz})\cos\phi]\gamma_v \quad (6\text{-}8)$$

The actual output of the two magnetometers, in units of instrument counts, is given by the equation (5-15).
In these equations B_x and B_y are the electrical bias values (in counts) which arise from a planned sensor scaling. G_x and G_y are the x and y-axis sensitivities in such units of counts/ gamma, where the earth's field strength may range from approximately 30,000 to 60,000 gamma.

Plugging equations (6-7) and (6-8) into (5-15) results in the following equations describing magnetometer output in terms of Euler angles and sensor misalignment errors;

$$M_x = B_x + G_x\gamma_h[\cos\phi\cos\psi - \sin\phi\cos(\theta+\varepsilon_{yz})\sin\psi + \varepsilon_{xz}\sin\theta\sin\psi] + G_x\gamma_v[2\varepsilon_{xz}\cos\phi + \varepsilon_{xz}\cos(\theta+\varepsilon_{yz})\sin\phi + \sin\phi\sin(\theta+\varepsilon_{yz}) + \varepsilon_{xz}\cos\theta] \quad (6\text{-}9)$$

and ...

$$M_y = B_y + G_y\gamma_h[-\sin\phi\cos\psi - \cos\phi\cos(\theta+\varepsilon_{yz})\sin\psi + \varepsilon_{yz}\sin\theta\sin\psi] + G_y\gamma_v[-2\varepsilon_{xz}\sin\phi + \cos\phi\sin(\theta+\varepsilon_{yz}) + \varepsilon_{yz}\cos\theta + \varepsilon_{yz}\cos(\theta+\varepsilon_{yz})\cos\phi] \quad (6\text{-}10)$$

6.2 Azimuth Scan Calibration

If an azimuth scan calibration is carried out as shown in Figure 16, the following assumptions can be made which greatly simplify the output equations (6-9) and (6-10).

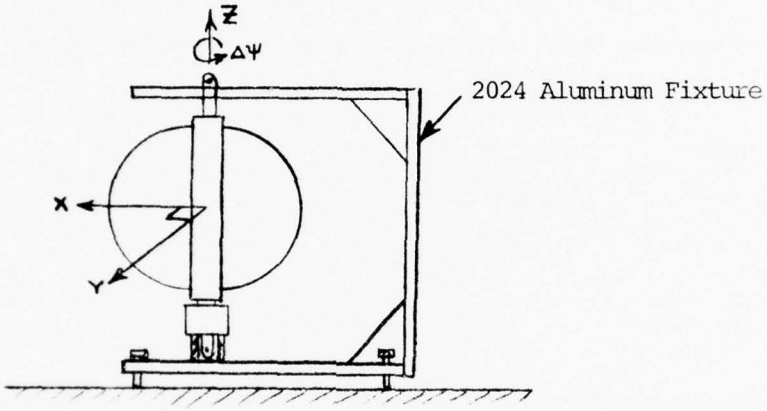

Figure 16 - "Azimuth Scan"
Magnetometer Field Calibration Setup

Azimuth Scan Assumptions

(1) $\theta = 0^{\circ} \longrightarrow \sin\theta = 0, \cos\theta = 1$

(2) $\phi = 0^{\circ} \longrightarrow \sin\phi = 0, \cos\phi = 1$

(3) $\cos(\theta + \varepsilon_{yz}) = 1$

(4) $\sin(\theta + \varepsilon_{yz}) = \varepsilon_{yz}$

(5) $\cos(\theta + \varepsilon_{yz}) = 1$

The resulting simplified versions of equations (6-9) and (6-10) are as follows:

$$M_x = B_x + G_x \left[\gamma_h \cos \psi + 3\gamma_v \varepsilon_{xz}\right] \quad (6\text{-}11)$$

$$M_y = B_y + G_y \left[-\gamma_h \sin \psi + 3\gamma_v \varepsilon_{yz}\right] \quad (6\text{-}12)$$

It can be seen that the output of each sensor axis is a sinusoidal term (varying with angle ψ) about the bias value as the mean. The bias on each axis is increased by the following amount:

$$\Delta B_x = 3\, G_x \gamma_v \varepsilon_{xz} \quad (6\text{-}13)$$

$$\Delta B_y = 3\, G_y \gamma_v \varepsilon_{yz} \quad (6\text{-}14)$$

..... where γ_v is a negative number.

This next section will show that this bias shift does not occur during an elevation scan calibration.

6.3 Elevation Scan Calibration

The strength of the total magnetic field is measured along with the dip angle in the "elevation scan" calibration test. The test setup employed is shown in Figure 17. For this test the z-axis is kept horizontal while the x and y axes are incrementally rotated through 360 degrees, stopping every 10-degrees to record data from all sensors. The x-y plane is aligned in a magnetic North-South direction using an independent, hand-held compass.

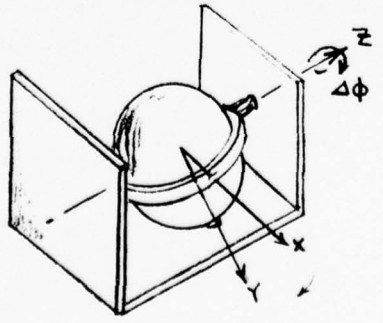

Figure 17 - "Elevation Scan"
Magnetometer Field Calibration Setup

For this test, the following assumptions are made:

(1) $\psi = 180^{o} \longrightarrow \sin \psi = 0 \quad \cos \psi = -1$

(2) $\theta = -90^{o} \longrightarrow \sin \theta = -1, \cos \theta = 0$

(3) vary ϕ

Substituting these values into equations (6-9) and (6-10) indicates that no constant bias shift arises in either magnetometer sensor in an elevation scan due to the misalignment errors assumed.

The calibration data of output versus rotation angle derived in both the azimuth and elevation scan were fitted to sinusoidal curves by a least squares minimization process. The generalized form of the equation is given as follows:

$$M = \text{counts} = B + C \sin (\phi + \zeta) + R (\phi) \qquad (6\text{-}15)$$

where: M = instrument output in counts

B = bias for a given axis

C = scale factor sensitivity

ϕ = rotation angle during calibration

ζ = phase angle

R(ϕ) = residual from curve fitting process

The results of the above curve fitting for all of the instrument calibrations done at PMRF (Kauai, Hawaii) are given in Table 9. The variation in bias between azimuth and elevation scans allows the estimation of sensor misalignment by equations (6-13) and (6-14). The variation of the estimated dip angle during elevation tests allows the estimation of sensor misalignment in the x - y plane (i.e., ε_{xy}, x-axis in y-direction, and ε_{yx}). A nominal value of 39.4^{o} was assumed for the dip angle taken from NAVOCEANO charts. The residual RMS error from the curve-fitting process is given in Table 9. In general this error is neglected because it is of small order. It is given for completeness of data portrayal. Interestingly enough the frequency of this error is at twice that of the rotation angle with a phasing which is not always uniform from unit to unit. The source of this periodic residual is

S/N	PHASE (DEGREES)	AMPLITUDE (COUNTS)	BIAS (COUNTS)	RESIDUAL RMS ERROR (Counts)
X-Az	-0.193	+156.044	526.667	1.29
Y-Az	-88.193	+180.994	493.389	1.49
X-EL	51.640	199.547	531.500	1.06
Y-EL	-37.069	232.290	486.944	1.46
X-Az	-2.028	+175.992	531.861	2.05
Y-Az	87.908	216.828	543.750	2.47
X-EL	49.425	224.822	544.028	2.41
Y-EL.	-40.744	276.429	527.500	3.57
X-EL	-50.340	225.354	518.278	1.19
Y-EL	42.388	+271.146	485.111	1.09
X-Az	0.711	+177.727	566.861	1.97
Y-Az	-88.345	+205.121	503.472	1.34
X-EL	53.136	225.249	573.611	1.78
Y-EL	-36.166	263.118	499.222	2.39
X-Az	0.930	+173.009	542.167	1.85
Y-Az	-87.962	+194.795	477.472	2.51
X-EL	53.069	222.255	550.139	1.00
Y-EL	-35.642	249.451	474.444	2.04

F1

F2

F2 Polihale Beach

F3

F4

TABLE 9 SUMMARY OF KAUAI MAGNETOMETER CALIBRATIONS.

unclear and not explained by the earlier math.

Magnetic anomaly charts for the MDE test area were employed to estimate the FVR magnetometer scale factor change at the test area relative to that at the calibration site. Two scale factors were derived - one for experiments 1, 2 and 3 and another for experiment 5, owing to a different (shallower) location. These factors and all of the pertinent magnetometer erros are given in Table 10.

These equations derived earlier in this section do not use the magnetometer misalignment errors in the x-y plane. In order to include these errors in the analysis, it is necessary to further revise the matrices (6-1) through (6-3) which gives rise to even more messy mathematics to achieve a precision that may seem unwarranted in light of the goals of the MDE. The low frequency average Euler angles derived for archiving did not correct for the misalignment errors described in Table 10.

When the real FVR ocean data from the Hawaii experiments were analyzed it was found that the instrument biases had changed from the values they exhibited during calibrations. Each instrument exhibited a different bias value in each experiment. Within a given experiment none of the bias changes were the same. The changes were obvious in the data because the accelerometers indicated the angle of the body x-y plane, but the magnetometer data was far different than expected under the specific circumstances. It was not known exactly why all the variations occurred. Later data analysis and tests indicated that the sensor scale factors did not change significantly. Laboratory tests, however, indicated that slight variations in the location of wire bundles within the FVR can give rise to small magnetometer bias changes and even smaller scale factor changes. It was also suspected that the following might help explain the problem:

(1) the local magnetic anomalies in the ocean itself, which are not revealed in NAVOCEANO charts, could give rise to the observed bias changes. This could be true because the charts are derived by filtering the data from aeromagnetic surveys. Limited detailed subsurface magnetic data indicates horizontal gradients in the magnetic field strength, but less than the observed changes in output.

FVR S/N	x - Axis	y - Axis
F1	SF_x (1-3) = 205.60	SF_y (1-3) = 239.33
	SF_x (5) = 203.13	SF_y (5) = 236.45
	$\varepsilon_{xz} = .73^{\circ}$	$\varepsilon_{yz} = -.84^{\circ}$
	$\varepsilon_{xy} = -1.04^{\circ}$	$\varepsilon_{yx} = 2.33^{\circ}$
F2	SF_x (1-3) = 231.63	SF_y (1-3) = 284.81
	SF_x (5) = 228.85	SF_y (5) = 281.39
	$\varepsilon_{xz} = 1.64^{\circ}$	$\varepsilon_{yz} = -1.78^{\circ}$
	$\varepsilon_{xy} = 1.18^{\circ}$	$\varepsilon_{yx} = -1.34^{\circ}$
F3	SF_x (1-3) = 232.06	SF_y (1-3) = 271.09
	SF_x (5) = 229.28	SF_y (5) = 267.84
	$\varepsilon_{xz} = .91^{\circ}$	$\varepsilon_{yz} = -.49^{\circ}$
	$\varepsilon_{xy} = -2.53^{\circ}$	$\varepsilon_{yx} = 3.23^{\circ}$
F4	SF_x (1-3) = 228.99	SF_y (1-3) = 257.00
	SF_x (5) = 226.25	SF_y (5) = 253.92
	$\varepsilon_{xz} = 1.09^{\circ}$	$\varepsilon_{yz} = -.37^{\circ}$
	$\varepsilon_{xy} = -2.47^{\circ}$	$\varepsilon_{yx} = 3.76^{\circ}$

Notes and Comments

1. SF (1-3) and SF (5) are the scale factors (counts) when sensors are aligned parallel to the magnetic vector for experiments 1 through 3 and 5 respectively (i.e., units are counts/ local earth's field).

2. Dip Angle assumed to be 39.4° at calibration site and 39.6° at test site.

3. Alignment error sign convention

   ε_{xy} = x - axis towards y

   ε_{xz} = x - axis towards z

   ε_{yx} = y - axis towards x

   ε_{yz} = y - axis towards z

4. Magnetic field strength ratios

   a. $\left[\gamma_{field\ (1-3)} / \gamma_{PMRF} \right] = 1.0303$

   b. $\left[\gamma_{field\ (5)} / \gamma_{PMRF} \right] = 1.0179$

Table 10 - Magnetometer Scale Factors and Estimated Alignment Errors During MDE Field Experiment

(2) the instruments could be retaining a residual magnetic field from the lab, the ship, their ON/OFF magnet, or other unknown source.

Ongoing instrument tests will hope to pin down the full nature of the problem.

In order to arrive at a best estimate of the new bias values for the MDE data, a new analysis was carried out. All of the FVR experiment data were scanned for portions representing conditions in which the x-y plane of the FVR body axes was very close to being horizontal (i.e., within 3°) as indicated by the accelerometer data. For these cases the extremes of the magnetometer data output were noted. The expected output from the magnetometers as a function of the accelerometer-derived Euler angles and an unknown azimuth angle was described analytically. The simulataneous analysis of two azimuth data points for the two sensors gave four equations in the four unknowns: E_x, E_y, A_{z1}, A_{z2}. E_x and E_y are the new and unknown biases and A_{z1} and A_{z2} are the azimuth rotations for the two data points selected. Many combinations of data points for each instrument were analyzed and a best estimate of the biases derived. In most cases the use of many different data point combinations produced a convergent solution to the same answers. The resulting estimates of sensor biases and instrument counts when pointing horizontal (i.e., m_{xh} and m_{yh}) are given in Table 11 for experiments 1,2,3, and 5 respectively for the four FVRs displaying serial numbers (S/N) F1, F2, F3, and F4. From the data presented in these tables, the non-dimensionalized magnetometer output are derived as follows:

$$\frac{\gamma_x}{\gamma_h} = \frac{m_x - E_x}{m_{xh} - E_x} \tag{6-16}$$

$$\frac{\gamma_y}{\gamma_h} = \frac{m_y - E_x}{m_{yh} - E_x} \tag{6-17}$$

where: m_x, m_y = x & y axis sensor output (Counts)

E_x, E_y = x & y axis bias value (Counts)

m_{xh}, m_{yh} = x & y axis sensor counts when sensor is horizontal and pointing in a magnetic north direction (Counts).

These non-dimensionalized quantities are those which are archived on the engineering unit tapes and employed in estimating the azimuth rotation Euler angles by equations (5-20) and (5-21).

Table 11

MDE - Magnetometer Calibration Data Summary

S/N	B_x (Counts)	B_y (Counts)	m_{xh} (Counts)	m_{yh} (Counts)
Experiment 01:				
F1	521.7	530.3	363.29	345.9
F2	539.6	567.7	361.13	348.25
F3	576.5	524.1	397.7	315.23
F4	552.0	505.3	375.56	307.28
Experiment 02:				
F1	548.0	502.5	389.59	318.10
F2	534.0	527.5	355.53	308.05
F3	690.0	426.0	511.20	217.13
F4	559.0	515.5	382.56	316.98
Experiment 03:				
F1	514.2	538.5	355.78	354.09
F2	517.0	478.3	338.53	258.85
F3	386.5	472.4	207.7	263.53
F4	543.0	506.3	366.56	308.28
Experiment 05:				
F1	531.5	505.0	377.99	322.82
F2	535.0	508.1	358.67	291.29
F3	372.5	440.5	195.84	234.13
F4	524.0	502.0	349.67	306.36

7.0 ARCHIVED DATA TAPE CONTENTS

The four following types of Draper Lab/MDE data tapes were archived with the data aligned in columns as shown:

(1) Low Frequency Temperature/Pressure Recorders (LFTP) data:

Data Column	Data Word (see Appendix B)	
1	Time (minutes since instrument turn-on at 1550 Z on 27 September 1976	
2	Instrument Time Count (see TAble B-2)	
3	Depth (meters)	
4	Pressure Offset (i.e., bias)	DATA NOT NEEDED IN MODEL VERIFICATION
5	Calibration Reference Voltage	
6	Identification Number	
7	Temperature (^{o}C)	

(2) High Frequency Temperature/Pressure Recorders (HFTP) data:

Data Column	Data Word (see Appendix B)
1	Time = T (Seconds since beginning of burst-1)
2	Instrument Time Count (see TAble B-1)
3	Temperature at time T
4	Pressure at time T
5	Pressure at time T + .48 sec.
6	Pressure at time T + 1.04 sec.
7	Pressure at time T + 1.52 sec.

(3) Force Vector Recorder (FVR) data:

Data Column	Data Word (see Appendix C)
1	Time (Seconds since beginning of burst-1)
2	Frame Count (0 to 63)
3	Mooring Line Tension (Pounds)
4	γ_x/γ_h
5	γ_y/γ_h
6	Specific Force, f_x (g's)
7	Specific Force, f_y (g's)
8	Specific Force, f_z (g's)

(4) Low Frequency Euler Angle Tape (from FVR data):

Data Column	Data Word
1	Number of frames used in average
2	Time at middle of averaging interval (seconds since start of burst-1)
3	Average Tension (Pounds)
4	Average γ_x/γ_h
5	Average γ_y/γ_h
6	Average specific force, f_x (g's)
7	Average specific force, f_y (g's)
8	Average specific force, f_z, (g's)
9	Average Euler angle, ϕ (degrees) (see Fig. 15)
10	Average Euler angle, θ (degrees) (see Fig. 15)
11	Average Euler angle, Ψ (degrees) (see Fig. 15)

It should be re-emphasized that the following archived records are incomplete or faulty for the reasons given. These same data gaps can be ascertained by examining the comment portions of Tables 2 through 5 under instrument summary.

Experiment	Instrument	Problem Bursts	Nature of Problem
CM Mooring	LFTP S/N 84	all	Recorder unlatched
1	FVR S/N F2	5-end	x-axis accelerometer failure
1	HFTP S/N 93	all	Instrument depth at extreme of sensor range producing clipped signal in presence of dynamics
2	HFTP S/N 93	22-end	Data breakup due to recorder problem

REFERENCES

(1) Chhabra, N. K. 1974, "Verification of a Computerized Model for Subsurface Mooring Dynamics Using Full Scale Ocean Test Data," Proceedings, Marine Technology Society, pp. 69-80.

(2) Chhabra, N. K., J. M. Dahlen, and M. R. Froidevaux, 1974, "Mooring Dynamics Experiment - Determination of a Verified Dynamic Model of the WHOI Intermediate Mooring," C. S. Draper Laboratory, Inc., Report R-823.

(3) Chhabra, N. K., 1976, "Mooring Mechanics - A Comprehensive Computer Study - Volume II," C. S. Draper Laboratory, Inc., Report R-1066.

(4) Dillon, D. B., 1973, "An Inventory of Current Mathematical Models of Scientific Data-Gathering Moors," Hydrospace-Challenger Report HCI TR4450 0001.

(5) Gould, W. J. and E. Sambuco, 1975, "The Effect of Mooring Type on Measured Values of Ocean Currents," Deep-Sea Research, V. 22, pp. 55-62.

(6) Heinmiller, Robert H. and Robert G. Walden, 1973, "Details of Woods Hole Moorings," W.H.O.I. Reference No. 73-71 (Unpublished Manuscript).

(7) Kalvaitis, A. N., 1974, "Effects of Vertical Motion on Vector Averaging (Savonius Rotor) and Electromagnetic Type Current Meters," NOAA Tech. Memo, NOS, NOIC3.

(8) Kaplan, P., A. I. Raff and T. P. Sargeant, 1972, "Experimental and Analytical Studies of Buoy Hull Motion in Waves," Oeanics Inc., Final Report to NDBC, NDBC Report No. NDBCM 611.3.

(9) Walden, R. G., D. H. DeBok, D. Meggitt, J. B. Gregory and W. A. Vachon, 1977, "The Mooring Dynamics Experimen t - A Major Study of the Dynamics of Buoys in the Deep Ocean," Paper No. 2883, Proceedings of Offshore Technology Conference.

(10) Wunsch, C. and J. Dahlen, 1974, "A Moored Temperature and Pressure Recorder," Deep-Sea Research, V. 21, pp. 145-154.

APPENDIX A

Summary of Averaged T/P Field Data

This section contains an average value from all of the HFTPs (temperature and depth) during every burst of the Mooring Dynamics Experiment. Furthermore, it also contains an average value for every hour that the LFTPs were deployed. These data are given in Tables A-1 through A-22.

HFTP S/N 90 IN EXPERIMENT NO. 1, DISCUS MRG., DATE 10-12-76

TIME (ZULU)[1] BURST		AVE. TEMP. (°C)	AVE. DEPTH (m)	TMAX[2] (°C)	TMIN (°C)	DMAX[3] (m)	DMIN (m)	NO. FRAMES	SIGNIF. EVENTS
16:04:55	1	24.007	0.077	24.042	23.994	0.239	-0.022	833	
16:48:36	2	25.171	5.624	26.014	24.114	19.884	-0.020	833	IN WATER 17:03
17:32:18	3	26.030	20.507	26.061	25.990	28.721	8.578	833	
18:15:59	4	26.063	33.646	26.084	26.061	34.439	31.970	833	
19:00:00	5	26.075	34.865	26.084	26.061	35.738	33.399	833	
19:43:41	6	26.050	35.659	26.061	26.037	36.517	34.308	833	
20:27:23	7	26.044	35.830	26.061	26.014	37.037	34.438	833	ANCHOR LAUNCH 20:27:27
21:11:04	8	26.057	36.132	26.061	26.037	37.037	35.218	833	
21:54:46	9	26.021	36.166	26.037	26.014	37.037	34.828	833	
22:38:27	10	26.001	36.343	26.014	25.967	37.427	35.087	833	
23:22:09	11	25.991	36.346	26.037	25.849	37.426	35.088	833	
00:05:50	12	25.981	36.344	26.014	25.872	37.297	35.217	833	
00:49:32	13	26.001	36.363	26.014	25.990	37.556	35.087	833	
01:33:13	14	26.008	36.365	26.014	25.990	37.427	35.218	833	
02:16:54	15	26.009	36.390	26.014	25.990	37.297	35.218	833	
03:00:35	16	25.990	36.430	26.014	25.990	37.686	35.087	833	
03:44:17	17	25.990	36.471	26.014	25.990	37.686	34.827	833	
04:27:58	18	25.991	36.458	26.014	25.990	37.556	34.827	833	
05:11:40	19	25.990	36.467	25.990	25.990	37.686	35.347	833	
05:55:21	20	26.001	36.484	26.014	25.990	37.686	35.088	833	
06:39:03	21	25.986	36.531	25.990	25.967	37.686	35.087	833	
07:22:44	22	25.948	36.616	25.967	25.943	38.075	35.217	833	
08:06:26	23	25.948	36.674	25.967	25.920	37.816	35.217	833	
08:50:07	24	26.057	36.711	26.108	25.990	37.818	35.348	833	
09:33:48	25	26.106	36.704	26.131	26.084	37.948	34.959	833	
10:17:29	26	26.106	36.712	26.108	26.084	37.818	35.479	777	

NOTES: (1) TIMES NOTED AT BEGINNING OF BURST

(2) TEMP. LEAST SIGNIF. BIT = .027 °C, RG. 2.9-30.3°C (3) DEPTH LSB = .127 m, RG. 0-122.1 m.

TABLE A-1, EXP. #1, S/N 90 HFTP DATA SUMMARY

HFTP S/N 91 IN EXPERIMENT NO. 1, DISCUS MRG., DATE: 10-12-76

TIME (ZULU)[1]	BURST	AVE. TEMP.[4] (°C)	AVE. DEPTH (m)	TMAX[2],[4] (°C)	TMIN (°C)	DMAX[3] (m)	DMIN (m)	NO. FRAMES	NOTES
16:04:55	1	24.174	46.141	24.249	23.746	46.161	46.025	833	
16:48:36	2	24.518	46.234	24.774	24.249	46.303	46.161	833	IN WATER 17:23 Z
17:32:18	3	26.043	46.645	26.074	[illegible]	46.654	45.830	833	
18:15:59	4	[illegible]	110.384	22.707	[illegible]	129.048	91.302	833	
19:00:00	5	[illegible]	117.117	[illegible]	[illegible]	128.475	107.377	833	
19:43:41	6	[illegible]	139.675	20.316	[illegible]	150.864	116.085	833	
20:27:23	7	[illegible]	139.521	19.889	[illegible]	153.448	131.824	833	ANCHOR LAUNCH 20:27:27
21:11:04	8	[illegible]	152.040	19.864	[illegible]	154.767	147.394	833	
21:54:46	9	19.596	151.986	19.763	19.409	153.736	150.187	833	
22:38:27	10	19.347	153.295	19.384	19.308	154.973	151.633	833	
23:22:09	11	[illegible]	151.363	19.282	[illegible]	155.120	147.896	833	
00:05:50	12	[illegible]	153.290	19.282	[illegible]	155.274	148.231	833	
00:49:32	13	19.059	153.854	19.384	18.388	155.816	152.033	833	
01:33:13	14	18.942	154.100	19.232	18.593	155.615	152.272	833	
02:16:54	15	18.831	154.397	19.155	18.388	155.960	152.822	833	
03:00:36	16	18.996	155.125	19.282	18.696	157.255	153.539	833	
03:44:17	17	19.272	155.690	19.333	18.619	157.316	153.634	833	
04:27:58	18	19.552	155.532	19.713	19.282	157.236	153.360	833	
05:11:40	19	20.086	155.226	20.291	[illegible]	157.023	150.575	833	
05:55:21	20	[illegible]	152.578	20.291	[illegible]	155.898	147.896	833	
06:39:03	21	[illegible]	153.208	20.316	[illegible]	155.737	147.896	833	
07:22:44	22	[illegible]	149.667	20.316	[illegible]	155.061	147.896	833	
08:06:26	23	[illegible]	149.530	[illegible]	[illegible]	150.910	147.896	833	
08:50:07	24	[illegible]	149.575	[illegible]	[illegible]	151.077	147.896	833	
09:33:48	25	[illegible]	149.917	[illegible]	[illegible]	151.412	147.729	833	
10:17:29	26	[illegible]	150.311	[illegible]	[illegible]	151.747	148.566	833	
11:01:10	27	[illegible]	150.224	[illegible]	[illegible]	151.412	149.236	74	

NOTES: (1) TIMES NOTED AT BEGINNING OF BURST (2) LSB (TEMP) = .027°C, RG. 2.9 - 30.3 °C
(3) LSB (DEPTH) = .169 m, RG. 46-218 m. (4) INTERMITTENT TEMP. SENSOR, BAD DATA CANCELLED

TABLE A-2, EXP. #1, S/N 91 HFTP DATA SUMMARY

HFTP S/N 92 IN EXPERIMENT NO. 1, DISCUS MRG., DATE: 10-12-76

BURST		AVE. TEMP. (°C)	AVE. DEPTH (m)	TMAX	TMIN	DMAX	DMIN	NO. FRAMES	SIGNIF. EVENTS
16:04:55	1	24.142	53.479	24.187	24.116	53.480	53.478	833	
16:48:36	2	24.823	53.496	26.034	24.211	53.526	53.481	833	IN WATER 17:09 Z
17:32:18	3	26.073	53.527	26.104	26.034	53.528	53.526	833	
18:15:59	4	25.771	63.784	26.127	25.138	74.882	62.132	833	
19:00:00	5	24.636	71.986	25.657	23.228	75.612	68.816	833	
19:43:41	6	24.092	75.946	24.545	23.444	77.822	71.743	833	
20:27:23	7	23.782	76.943	24.116	23.565	79.272	72.948	833	ANCHOR LAUNCH 20:27:27
21:11:04	8	23.413	77.040	23.613	23.131	78.429	75.873	833	
21:54:46	9	23.405	76.950	23.516	23.228	78.383	75.365	833	
22:38:27	10	23.056	77.476	23.155	22.914	78.924	75.861	833	
23:22:09	11	22.959	77.562	23.179	22.744	79.045	76.103	833	
00:05:50	12	22.942	77.511	23.107	22.671	79.002	76.109	833	
00:49:32	13	22.663	77.631	22.865	22.429	79.291	75.974	833	
01:33:13	14	22.670	77.715	22.744	22.429	79.207	76.226	833	
02:16:54	15	22.796	77.814	23.035	22.599	79.168	76.396	833	
03:00:35	16	22.627	77.961	22.696	22.550	79.958	76.393	833	
03:44:17	17	23.936	78.183	24.972	23.228	79.863	76.207	833	
04:27:58	18	24.834	78.108	25.043	24.545	79.730	76.071	833	
05:11:40	19	24.482	78.028	24.853	24.116	79.593	76.561	833	
05:55:21	20	24.616	77.935	25.350	23.709	79.529	76.172	833	
06:39:03	21	23.626	77.901	23.924	23.396	79.318	76.086	833	
07:22:44	22	23.944	78.116	24.354	23.444	79.829	76.430	833	
08:06:26	23	24.096	78.166	24.378	23.876	79.707	76.385	833	
08:50:07	24	23.685	78.214	23.852	23.565	79.823	76.502	833	
09:33:48	25	23.523	78.246	23.565	23.493	79.732	76.165	833	
10:17:29	26	23.443	78.306	23.468	23.203	79.731	76.877	833	
11:01:10	27	22.865	77.931	22.865	22.865	78.162	77.700	3	

NOTES: (1) TIMES NOTED AT BEGINNING OF BURST (2) LSB (TEMP) = .027 °C, RG. 2.9 - 30.3°C
(3) LSB (DEPTH) = .042 m, RG. 53.6 - 96.4m.

TABLE A-3, Exp. #1, S/N 92 HFTP DATA SUMMARY

HFTP S/N 93 IN EXPERIMENT NO. 1

TIME (ZULU) BURST		AVE. TEMP.	AVE. DEPTH	TMAX	TMIN	DMAX	DMIN	NO. FRAMES	SIGNIF. EVENTS
16:04:55	1	23.974	0.159	24.016	23.944	0.184	0.143	833	
16:48:36	2	25.503	7.422	26.064	24.179	18.448	0.143	833	IN WATER 16:57Z
17:32:18	3	26.080	13.406	26.117	26.046	18.303	5.275	833	
18:15:59	4	26.131	18.146	26.135	26.117	18.988	16.121	833	
19:00:00	5	26.135	18.368	26.135	26.135	18.988	15.872	833	
19:43:41	6	26.135	18.525	26.135	26.117	18.988	16.495	833	
20:27:23	7	26.134	18.627	26.135	26.117	18.988	16.952	833	ANCHOR LAUNCH 20:27:27
21:11:04	8	26.123	18.706	26.135	26.117	18.988	17.326	833	
21:54:46	9	26.101	18.734	26.117	26.099	18.988	17.139	833	
22:38:27	10	26.101	18.778	26.117	26.081	18.988	17.347	833	
23:22:09	11	26.100	18.767	26.117	26.081	18.988	17.472	833	
00:05:50	12	26.093	18.769	26.099	26.081	18.988	17.513	833	
00:49:32	13	26.090	18.773	26.099	26.081	18.988	17.472	833	
01:33:13	14	26.083	18.759	26.099	26.081	18.988	17.575	833	
02:16:54	15	26.068	18.767	26.081	26.064	18.988	17.472	833	
03:00:35	16	26.049	18.775	26.064	26.046	18.988	17.285	833	
03:44:17	17	26.047	18.779	26.064	26.046	18.988	17.014	833	
04:27:58	18	26.046	18.782	26.046	26.028	18.988	17.201	833	
05:11:40	19	26.043	18.777	26.064	26.028	18.988	17.575	833	
05:55:21	20	26.054	18.793	26.064	26.046	18.988	17.555	833	
06:39:03	21	26.041	18.809	26.046	26.028	18.988	17.368	833	
07:22:44	22	26.003	18.821	26.010	25.992	18.988	17.596	833	
08:06:26	23	25.998	18.837	26.028	25.974	18.988	17.513	833	
08:50:07	24	26.111	18.854	26.171	26.046	18.988	17.575	833	
09:33:48	25	26.171	18.860	26.171	26.153	18.988	17.326	833	
10:17:29	26	26.166	18.879	26.171	26.153	18.988	17.887	745	

NOTES: (1) TIMES NOTED AT BEGINNING OF BURST.
(2) LSB (TEMP.) = .019 °C, RG. = 10.7 - 29.7 °C (3) LSB (DEPTH) = .021 m
RG = ~2.4 to 19 m

TABLE A-4, Exp #1, S/N 93 HFTP DATA SUMMARY

EXPERIMENT NO. 1		LFTP S/N : 15		
HOUR	Time (GMT)	Average Depth (m)	Average Temp. (°C)	Comments
1	10-12-96 2100	1440	2.85	
2	2200	1398	2.98	
3	2300	1391	3.01	
4	0000	1386	2.96	
5	0100	1403	2.93	
6	0200	1424	2.92	
7	0300	1434	2.84	
8	0400	1442	2.82	
9	0500	1434	2.82	
10	0600	1418	2.82	
11	0700	1413	2.79	
12	0800	1405	2.77	
13	0900	1400	2.77	
14	1000	1401	2.93	
15	1100	1401	2.95	
16	1200	1399	3.08	
17	1300	1391	2.97	
18	1400	1386	2.96	

TABLE A-5, EXP. #1, S/N 15 LFTP

DATA SUMMARY

EXPERIMENT NO. 1		LFTP S/N : 85		
HOUR	Time (GMT)	Average Depth (m)	Average Temp. (°C)	Comments
1	10-12-76 2100	430	7.28	
2	2200	428	7.15	
3	2300	431	7.09	
4	0000	432	7.21	
5	10-13-76 0100	434	7.25	
6	0200	436	7.18	
7	0300	441	6.85	
8	0400	442	7.10	
9	0500	440	7.20	
10	0600	435	7.90	
11	0700	435	8.05	
12	0800	432	7.82	
13	0900	432	7.75	
14	1000	435	7.72	
15	1100	435	7.64	
16	1200	436	7.64	
17	1300	436	7.50	
18	1400	437	7.40	

TABLE A-6, EXP. #1, S/N 85 LFTP

DATA SUMMARY

HFTP S/N 90 IN EXPERIMENT NO. 2, SPAR MOORING, 18 OCT. '76

TIME (ZULU)	BURST	AVE. TEMP. (°C)	AVE. DEPTH (m)	TMAX (°C)	TMIN (°C)	DMAX (m)	DMIN (m)	NO. FRAMES	SIGNIF. EVENTS
14:21:33	1	24.321	0.520	24.497	24.186	0.634	0.500	833	
15:05:14	2	23.990	0.501	24.090	23.899	0.629	0.497	833	
15:48:56	3	23.805	0.496	23.826	23.802	0.626	0.236	833	
16:32:37	4	25.083	0.800	26.460	23.778	1.306	0.495	833	IN WATER 16:48Z
17:16:19	5	26.462	0.819	26.484	26.437	0.917	0.527	833	
18:00:00	6	26.453	0.869	26.484	26.437	1.306	0.527	833	
18:43:41	7	26.522	0.621	26.531	26.484	0.787	0.527	833	
19:27:33	8	26.582	0.760	26.624	26.554	1.048	0.528	833	
20:11:04	9	26.678	0.590	26.718	26.624	0.790	0.529	833	20:27:45 ANCHOR LAUNCH
20:54:46	10	26.416	30.030	26.460	26.131	52.370	16.641	833	
21:38:27	11	26.504	9.097	26.531	26.484	11.313	7.285	833	
22:22:09	12	26.621	3.100	26.858	26.531	5.076	1.569	833	
23:05:50	13	27.067	1.004	27.139	26.975	1.313	0.793	833	
23:49:32	14	27.128	0.806	27.209	27.045	0.925	0.664	833	
00:33:13	15	27.117	0.817	27.162	27.069	1.054	0.534	833	
01:16:55	16	27.171	0.869	27.232	27.092	1.056	0.794	833	
02:00:36	17	26.977	1.029	27.489	26.460	2.216	0.533	833	
02:44:17	18	26.348	8.775	26.437	26.296	11.961	4.685	833	
03:27:59	19	26.271	13.235	26.272	26.249	14.300	12.221	833	
04:11:40	20	26.224	13.151	26.249	26.178	13.910	11.700	833	
04:55:22	21	26.153	15.388	26.178	26.131	17.287	13.778	833	
05:39:03	22	26.203	18.473	26.272	26.155	20.016	14.560	833	
06:22:45	23	26.539	7.121	26.975	26.296	10.532	4.431	833	
07:06:26	24	26.642	5.772	26.882	26.531	6.896	4.820	833	
07:50:07	25	26.560	7.065	26.601	26.484	7.935	5.596	833	
08:33:49	26	26.495	3.640	26.554	26.437	4.297	2.606	597	

NOTES: (1) TIMES NOTED AT BEGINNING OF BURST.

(2) LSB (TEMP) = LEAST SIGNIF. BIT = .027°C, RG = 2.9 - 30.3°C

(3) LSB (DEPTH) = .127 m, RG = 0 - 122.1 m

TABLE A-7, EXP. #2, S/N 90 HFTP DATA SUMMARY

HFTP S/N 91 IN EXPERIMENT NO. 2, SPAR MOORING, 18 OCT. '76

TIME (GMT) BURST		AVE. TEMP. (°C)	AVE. DEPTH (m)	TMAX (°C)	TMIN (°C)	DMAX (m)	DMIN (m)	NO. FRAMES	SIGNIF. EVENTS
14:21:33	1	24.008	46.096	24.177	23.866	46.142	46.057	833	
15:05:14	2	23.693	46.011	23.770	23.601	46.032	45.986	833	
15:48:56	3	23.531	45.967	23.553	23.529	45.973	45.967	833	
16:32:37	4	23.538	45.969	23.601	23.505	45.986	45.960	833	
17:16:19	5	23.832	46.048	24.081	23.649	46.116	45.999	833	IN WATER 17:58 Z
18:00:00	6	26.441	46.753	26.450	26.427	46.755	46.749	833	
18:43:41	7	26.466	46.760	26.473	26.450	46.762	46.755	833	
19:27:23	8	26.474	46.762	26.497	26.473	46.768	46.762	833	
20:11:04	9	26.479	46.763	26.497	26.473	46.768	46.762	833	20:27:45 ANCHOR LAUNCH
20:54:46	10	20.886	133.120	21.606	19.662	153.394	122.104	833	
21:38:27	11	22.011	116.802	22.170	21.827	119.338	114.885	833	
22:22:09	12	22.321	112.059	22.463	22.195	113.959	110.231	833	
23:05:50	13	22.643	109.870	22.901	22.488	110.631	108.971	833	
23:49:32	14	23.114	109.622	23.457	22.852	110.460	108.786	833	
00:33:13	15	23.136	110.049	23.457	22.877	110.742	109.127	833	
01:16:55	16	23.102	110.094	23.215	23.022	110.949	109.436	833	
02:00:36	17	22.362	113.496	22.780	22.048	116.706	111.353	833	
02:44:17	18	21.460	122.142	21.778	21.187	125.532	118.635	833	
03:27:59	19	21.259	125.199	21.434	21.137	126.677	124.033	833	
04:11:40	20	21.437	124.304	21.508	21.409	125.766	122.727	833	
04:55:22	21	21.448	125.616	21.483	21.409	127.426	65.496	737	

BAD DATA AFTER 21ST BURST

NOTES: (1) TIMES NOTED AT BEGINNING OF BURST

(2) LSB (TEMP) = .027 °C, RG. 2.9 - 30.3 °C

(3) LSB (DEPTH) = .169 m, RG. 46 - 218 m (4) BAD TAPE RCDR REPLACED AFTER

TABLE A-8, EXP. #2, S/N 91 HFTP DATA SUMMARY

HFTP S/N 92 IN EXPERIMENT NO. 2, SPAR MOORING, 18 OCT. '76

TIME (ZULU) BURST		AVE. TEMP. (°C)	AVE. DEPTH (m)	TMAX (°C)	TMIN (°C)	DMAX (m)	DMIN (m)	NO. FRAMES	SIGNIF. EVENTS
14:21:33	1	25.084	53.502	26.479	24.378	53.537	53.485	833	IN WATER 14:40Z
15:05:14	2	25.577	56.895	26.151	24.663	67.761	53.518	833	
15:48:56	3	23.979	68.691	24.449	23.541	74.447	64.560	833	
16:32:37	4	23.723	75.166	24.330	23.468	81.160	57.679	833	
17:16:19	5	23.322	79.998	23.900	23.059	81.408	74.287	833	
18:00:00	6	23.446	79.555	23.852	23.203	81.402	76.203	833	
18:43:41	7	23.564	80.115	23.828	23.276	81.153	78.565	833	
19:27:23	8	24.204	80.234	24.687	23.805	81.346	77.917	833	
20:11:04	9	24.833	78.485	25.539	24.735	81.235	68.035	833	ANCHOR LAUNCH 20:27:45
20:54:46	10	24.654	80.230	24.687	24.568	80.978	79.427	833	
21:38:27	11	24.241	80.349	24.521	24.044	81.218	79.498	833	
22:22:09	12	24.082	80.425	24.139	24.020	81.299	79.410	833	
23:05:50	13	24.300	80.465	24.449	24.163	81.226	79.667	833	
23:49:32	14	24.401	80.481	24.473	24.235	81.267	79.672	833	
00:33:13	15	24.636	80.480	24.759	24.521	81.359	79.594	833	
01:16:55	16	24.708	80.482	24.853	24.497	81.317	79.680	833	
02:00:36	17	24.275	80.366	24.449	24.187	81.183	79.416	833	
02:44:17	18	24.262	80.242	24.354	24.163	81.095	79.416	833	
03:27:59	19	24.197	80.219	24.378	24.116	81.094	79.372	833	
04:11:40	20	24.328	80.208	24.545	24.020	81.017	79.411	833	
04:55:22	21	24.407	80.248	24.592	24.163	81.102	79.372	833	
05:39:03	22	24.383	80.216	24.901	23.996	80.968	79.330	833	
06:22:45	23	24.881	80.362	24.925	24.806	81.277	79.473	833	
07:06:26	24	24.926	80.380	25.067	24.853	81.279	79.390	833	
07:50:07	25	25.148	80.360	25.280	25.067	81.076	79.606	833	
08:33:49	26	25.267	80.392	25.398	25.161	81.040	79.736	699	

NOTES: (1) TIMES NOTED AT BEGINNING OF BURST

(2) LSB (TEMP) = .027°C, RG = 2.9 - 30.3°C (3) LSB (DEPTH) = .042 m, RG = 53.6 - 96.4 m

TABLE A-9, EXP. #2, S/N 92 HFTP DATA SUMMARY

HFTP S/N 93 IN EXPERIMENT NO. 2, SPAR MOORING, 18 OCT '76

TIME (GMT) / BURST		AVE. TEMP. (°C)	AVE. DEPTH (m)	TMAX (°C)	TMIN (°C)	DMAX (m)	DMIN (m)	NO. FRAMES	SIGNIF. EVENTS
14:21:33	1	25.188	7.930	25.259	19.335	28.440	7.884	833	
15:05:14	2	25.314	7.924	25.331	25.295	7.925	7.924	833	IN WATER 15:247
15:48:56	3	25.388	7.925	25.420	25.367	7.925	7.925	833	
16:32:37	4	25.479	7.926	25.510	25.456	7.926	7.925	833	
17:16:19	5	25.547	7.926	25.564	25.545	7.926	7.926	833	
18:00:00	6	25.571	7.926	25.581	25.564	7.926	7.926	833	
18:43:41	7	25.581	7.926	25.581	25.581	7.926	7.926	833	
19:27:23	8	25.582	7.926	25.599	25.581	7.926	7.926	833	
20:11:04	9	24.643	7.920	24.864	24.468	7.921	7.919	833	ANCHOR LAUNCH 20:27:45
20:54:46	10	24.777	7.921	26.527	24.107	7.933	7.916	833	
21:38:27	11	26.527	8.738	26.545	26.527	12.835	7.933	833	
22:22:09	12	26.469	16.195	26.527	26.384	18.213	10.882	833	
23:05:50	13	26.508	17.247	26.527	26.491	17.944	14.309	833	
23:49:32	14	26.477	16.950	26.491	26.473	18.068	15.181	833	
00:33:13	15	26.508	17.239	26.527	26.491	17.778	16.532	833	
01:16:55	16	26.515	17.327	26.527	26.509	17.965	16.158	833	
02:00:36	17	26.510	16.438	26.527	26.491	17.799	11.713	833	
02:44:17	18	26.487	17.368	26.491	26.473	17.902	16.947	833	
03:27:59	19	26.490	17.415	26.491	26.473	17.923	16.926	833	
04:11:40	20	26.475	17.470	26.491	26.456	17.985	17.009	833	
04:55:22	21	26.460	17.489	26.473	26.456	18.005	16.988	833	
05:39:03	22	26.440	17.498	26.456	26.367	17.923	17.071	833	
06:22:45	23	26.368	17.497	26.384	26.367	18.026	16.987	833	
07:06:26	24	26.387	17.525	26.402	26.367	18.068	16.905	833	
07:50:07	25	26.342	17.515	26.367	26.331	18.005	16.987	833	
08:33:49	26	26.379	17.438	26.384	26.367	17.901	16.925	716	

NOTES: (1) TIMES NOTED AT BEGINNING OF BURST.
(2) LSB(TEMP) = .019 °C, RG = 10.7 - 29.7 °C (3) LSB(DEPTH) = .021 m, RG = 7.4 - 28.4 m.

TABLE A-10, EXP. #2, S/N 93 HFTP DATA SUMMARY

EXPERIMENT NO. 2		LFTP S/N : 15		
HOUR	Time (GMT)	Average Depth (m)	Average Temp. (°C)	Comments
1	10-18-76 2100	1375	3.07	
2	2200	1374	3.05	
3	2300	1374	3.04	
4	0000	1374	3.02	
5	0100	1374	3.01	
6	0200	1375	2.91	
7	0300	1377	2.91	
8	0400	1377	2.93	
9	0500	1377	2.91	
10	0600	1376	2.99	
11	0700	1375	3.02	
12	0800	1375	3.01	
13	0900	1375	2.93	
14	1000			ANCHOR RELEASED 1000 (10-19-76)
15	1100			
16	1200			
17	1300			
18	1400			

TABLE A-11, EXP. #2, S/N 15

LFTP DATA SUMMARY

EXPERIMENT NO. 2		LFTP S/N : 85		
HOUR	Time (GMT)	Average Depth (m)	Average Temp. (°C)	Comments
1	10-18-76 2100	406	8.60	VARIATIONS
2	2200	400	9.15	"
3	2300	397	9.30	
4	0000	397	8.98	
5	10-19-76 0100	397	8.70	
6	0200	403	8.35	
7	0300	410	7.90	
8	0400	409	7.81	
9	0500	411	7.97	
10	0600	405	7.96	
11	0700	403	8.15	
12	0800	401	8.25	
13	0900	400	8.28	
14	1000			ANCHOR RELEASED
15				
16				
17				
18				

TABLE A-12, EXP. #2, S/N 85
LFTP DATA SUMMARY

HFTP S/N 90 IN EXPERIMENT NO. 3, TAUT DISCUS MRG, 22 OCT. '76

TIME (ZULU) ↓ BURST		AVE. TEMP. (°C)	AVE. DEPTH (m)	TMAX (°C)	TMIN (°C)	DMAX (m)	DMIN (m)	NO. FRAMES	SIGNIF. EVENTS
12:44:40	1	25.593	4.581	26.155	25.210	21.575	-0.007	833	IN WATER 13:04 Z
13:28:21	2	26.124	31.009	26.155	26.084	33.789	27.033	833	
14:12:03	3	25.979	33.685	26.037	25.943	34.568	32.488	833	
14:55:44	4	25.983	31.716	26.014	25.943	34.827	28.460	833	
15:39:26	5	26.033	34.288	26.061	25.990	36.777	32.489	833	ANCHOR LAUNCH 15:44:28
16:23:07	6	25.964	35.000	25.990	25.943	35.737	34.047	833	
17:06:49	7	25.952	35.015	25.990	25.943	35.867	34.177	833	
17:50:30	8	25.967	35.151	25.990	25.920	35.997	34.307	833	
18:34:12	9	25.959	35.201	25.967	25.943	35.867	34.307	833	
19:17:53	10	25.957	35.201	25.967	25.967	36.127	34.307	833	
20:01:35	11	25.957	35.458	25.967	25.943	37.036	33.268	833	
20:45:16	12	25.943	36.402	25.943	25.943	37.166	35.606	833	
21:28:57	13	26.037	36.775	26.084	25.990	37.167	35.608	833	
22:12:38	14	26.058	36.768	26.061	26.037	37.167	35.608	833	
22:56:20	15	26.037	36.397	26.061	26.014	37.297	35.348	833	
23:40:01	16	26.013	36.472	26.037	25.990	37.297	35.607	833	
00:23:43	17	26.048	36.527	26.061	26.014	37.427	35.608	833	
01:07:24	18	26.053	36.504	26.061	26.037	37.557	35.608	833	
01:51:05	19	26.050	36.480	26.061	26.037	37.427	35.478	833	
02:34:46	20	26.033	36.448	26.037	26.014	37.297	35.608	833	
03:18:28	21	26.010	36.443	26.014	25.990	37.427	35.219	833	
04:02:09	22	25.994	36.444	26.014	25.967	37.426	35.347	833	
04:45:51	23	25.974	36.477	25.990	25.967	37.296	35.347	833	
05:29:32	24	25.985	36.139	26.037	25.967	37.166	35.087	833	
06:13:14	25	26.025	36.119	26.084	25.990	37.037	35.088	833	
06:56:55	26	26.076	31.743	26.296	26.014	36.648	15.599	547	

NOTES: (1) TIMES NOTED AT BEGINNING OF BURST.
(2) LSB (Temp.) = .027°C, RG. = 2.9 - 30.3°C, (3) LSB (DEPTH) = .127 m., RG. 0 - 122.1 m

TABLE A-13, EXP. #3, S/N 90 HFTP DATA SUMMARY

HFTP S/N 91 IN EXPERIMENT NO. 3, TAUT DISCUS MRG, 22 OCT '76

TIME (GMT) / BURST		AVE. TEMP. (°C)	AVE. DEPTH (m)	TMAX (°C)	TMIN (°C)	DMAX (m)	DMIN (m)	NO. FRAMES	SIGNIF EVENTS
12:44:40	1	24.647	46.268	24.774	24.535	46.303	46.238	833	IN WATER 13:24 Z
13:28:21	2	25.172	76.391	26.121	22.561	121.382	46.660	833	
14:12:03	3	22.677	119.919	23.818	22.219	132.322	104.622	833	
14:55:44	4	24.351	96.141	25.862	22.170	134.491	73.005	833	
15:39:26	5	22.867	127.250	24.702	21.631	156.102	101.184	833	ANCHOR LAUNCH 15:44:28
16:23:07	6	21.043	153.561	21.532	20.839	154.539	152.363	833	
17:06:49	7	20.823	153.758	20.839	20.765	155.021	152.852	833	
17:50:30	8	20.707	154.395	20.740	20.640	155.329	153.327	833	
18:34:12	9	20.452	154.588	20.566	20.391	155.443	153.589	833	
19:17:53	10	19.975	154.459	20.291	19.788	155.637	153.421	833	
20:01:35	11	19.745	154.629	19.940	19.409	156.279	152.256	833	
20:45:16	12	19.826	155.565	19.964	19.687	156.447	154.432	833	
21:28:57	13	20.043	155.451	20.115	19.839	156.293	154.459	833	
22:12:38	14	20.311	155.417	20.391	20.115	156.407	154.519	833	
22:56:20	15	19.970	155.590	20.090	19.839	156.822	154.445	833	
23:40:01	16	20.461	155.998	20.516	20.266	157.103	154.927	833	
00:23:43	17	20.604	156.306	20.765	20.491	157.317	155.282	833	
01:07:24	18	20.836	156.169	20.964	20.740	157.357	155.027	833	
01:51:05	19	20.942	156.041	21.409	20.839	157.082	155.006	833	
02:34:46	20	21.303	155.886	21.508	21.236	156.827	154.818	833	
03:18:28	21	21.566	155.868	21.655	21.508	156.906	154.556	833	
04:02:09	22	21.906	155.899	22.097	21.754	157.011	154.648	833	
04:45:51	23	22.042	155.955	22.146	21.877	157.185	154.668	833	
05:29:32	24	21.252	153.897	21.557	21.063	155.012	152.758	833	
06:13:14	25	20.852	153.623	21.013	20.715	155.181	151.995	833	
06:56:55	26	25.380	70.238	26.407	22.973	100.385	46.609	588	

NOTES: (1) TIMES NOTED AT BEGINNING OF BURST.
(2) LSB (TEMP) = .027°C., RG = 2.9 – 30.3°C (3) LSB (DEPTH) = .169 m, RG. 46 – 218 m

TABLE A-14, EXP. #3, S/N 91 HFTP DATA SUMMARY

HFTP S/N 92 IN EXPERIMENT NO. 3, TAUT DISCUS MRG., 22 OCT. '76

TIME (ZULU) BURST		AVE. TEMP. (°C)	AVE. DEPTH (m)	TMAX (°C)	TMIN (°C)	DMAX (m)	DMIN (m)	NO. FRAMES	SIGNIF. EVENTS
12:44:40	1	25.268	53.506	25.398	25.019	53.510	53.501	833	IN WATER 13:10 Z
13:28:21	2	25.916	64.012	26.151	25.704	73.248	53.527	833	
14:12:03	3	25.882	70.570	25.940	25.657	73.460	66.490	833	
14:55:44	4	25.930	61.635	26.127	25.350	74.284	53.526	833	
15:39:26	5	25.952	71.699	26.010	25.916	73.587	64.899	833	ANCHOR LAUNCH 15:44:28
16:23:07	6	25.906	76.386	25.963	25.822	77.322	75.178	833	
17:06:49	7	25.498	76.410	25.846	24.996	77.506	75.499	833	
17:50:30	8	25.116	76.723	25.727	24.877	77.638	75.626	833	
18:34:12	9	25.332	76.825	25.398	25.161	77.683	75.836	833	
19:17:53	10	24.240	76.749	25.067	23.107	77.809	75.809	833	
20:01:35	11	22.689	76.966	22.880	22.575	78.536	74.590	833	
20:45:16	12	22.668	77.908	22.696	22.599	78.785	76.897	833	
21:28:57	13	22.807	77.849	23.083	22.429	78.795	77.028	833	
22:12:38	14	24.177	77.956	25.043	23.493	78.823	76.895	833	
22:56:20	15	24.029	77.927	24.449	23.805	79.000	76.720	833	
23:40:01	16	24.792	78.140	25.209	24.354	79.189	77.080	833	
00:23:43	17	25.324	78.286	25.445	25.256	79.360	77.178	833	
01:07:24	18	25.677	78.217	25.775	25.516	79.535	77.189	833	
01:51:05	19	25.871	78.146	25.916	25.704	79.208	76.983	833	
02:34:46	20	25.880	78.071	25.940	25.775	79.080	77.109	833	
03:18:28	21	25.861	78.040	25.940	25.728	79.042	76.730	833	
04:02:09	22	25.571	78.050	25.798	25.090	79.272	76.803	833	
04:45:51	23	25.357	78.116	25.563	24.908	79.199	76.924	833	
05:29:32	24	25.480	77.214	25.587	25.280	78.269	76.135	833	
06:13:14	25	25.300	77.126	25.681	24.925	73.403	75.825	833	
06:56:55	26	25.912	63.753	26.268	25.704	76.182	53.523	600	

NOTES: (1) TIMES NOTED AT BEGINNING OF BURST
(2) LSB (TEMP) = .027°C, RG. = 2.9 - 30.3°C. (3) LSB (DEPTH) = .042 m, RG. = 53.6 - 96.4 m.

TABLE A-15, EXP. #3, S/N 92 HFTP DATA SUMMARY

HFTP S/N 93 IN EXPERIMENT NO. 3, TAUT DISCUS MRG., 22 OCT. '76

TIME (ZULU) BURST		AVE. TEMP. (°C)	AVE. DEPTH (m)	TMAX (°C)	TMIN (°C)	DMAX (m)	DMIN (m)	NO. FRAMES	SIGNIF EVENTS
12:44:40	1	25.586	10.021	26.206	24.882	15.865	7.922	833	IN WATER 12:54 Z
13:28:21	2	26.176	15.887	26.206	26.135	17.069	14.577	833	
14:12:03	3	26.152	16.999	26.171	26.099	17.692	16.072	833	
14:55:44	4	26.111	16.784	26.135	26.081	17.941	15.615	833	
15:39:26	5	26.089	17.396	26.099	26.064	18.772	16.445	833	ANCHOR LAUNCH 15:44:28
16:23:07	6	26.049	17.500	26.064	26.010	18.169	16.694	833	
17:06:49	7	26.017	17.511	26.028	25.992	18.210	16.860	833	
17:50:30	8	25.993	17.587	26.010	25.992	18.252	16.819	833	
18:34:12	9	26.014	17.620	26.028	25.992	18.273	17.006	833	
19:17:53	10	26.043	17.634	26.064	26.028	18.397	16.964	833	
20:01:35	11	26.050	17.909	26.081	26.010	19.332	15.864	833	
20:45:16	12	26.090	18.860	26.099	26.081	19.540	18.148	833	
21:28:57	13	26.105	18.844	26.117	26.099	19.520	18.169	833	
22:12:38	14	26.117	18.839	26.135	26.099	19.457	18.232	833	
22:56:20	15	26.120	18.849	26.135	26.117	19.623	17.983	833	
23:40:01	16	26.119	18.883	26.135	26.099	19.604	18.149	833	
00:23:43	17	26.181	18.906	26.224	26.117	19.769	18.087	833	
01:07:24	18	26.190	18.896	26.224	26.153	19.790	18.087	833	
01:51:05	19	26.204	18.884	26.224	26.189	19.666	17.983	833	
02:34:46	20	26.149	18.870	26.189	26.135	19.644	18.128	833	
03:18:28	21	26.111	18.866	26.153	26.081	19.603	17.796	833	
04:02:09	22	26.086	18.867	26.099	26.064	19.769	17.941	833	
04:45:51	23	26.041	18.887	26.064	26.028	19.623	17.982	833	
05:29:32	24	26.157	18.734	26.171	26.135	19.561	17.900	833	
06:13:14	25	26.172	18.734	26.349	26.135	19.479	17.817	833	
06:56:55	26	26.265	17.186	25.456	26.171	19.395	10.300	833	

NOTES: (1) TIMES NOTED AT BEGINNING OF BURST.
(2) LSB (TEMP) = .019 °C, RG = 10.7 - 29.7 °C (3) LSB (DEPTH) = .021 m. RG. = 7.4 - 28.4 m.

TABLE A-16, EXP. #3, S/N 93 HFTP DATA SUMMARY

EXPERIMENT NO. 3		LFTP S/N : 15		
HOUR	Time (GMT)	Average Depth (m)	Average Temp. (°C)	Comments
1	10-22-76 1600	1360	2.99	ANCHOR LAUNCH AT 1544
2	1700	1375	2.86	
3	1800	1367	2.93	
4	1900	1363	2.98	
5	2000	1363	3.08	
6	2100	1363	3.05	
7	2200	1368	3.10	
8	2300	1375	3.02	
9	0000	1365	3.00	
10	10-23-76 0100	1360	2.99	
11	0200	1358	2.94	
12	0300	1360	2.94	
13	0400	1364	2.91	
14	0500	1365	2.93	ANCHOR RELEASE AT 0505
15	0600			
16				
17				
18				

TABLE A-17, EXP. #3, S/N 15

LFTP DATA SUMMARY

EXPERIMENT NO. 3		LFTP S/N: 85		
HOUR	Time (GMT)	Average Depth (m)	Average Temp. (°C)	Comments
1	10-22-76 1600	440	7.55	
2	1700	440	7.65	
3	1800	442	7.30	
4	1900	442	7.28	
5	2000	442	7.34	
6	2100	443	7.32	
7	2200	442	7.42	
8	2300	443	7.44	
9	0000	442	7.30	
10	10-23-76 0100	442	7.44	
11	0200	442	7.58	
12	0300	442	7.80	
13	0400	442	8.04	
14	0500	436	8.30	
15	0600	435	8.03	
16				
17				
18				

TABLE A-18, EXP. #3, S/N 85

LFTP DATA SUMMARY

AD-A045 801 CHARLES STARK DRAPER LAB INC CAMBRIDGE MASS F/G 8/3
THE C. S. DRAPER LABORATORY ROLE IN THE MOORING DYNAMICS EXPERI--ETC(U)
APR 77 W A VACHON, J R SCHOLTEN N00014-75-C-1065
UNCLASSIFIED R-1093 NL

2 OF 2
ADA045801

END
DATE FILMED
11-77
DDC

EXPERIMENT NO. 4		LFTP S/N: 15		
HOUR	Time (GMT)	Average Depth (m)	Average Temp. (°C)	Comments
1	10-26-96 1800	1392	2.98	ON BOTTOM ~1815
2	1900	1393	2.95	
3	2000	1393	2.93	
4	2100	1394	2.93	
5	2200	1394	3.02	
6	2300	1394	2.96	
7	0000	1393	2.99	
8	10-27-96 0100	1394	3.05	
9	0200	1394	3.02	
10	0300	1393	2.99	
11	0400	1394	2.96	
12	0500	1394	2.96	
13	0600			ANCHOR RELEASED
14	0700			
15	0800			
16	0900			
17				
18				

TABLE A-19, Exp. #4, S/N 15

LFTP DATA SUMMARY

EXPERIMENT NO. 4		LFTP S/N: 85		
HOUR	Time (GMT)	Average Depth (m)	Average Temp. (°C)	Comments
1	10-26-76 1800	3.90	9.35 (when bottomed)	STILL DECENDING
2	1900	391	9.15	
3	2000	391	9.12	
4	2100	391	8.40	
5	2200	391	8.31	
6	2300	391	8.20	
7	0000	391	8.09	
8	10-27-76 0100	391	8.19	
9	0200	391	8.12	
10	0300	391	8.01	
11	0400	391	8.25	
12	0500	391	8.75	
13	0600			ANCHOR RELEASED
14	0700			
15				
16				
17				
18				

TABLE A-20, EXP. #4, S/N 85

LFTP DATA SUMMARY

HFTP S/N 90 IN EXPERIMENT NO. 5, CEL SUBSURFACE MRG., 1 NOV. '76

TIME (BULU)[1] ↓BURST		AVE. TEMP. (°C)	AVE. DEPTH (m)	TMAX (°C)	TMIN (°C)	DMAX (m)	DMIN (m)	NO. FRAMES	SIGNIF. EVENTS
15:03:56	1	25.371	1.867	25.635	24.806	11.692	-0.012	833	
15:47:57	2	25.613	10.777	25.613	25.613	12.083	8.574	833	
16:31:18	3	25.612	11.577	25.613	25.589	12.213	10.913	833	
17:15:00	4	25.490	43.412	25.613	24.688	75.357	10.133	833	ANCHOR LAUNCH
17:58:41	5	25.471	55.035	25.494	25.471	55.220	54.830	833	
18:42:28	6	25.539	55.047	25.566	25.518	55.351	54.831	833	
19:26:04	7	25.444	64.774	25.518	24.949	76.392	55.610	833	
20:09:46	8	25.518	55.746	25.518	25.518	56.390	55.350	833	MOORING PULL-OVER
20:53:27	9	25.494	56.220	25.494	25.494	56.519	55.870	833	
21:37:09	10	25.502	55.480	25.518	25.494	59.118	54.051	833	MOORING PULL-OVER
22:21:50	11	25.517	55.158	25.518	25.494	55.610	54.831	833	
23:04:31	12	25.417	59.264	25.518	23.946	83.779	54.571	833	MOORING PULL-OVER
23:48:12	13	25.519	54.448	25.518	25.518	54.701	54.051	833	
00:31:54	14	25.538	55.750	25.542	25.518	68.992	53.792	833	MOORING PULL-OVER
01:15:35	15	25.543	54.149	25.566	25.542	54.441	53.792	833	
01:59:18	16	25.552	55.579	25.566	25.542	67.174	54.051	833	MOORING PULL-OVER
02:42:59	17	25.557	53.995	25.566	25.518	54.312	53.791	833	
03:26:40	18	25.724	13.354	25.754	25.518	54.051	10.914	833	ANCHOR RELEASE
04:20:21	19	25.736	7.045	25.849	25.258	11.824	-0.007	501	

NOTES: (1) TIMES NOTED AT BEGINNING OF BURST
(2) LSB (TEMP) = .027 °C, RG = 2.9 - [illegible] °C
(3) LSB (DEPTH) = .127 m., RG = 0 - 122.1 m.

TABLE A-21, EXP. #5, S/N 90 HFTP DATA SUMMARY

EXPERIMENT NO. 5		LFTP S/N: 85		
HOUR	TIME (GMT)	AVERAGE DEPTH (m)	AVERAGE TEMP. (°C)	COMMENTS
1	11-1-76 1800	404	8.2	ANCHOR LAUNCH 1717
2	1900	404	8.48	
3	2000	404	8.47	
4	2100	405	8.58	
5	2200	404	8.58	
6	2300	404	8.60	
7	0000	404	8.64	
8	0100	404	9.02	
9	0200	404	9.03	
10	0300	403	9.00	
11	0400			ANCHOR RELEASE 0327
12				
13				
14				
15				
16				
17				
18				

TABLE A-22, EXP. #5, S/N 85

LFTP DATA SUMMARY

APPENDIX B

T/P Timing, Calibrations and Word Structure

For users of the archived data from TPs it is useful to know how the data on the archived tapes were derived. Tables B-1 and B-2 contain explanations of the time counts on the HFTP and LFTP respectively.

The data are processed in two stages. First, the sea instrument tape cassettes are copied bit-for-bit onto an IBM compatible 7-track tape (at 800 characters per inch). The manner of packing of a single frame of T/P data (96 bits) on this intermediate tape is given in Tables B-3 and B-4 for the FHTPs and LFTPs, respectively. The final, archived, tape is generated from the intermediate tape by a special PL/I language computer program. The archived data is written in a simple FORTRAN-compatible format, given in Table B-5.

In order to have the HFTPs strobe in close synchronism with the FVRs it is necessary to artifically delay their start by 5.12 seconds (see section 4.4). The timing after this follows a repeating history where the first temperature and pressure word are strobed .08 seconds later. Subsequently temperature is sampled every frame (i.e., 2.08 seconds) while in between pressure is sampled on the average every 0.52 seconds. In fact, the time of the pressure word (after the first strobe/frame) increments by 0.48 seconds, 0.56 seconds, 0.48 seconds, and finally by 0.56 seconds - for a total of 2.08 seconds per frame. The time word on the HFTP data tapes will reflect this fact.

The archived data from the T/Ps contain temperature and depth information in ^{o}C and meters respectively. The temperature data are a direct result of the calibrations themselves. The depth data are, however, calculated from the pressure data in order to be presented in a form directly useful for model verification. For those data users wishing to recreate the basic pressure word or possibly then recreate a new depth estimate based on a new model of the pressure-depth relationship the relationship that was used in deriving the archived depth words is given by equation (B-1). In (B-1) the following values

$$D = C_1 P + C_2 P^2 \qquad \text{(B-1)}$$

for C_1 and C_2 are assumed:

$$C_1 = .68372608$$

$$C_2 = -9.50103555 \times 10^{-7}$$

The units of P are psig (pounds per square inch above an assumed atmospheric pressure of 14.473 pounds per square inch or 29.6 inches of mercury at $23^{\circ}C$) and the units of D are in meters.

J. Scholten
15 Mar. 1977

TABLE B-1

HFTP "Time Count"

The "time count" register on the high-frequency temperature-pressure recorder increments every 2.56 seconds, and is initialized to zero at 5.20 sec. into each burst. Since there are 2.08 seconds between frames, the time count increments exactly 13 times for each 16 frames.

For example:

FRAME NO.	TIME (SEC.)	TIME COUNT
1	5.20	0
2	7.28	0
3	9.36	1
4	11.44	2
5	13.52	3
6	15.60	4
7	17.68	4
8	19.76	5
9	21.84	6
10	23.92	7
11	26.00	8
12	28.08	9
13	30.16	9
14	32.24	10
15	34.32	11
16	36.40	12
17	38.48	13
18	40.56	13

J. Scholten
15 March 1977

TABLE B-2

LFTP "Time Count"

The "time count" register of the low-frequency temperature-pressure recorder is initialized to zero at instrument start (i.e. magnet off, frame no. zero), and is incremented by <u>two</u> for each frame (4 minutes). In addition, the lowest-order ("ones") bit of the register is switched "on" during alternate series of eight frames, starting at frame 8. In particular:

FRAME NO.	TIME (MINUTES)	TIME COUNT	"ONES" BIT
0	0	0	0
1	4	2	0
2	8	4	0
3	12	6	0
4	16	8	0
5	20	10	0
6	24	12	0
7	28	14	0
8	32	17	1
9	36	19	1
10	40	21	1
11	44	23	1
12	48	25	1
13	52	27	1
14	56	29	1
15	60	31	1
16	64	32	0
17	68	34	0
18	72	36	0
19	76	38	0

J. Scholten
March 1977
(after J. McKenna)

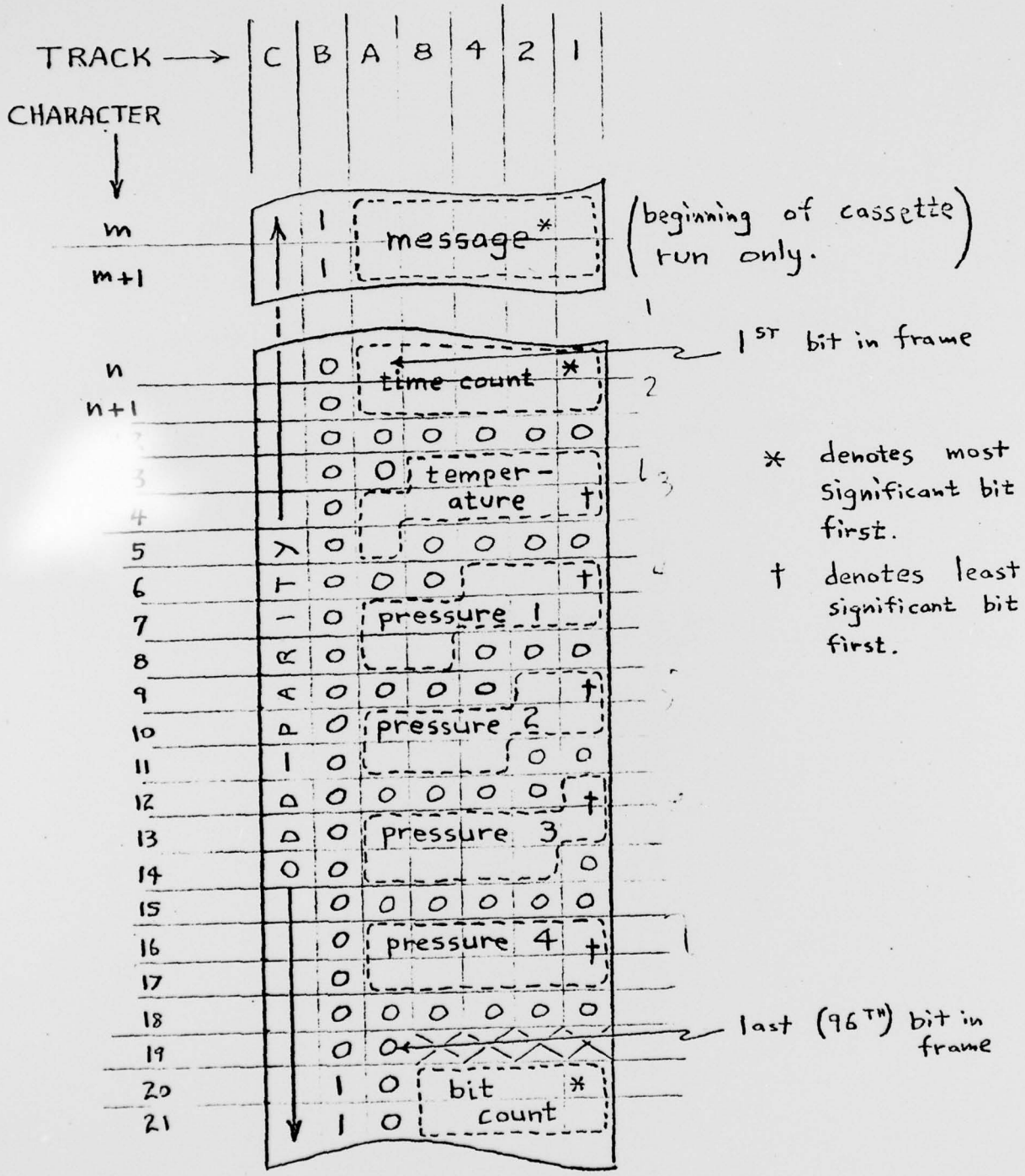

HIGH-FREQUENCY TEMPERATURE-PRESSURE RECORDER.
TFA FORMAT

TABLE B-3

J. Scholten
March 1977
(after J. McKenna)

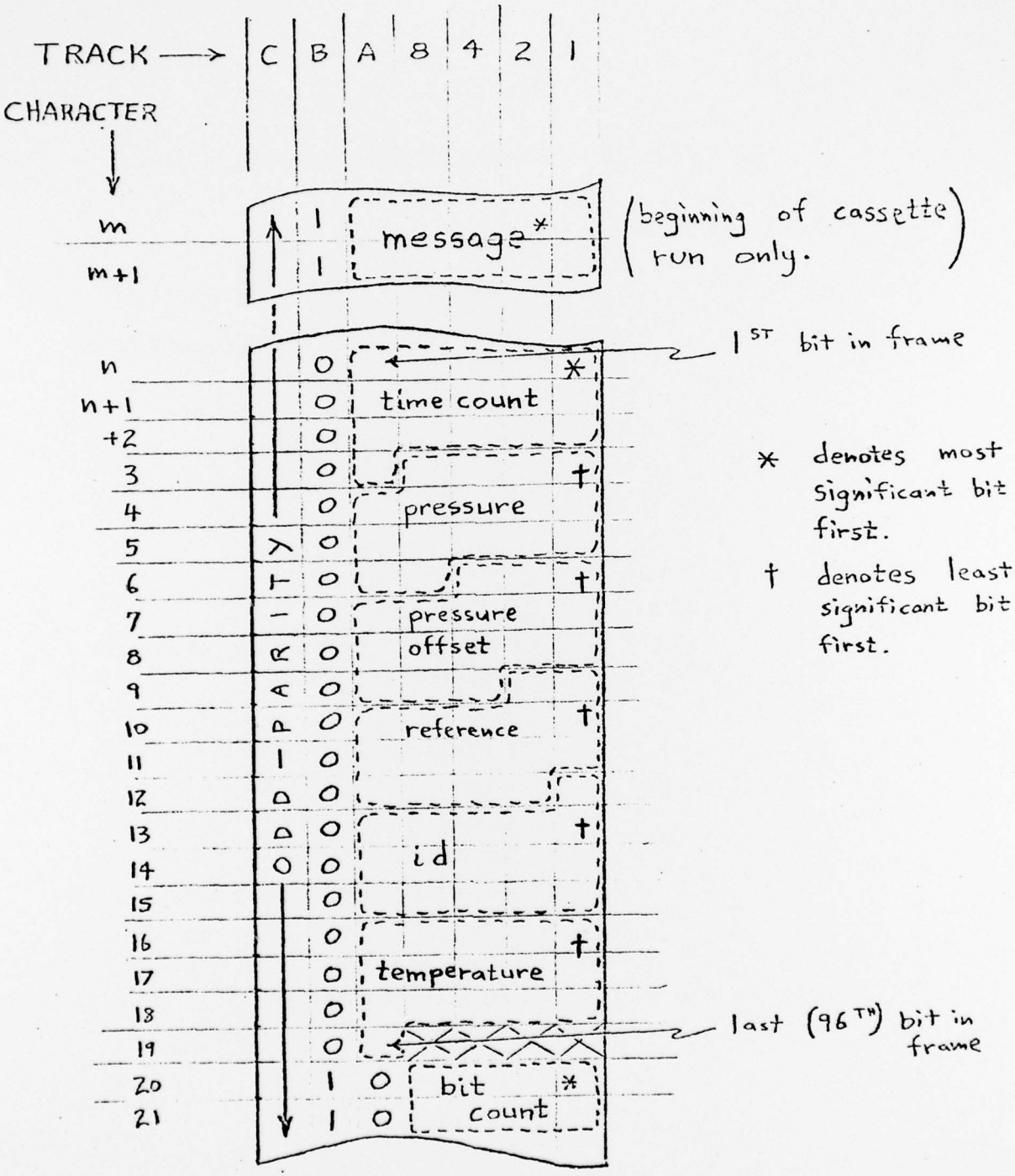

LOW-FREQUENCY TEMPERATURE-PRESSURE RECORDER

TFA FORMAT

TABLE B-4

TABLE B-5

Data Format for Temperature/Pressure Recorders

HFTP Archived Data Format:

FORTRAN FORMAT	DESCRIPTION
F 11.2	Time (sec. after start of first burst)
I 11	Time count
F 11.6	Temperature (^{O}C)
4 F 11.6	Depths (m.)
3 X	(Blanks to make 80 characters)

LFTP Archived Data Format:

I 11	Time (mins. after instrument start)*
I 11	Time Count
F 11.3	Depth (m.)
I 11	Pressure Offset
I 11	Reference
I 11	I. D.
F 11.6	Temperature (^{O}C)
3 X	(Blanks to make 80 characters)

* Instrument started at 1530 Z on 27 September 1976.

NOTE:

In both cases tape attributes are:

7-Tracks, Even parity
800 BPI
80 BCD characters per logical record
1600 BCD characters per physical record (block)

APPENDIX C

FVR Timing, Calibration, and Word Structure

The overall burst timing of the FVR is given in Table 6 with 1810, 6-word frames (plus time) per burst. The timing of each FVR frame is, however, taken at 0.08 seconds into the 0.52-second burst. Each of the 6 data channels is simultaneously strobed and fed to a sample and hold circuit from which the data are sequentially read onto the magnetic tape cassette. Figure C-1 shows the manner in which the data are packed on the cassette tape. Notice that the first frame of each burst is time and frame count. Each succeeding frame contains real data. When the data are finally placed on the 7-track tape by the Tape Format Adapter (TFA) the first and succeeding frames of each burst are packed as shown in Figures C-2 and C-3 respectively. It should be observed that the frame count is a 6-bit word and thus increments from 0 to 63 and is then reinitialized. These raw data (in units of instrument counts) are then converted to engineering units by using the magnetometer calibration values shown in Table 10 and the load cell and accelerometer calibrations shown in Table C-4. The resulting basic engineering unit archived data tapes contain the following data columns:

Time (since the beginning of the first burst),
frame count (0 to 63), tension (pounds),

γ_x/γ_h, γ_y/γ_h, f_x(g's), f_y(g's), and f_z(g's) .

The non-dimensionalized magnetometer data are derived by applying equations (5-17).

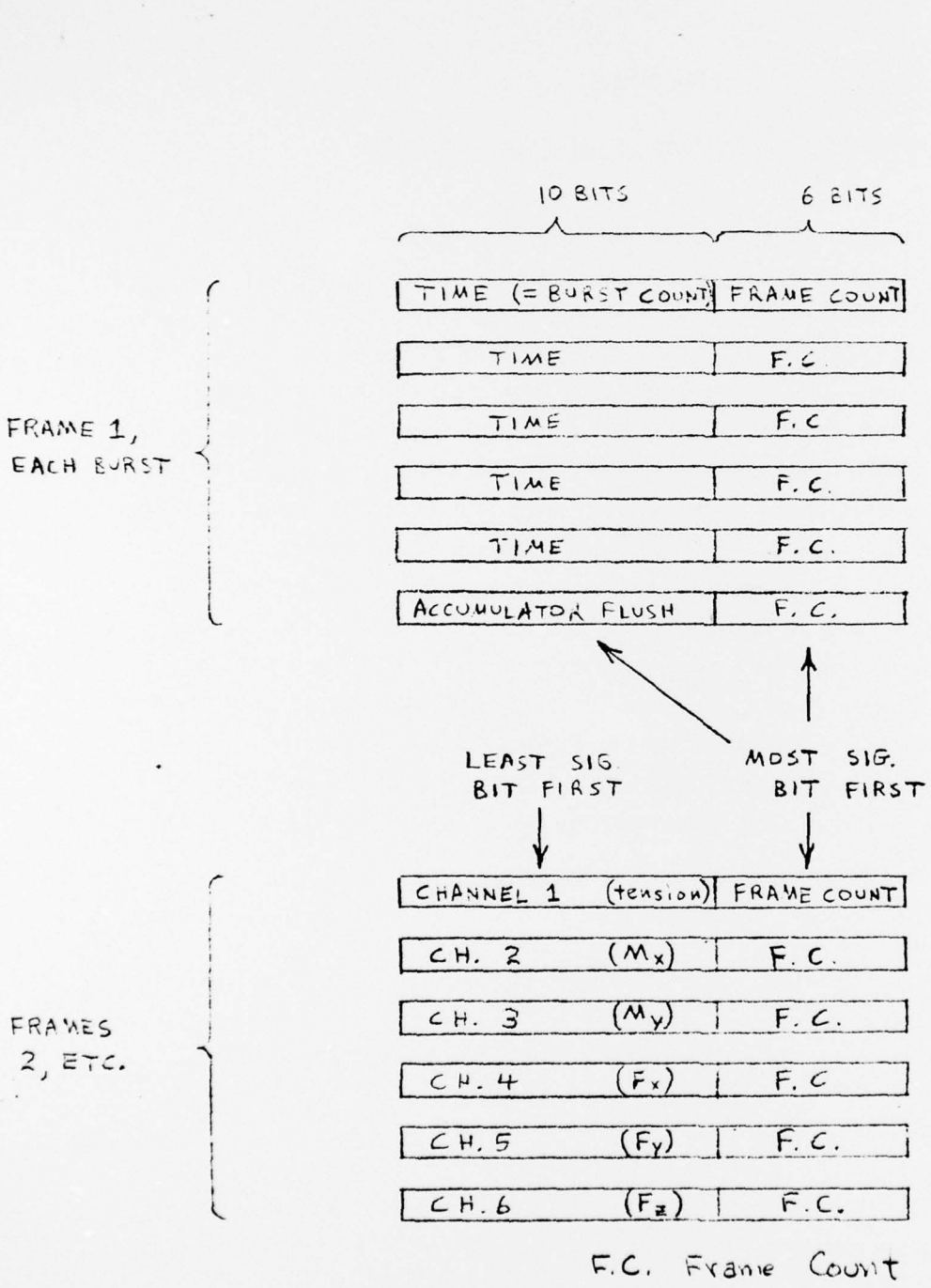

FIGURE C-1
FVR BIT FORMATTING

J. Scholten
March 1977
(after J. McKenna)

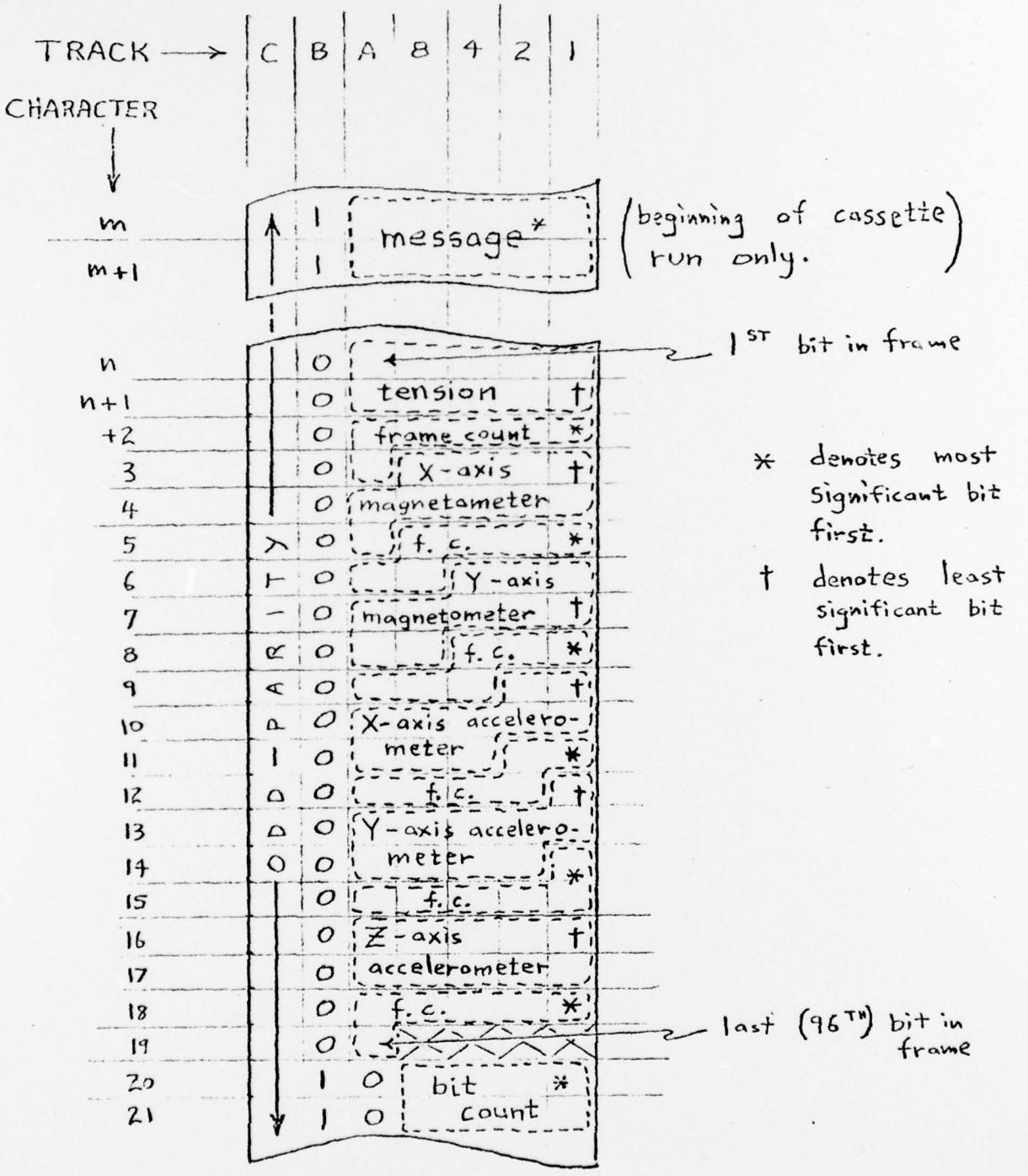

FORCE VECTOR RECORDER
TFA FORMAT
FRAMES 2, ETC., EACH BURST

TABLE C-2

J. Scholten
March 1977
(after J. McKenna)

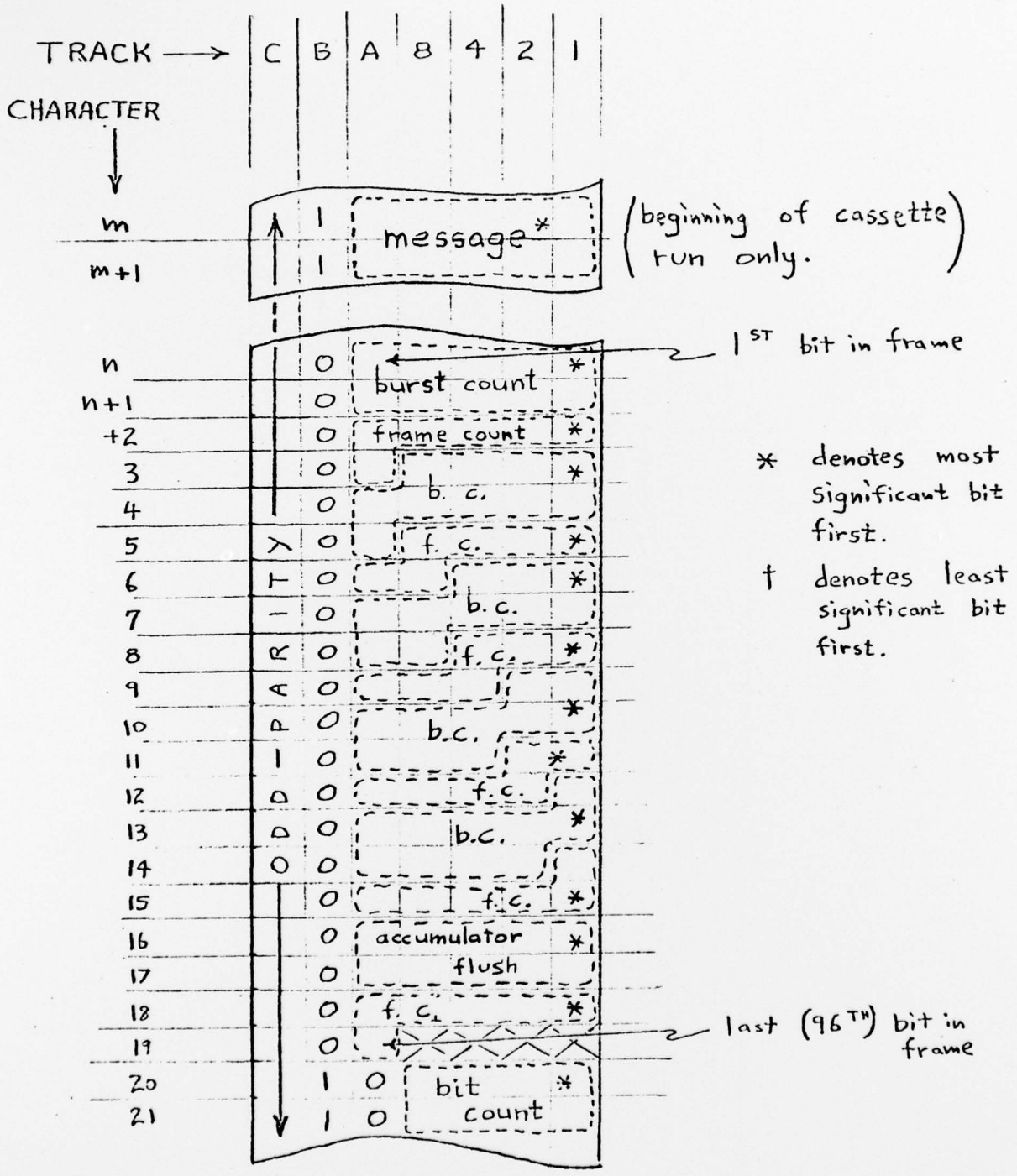

FORCE VECTOR RECORDER
TFA FORMAT
FRAME NO. 1, EACH BURST

TABLE C-3

FVR S/N	LOAD CELL $C_L = B_L + (SF)_L L$	x - ACCELEROMETER $A_x = B_x + (SF)_x f_x$	y - ACCELEROMETER $A_y = B_y + (SF)_y f_y$	z-ACCELEROMETER $A_z = B_z + (SF)_z f_z$
F1	B_L = 10 Counts $(SF)_L$ = .3236 cts/lb	B_x = 514 counts $(SF)_x$ = -518.6 cts/g	B_y = 519 Counts $(SF)_y$ = -507.5 cts/g	B_z = 1020 counts $(SF)_z$ = -511 cts/g
F2	B_L = 0 Counts $(SF)_L$ = .3227 cts/lb	EXPERIMENT No. 1 : (+) B_x = 518 counts $(SF)_x$ = -254 cts/g EXPERIMENTS 2,3,5: B_x = 519 cts/g $(SF)_x$ = -404 cts/g	B_y = 515.5 Counts $(SF)_y$ = -335.5 cts/g	B_z = 774 Counts $(SF)_z$ = -250.9 cts/g
F3	B_L = -1.6 Counts $(SF)_L$ = .3189 cts/lb	B_x = 513 Counts $(SF)_x$ = -256 cts/g	EXPERIMENT No. 1 (§) B_y = 519 Counts $(SF)_y$ = -340 cts/g EXPERIMENTS 2,3,5: B_y = 519 Counts $(SF)_y$ = -340 cts/g	B_z = 772 Counts $(SF)_z$ = -251.5 cts/g
F4	B_L = 32 Counts $(SF)_L$ = .3211 cts/lb	B_x = 510 Counts $(SF)_x$ = -255 cts/g	B_y = 509 Counts $(SF)_y$ = -341 cts/g	B_z = 764 Counts $(SF)_z$ = -250 cts/g

(+) FIRST 4 BURSTS ONLY THEN FAILURE (§) WORKED FOR COMPLETE EXP. No. 1

TABLE C-4: LOAD CELL & ACCELEROMETER CALIBRATION SUMMARY FOR MDE FIELD EXPERIMENT

WV 3/25/77

TABLE C-5

FVR Archived Data Format:

FORTRAN FORMAT	DESCRIPTION
F 11.2	Time (sec. after start of first burst)
I 8	Time Count
F 11.4	Tension (lbs.)
F 10.6	γ_x/γ_h
F 10.6	γ_y/γ_h
F 10.6	f_x (g's) = specific force$_x$
F 10.6	f_y (g's) = specific force$_y$
F 10.6	f_z (g's) = specific force$_z$

NOTE:

Tape attributes are the same as for T/P's (see Table B-5)

TABLE C-6

FVR Euler Angle Archived Data Format:

FORTRAN FORMAT	DESCRIPTION
I 10	Number of frames averaged
F 11.2	Time at mid-average (sec. after instrument start)
F 11.4	Tension (lbs.)
F 11.6	γ_x/γ_h
F 11.6	γ_y/γ_h
F 11.6	f_x (g's)
F 11.6	f_y (g's)
F 11.6	f_z (g's)
F 11.2	ϕ (deg.)
F 11.2	θ (deg.)
F 11.2	ψ (deg.)

Tape attributes are: 7-Tracks, Even parity
800 BPI
120 BCD characters per logical record
1200 BCD characters per physical record (block)

MANDATORY DISTRIBUTION LIST

FOR UNCLASSIFIED TECHNICAL REPORTS, REPRINTS, & FINAL REPORTS
PUBLISHED BY OCEANOGRAPHIC CONTRACTORS
OF THE OCEAN SCIENCE AND TECHNOLOGY DIVISION
OF THE OFFICE OF NAVAL RESEARCH
(REVISED JAN 1975)

1 Director of Defense Research and Engineering
Office of the Secretary of Defense
Washington, D. C. 20301
ATTN: Office, Assistant Director (Research)

Office of Naval Research
Arlington, Virginia 22217
3 ATTN: (Code 480)*
1 ATTN: (Code 460)
1 ATTN: (Code 102-OS)
6 ATTN: (Code 102IP)
1 ATTN: Code 200
1 ONR ResRep (if any)

Director
Naval Research Laboratory
Washington, D. C. 20375
6 ATTN: Library, Code 2620

12** Defense Documentation Center
Cameron Station
Alexandria, Virginia 22314

Commander
Naval Oceanographic Office
Washington, D. C. 20390
1 ATTN: Code 1640
1 ATTN: Code 70

1 NODC/NOAA
Rockville, MD 20882

TOTAL REQUIRED - 35 copies

* Add one separate copy of Form DD-1473

** Send with these 12 copies two completed forms DDC-50, one self addressed back to contractor, the other addressed to ONR, Code 480

DISTRIBUTION (cont'd)

Charles Stark Draper Laboratory, Inc.

5 Librar
1 Arau ichard
1 Bowdi , Philip N.
1 Chhabra Narender
1 Dahlen, John M.
1 McKenna, John F.
1 Reid, Robert W.
5 Scholten, James S.
1 Shillingford, John T.
1 Soikkeli, Matti
1 Suomala, John B.
1 Toth, William E.
5 Vachon, William

M.I.T. Department of Earth & Planetary Physics

1 Wunsch, Prof. Carl I.

M.I.T. Department of Meteorology

1 Heinmiller, Robert

M.I.T. Department of Naval Architecture & Marine Engineering

1 Newman, Prof. John N.

Research Laboratories:

1 Davis, Dr. Russ
Scripps Institution of Oceanography
La Jolla, CA 92037

1 Nath, Dr. John
Department of Oceanography
Oregon State University
Corvallis, OR 97331

1 Savage, Dr. Godfrey H.
Director, Engineering Design & Development Lab
University of New Hampshire
Durham, NH 03824

DISTRIBUTION (cont'd)

Research Laboratories (cont'd.):

1 Christenson, Lt. Tom
Ocean Science and Technology Division
NORDA, Code 450
NSTL Station
Bay St. Louis, Miss. 39520

1 Gregory, John B.
U. S. Geological Survey
620 National Center
Reston, VA 22092

3 Walden, Robert
Woods Hole Oceanographic Institute
Woods Hole, MA 02543

1 Collins, Dr. Curt
National Science Foundation
1800 G Street, N.W.
Washington, DC 20550

5 Director
2 Barry, Lt. Craig
1 Kerut, Edmund
1 Livingston, Dr. Layne
1 Michelena, Dr. Edwards
NOAA Data Buoy Office
Code C-623A
NSTL Station
Bay St. Louis, MS 39529

1 Ringenbach, Maurice
1 Kalvaitis, Allan
NOAA/OMT
Test and Evaluation Lab
Rockville, MD 20852

1 Brooks, Dr. Davis
1 Merritt, Hal
1 Trampus, Dr. Anthony
Sperry Rand
NSTL Station
Bay St. Louis, Miss. 39529

1 Escowitz, Edward C.
Chesapeake Division - Bldg. 200
Naval Facilities Engineering Command
Washington Navy Yard
Washington, D.C. 20374
Attn: Code: FPO-1E4

DISTRIBUTION (cont'd)

1 Kim, Michael W. D.
Chesapeake Division - Bldg 57
Naval Facilities Engineering Command
Washington Navy Yard
Washington, D.C. 20374
Attn: Code FPO-1E5

1 Bonde, Les
EG&G/WASCI
2150 Field Road
Rockville, MD 20850

1 DeBok, Lt. Donald H.
U. S. Coast Guard
Research & Development Center
Groton, Conn.

1 Halpern, Dr. David
1 Milburn, Hugh
NOAA-PMEL
3711 15th Avenue, NE
Seattle, WA 98105